DISTRIBUTED NONLINEAR STABILITY ANALYSIS OF ROTATING STALL

by

Catherine Mansoux

Ingénieur de l'Ecole Polytechnique (1991)

Submitted to the Department of Aeronautics and Astronautics
in Partial Fulfillment of the Requirements for the Degree of

Master of Science in Aeronautics and Astronautics

at the

Massachusetts Institute of Technology
May 1994

Signature of Author _____
Department of Aeronautics and Astronautics
March 31, 1994

Certified by _____
Professor James D. Paduano
Thesis Supervisor

Accepted by _____
Professor Harold Y. Wachman
Chairman, Department Graduate Committee

Distributed Nonlinear Stability Analysis of Rotating Stall

by

Catherine Mansoux

Abstract

Linear stability addresses only the local behavior of a nonlinear system around its equilibrium point, whereas a nonlinear stability analysis can provide more general information, for instance the size of the domain of attraction of the equilibrium. This issue is critical since a linearly stable equilibrium that has a small domain of attraction can be destabilized by a big enough perturbation, sometimes even by noise. This phenomenon occurs in compression systems; the compressor enters rotating stall before the linearly-predicted stall inception point. This thesis presents a method for nonlinear stability analysis of rotating stall using Lyapunov stability theory. The method allows one to estimate domains of attraction at any operating point, for various compression system parameters. A nonlinear state-space representation of rotating stall based on the Moore-Greitzer model is used. Examples are given that show trends in the inception behavior of rotating stall depending on the properties of the compression system. A more elaborate model of rotating stall is then presented, and it is shown why and how Absolute Stability Theory can be applied.

Acknowledgments

First, I would like to thank Professor Greitzer and Professor Epstein for their warm welcome at the Gas Turbine Laboratory and their continuous interest in this work. To my advisor, Professor Paduano, I express my thanks for his time, assistance and invaluable guidance throughout this year. He helped me understand many of the concepts surrounding the Lyapunov analysis and rotating stall.

I would also like to take advantage of this page to say how grateful I am to all the students met in this unique environment. Special thanks go to Hong Shu for her friendship and all the so different but delicious food she made me discover. My very best wishes for the continuation of her studies. To Harold Weigl for the H-infinity controller of Chapter 3 and all the fruitful discussions we had. It was very constructive to work together. And to the GTL French connection: Merci, it made me feel a little bit at home.

Finally, I would like to thank the Délégation Générale pour l'Armement for its financial support that made it possible for me to carry out this research work under excellent conditions. This work was also supported by the US Air Force Office of Research, Major Daniel B. Fant, Technical monitor. This support is gratefully acknowledged.

Contents

List of Figures

List of Tables

Nomenclature

V	Lyapunov function
$\underline{x}$	State vector
Ω	Region of negative $\dot{V}$
D_c	Largest ellipsoid $\{\underline{x} / V(\underline{x}) = c\}$ to fit inside Ω, domain of attraction
m,μ,λ	Compression system geometric parameters (I)
l_c,B	Compression system geometric parameters (II)
ϕ	Nondimensional flow coefficient in compressor duct
$\delta\phi$	Perturbation of flow coefficient around annulus of compressor
$\underline{\phi}$	(Mx1) vector containing flow coefficients at distributed values of θ
$\delta\Phi$	Nondimensional velocity potential
ψ	Nondimensional instantaneous local pressure rise in plenum
ψ_c	Pressure rise delivered across compressor
ψ_T	Pressure drop imposed across throttle
ϕ_T	Inverse of ψ_T
K_t	Throttle constant
Q	Throttle local slope
t	Time nondimensionalized by rotor revolution period
θ	Circumferential angle around compressor annulus
η	Nondimensional axial distance along compressor duct, zero at compressor face
∇	Laplacian
N	Number of harmonics modeled in finite order approximation
M	2N+1
n	Harmonic number
k	Location around annulus, $k \in [0;2N]$
F	Fourier transform matrix in complex form
F_{ext}	Extended Fourier transform matrix in complex form
G	Fourier transform matrix in real form
A	Flowfield transformation operator
E	Flowfield transformation operator

D_A	Matrix of eigenvalues of A using transformation F
D_E	Matrix of eigenvalues of E using transformation F
D_A^G	Matrix of eigenvalues of A using transformation G
D_E^G	Matrix of eigenvalues of E using transformation G
$\underline{S}$	Length-N vector to take mean of a distributed vector quantity
$\underline{T}$	Length-N vector for zeroth mode of surge/stall model
f	$\tilde{\phi}$-dependent part of $\dot{\tilde{V}}$
g	$\tilde{\bar{\psi}}$-dependent part of $\dot{\tilde{V}}$
d	Size of domain of attraction
ψ_i	Ideal characteristic of compressor assumed isentropic
L_{ss}	Steady-state losses
L	Unsteady losses
r	Rotor
s	Stator
i	Ideal
τ	Nondimensional convection time through a blade row
C_i, C_r, C_S	Value of $\tilde{\psi}_i$, $\tilde{L}_{ss}^{(r)}$ and $\tilde{L}_{ss}^{(s)}$ at $\tilde{\phi} = 0$
D_i, D_r, D_S	Slope of $\tilde{\psi}_i$, $\tilde{L}_{ss}^{(r)}$ and $\tilde{L}_{ss}^{(s)}$ at $\tilde{\phi} = 0$
$\tilde{H}_i, \tilde{H}_r, \tilde{H}_s$	Nonlinear part of $\tilde{\psi}_i$, $\tilde{L}_{ss}^{(r)}$ and $\tilde{L}_{ss}^{(s)}$ at $\tilde{\phi} = 0$
A,B,C	State-space matrices
$\underline{X}, \underline{U}, \underline{Y}$	State, input and output vectors of state-space representation
$\underline{\Psi}$	Nonlinearity vector
α	Slope, lower limit of 1D sector condition
β	Slope, higher limit of 1D sector condition
[a;b]	Interval of validity of 1D sector condition
K_{min}	Matrix of lower limit slopes for multivariable sector condition
K_{max}	Matrix of higher limit slopes for multivariable sector condition
Γ	Domain of validity of multivariable sector condition
P	Solution of Ricatti equation, defines quadratic Lyapunov function V
H	Hamiltonian matrix
ε	Rate of convergence of trajectories to the origin
U	Rotor speed
γ	Stagger angle of servo-controlled guide vanes
R	Dissipation matrix
N	Multiplier matrix

$\dot{(.)}$	Derivative with respect to nondimensional time t
$\overline{(.)}$	Annulus average
$(.)^*$	Value of argument at equilibrium point
$\tilde{(.)}$	Value of argument in local coordinate system about equilibrium point
$\hat{(.)}$	Spatial Fourier coefficient (argument is a function of θ)
$(.)^T$	Conjugate transpose (argument is a matrix)
$(.)^i$	Internal or linear part
$(.)^e$	External or nonlinear part
Real(.)	Real part
Imag(.)	Imaginary part
$I_{(.)}$	Identity matrix of dimension (.)

D.A.	Domain of attraction
S.I.P.	Stall inception point
D.F.T.	Discrete Fourier Transform
C.L.	Closed-loop
O.L.	Open-loop

Introduction

Rotating stall and surge are violent limit cycle-type oscillations in axial compressors, which result when perturbations (in flow velocity, pressure, etc.) become unstable. Originally treated separately, these two phenomena are now recognized to be coupled oscillation modes of the compression system -- surge is the zeroth order or planar oscillation mode, while rotating stall is the limit cycle resulting from higher-order, rotating-wave disturbances. The importance of these phenomena to the safety and performance of gas turbine engines is widely recognized [1], and various efforts to either avoid or control both rotating stall and surge have been studied [2,3,4,5,6].

This thesis presents a nonlinear stability analysis of rotating stall as opposed to the linear stability analyses that have been presented in the past [3,7,8]. To model the rotating stall phenomenon we use a state-space representation based on the Moore-Greitzer equations [9,10], which include nonlinearity through the compressor characteristic. The model of rotating stall is therefore nonlinear and a simple linear stability analysis is not enough to capture the whole behavior of the system. Linear stability addresses only its local behavior around an equilibrium point. A further step in the analysis is then: given a linearly stable equilibrium point, to measure from a nonlinear perspective how stable the equilibrium is. This issue is addressed by the calculation of the domain of attraction of the equilibrium point which requires a method of nonlinear stability analysis. We will use a Lyapunov analysis method. Lyapunov methods are the foundation for various nonlinear control design procedures (such as feedback linearization, sliding mode control and Lyapunov control). Thus such a choice seems to be well adapted to the problem we are dealing with.

Basic compression system modeling

A detailed model of rotating stall will be presented in Section 2.1 but in order to facilitate the discussion of the nonlinear analysis we present here a brief description of the phenomenology of compressor operation.

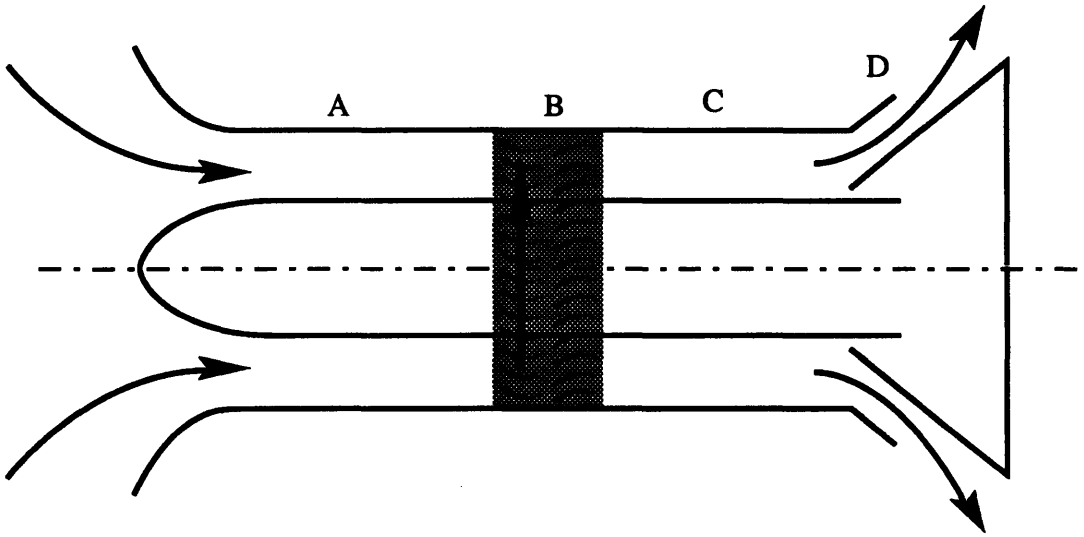

Figure I.1: Compression system components: A - inlet duct, B - compressor, C - downstream duct, D - throttle.

Consider the schematic diagram of an axial compressor in Figure I.1. It consists of an upstream annular duct, a compressor modeled as an actuator disk, a downstream annular duct, and a throttle. During stable operation, flow through the compressor can be assumed to be circumferentially uniform (axisymmetric), and a single non-dimensional measure of flow through the compressor determines the system state. One such measure is the 'flow coefficient', which is simply the nondimensionalized value of the axial velocity:

$$\phi = \frac{\text{(axial velocity)}}{\text{(rotor speed)}} \qquad \text{(I.1)}$$

During quasi-steady operation, the total-to-static pressure rise delivered by the compressor is simply determined by its 'pressure rise characteristic,' denoted $\psi_c(\phi)$ (Refer to Figure I.2). The pressure rise is balanced by a pressure loss across a throttling device, which can

be either a simple flow restriction (used for testing compressors as components) or the combustor and turbine in a gas turbine engine. The balance between pressure rise across the compressor and pressure drop across the throttle is depicted as an intersection between the characteristics of the two devices, $\psi_c(\phi)$ and $\psi_T(\phi)$, where, for low pressure ratios, $\psi_T(\phi)$ is usually taken to be a quadratic function of ϕ:

$$\psi_T(\phi) = \frac{1}{2} K_T \phi^2 \qquad \text{(I.2)}$$

K_T depends on the degree of throttle closure. In a typical experiment, the throttle is slowly closed, the throttle characteristic becomes steeper (modeled by increasing K_T in (I.2)), the intersection point between $\psi_c(\phi)$ and $\psi_T(\phi)$ changes, and the equilibrium operating point of the compressor moves from high flow to low flow (see Figure I.2).

The stability of the equilibrium point represented by the intersection between $\psi_c(\phi)$ and $\psi_T(\phi)$ has been the topic of numerous studies, due to its importance in the safe, high performance operation of gas turbine engines.

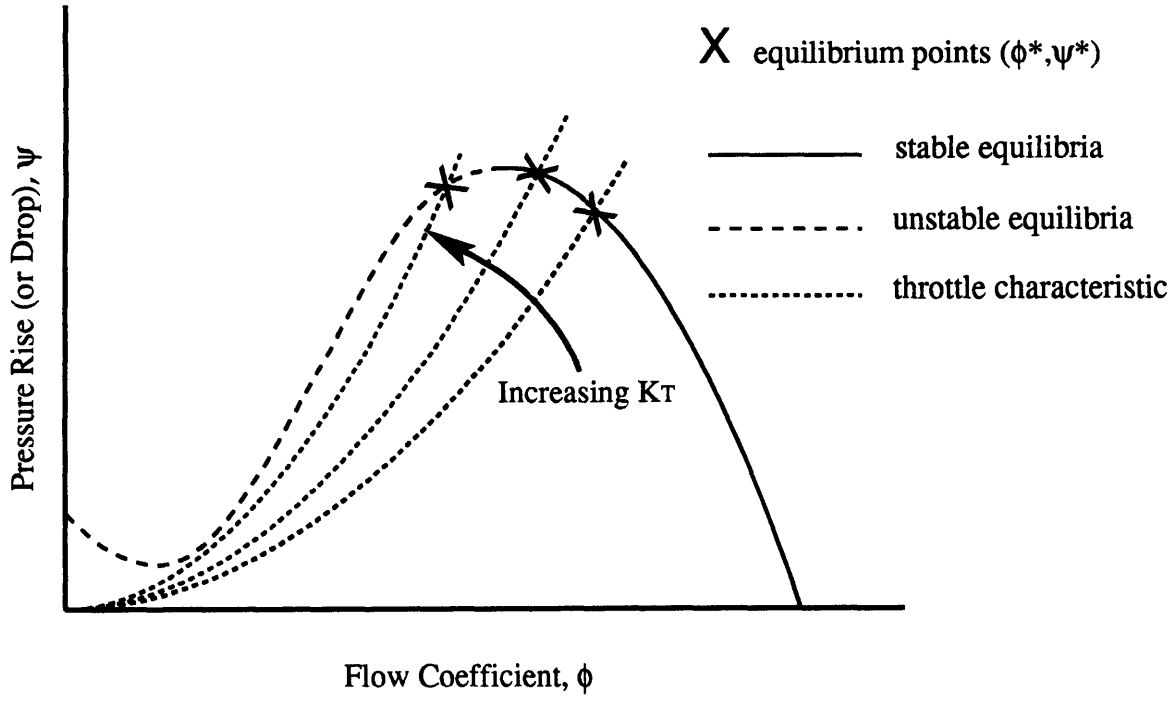

Figure I.2: Compressor and throttle behavior during a typical experimental test.

In chapter one, principles of the Lyapunov Analysis are presented. Then it is shown how a Lyapunov analysis of surge has been successfully implemented and how the initial choice of the Lyapunov function is critical to the physical meaningfulness of the results that follow. A first state-space representation of rotating stall based on the Moore-Greitzer model is presented and a Lyapunov function is proposed. It allows to estimate the domain of attraction at any operating point for various compression systems. Examples are given that explain trends in the inception behavior of rotating stall depending on properties of the compression system. A 1D Lyapunov analysis is performed that explains the 'stabilization' of the system by a simple nonlinear control. A more elaborate model of rotating stall is then presented that includes effects of unsteady losses and basic linear control schemes. It is explained why and how a new technique, Absolute Stability Theory, can be applied to the model. Domains of attraction are then calculated and compared with results from first model.

Chapter 1

Motivations for the Nonlinear Stability Analysis of Rotating Stall

1.1 Notion of Domain of Attraction.

From now on, when studying the stability of an equilibrium, it will always be first translated to the origin through a change of axes. Consider a linearly stable equilibrium point $\underline{x}=\underline{0}$ of a system whose dynamics are: $\dot{\underline{x}} = f(\underline{x})$ where $\underline{x}$ is the state vector and f is a nonlinear function (see [11]).

The Domain of Attraction (D.A.) is defined as the largest set of points around the equilibrium such that trajectories initiated at these points eventually converge to the origin. If the equilibrium has an infinite D.A. it is said to be globally stable (Figure 1.1(i)) whereas if it has a finite D.A. it is said to be locally stable (Figure 1.1(ii)). This happens when we have more than 2 coexistent equilibria.

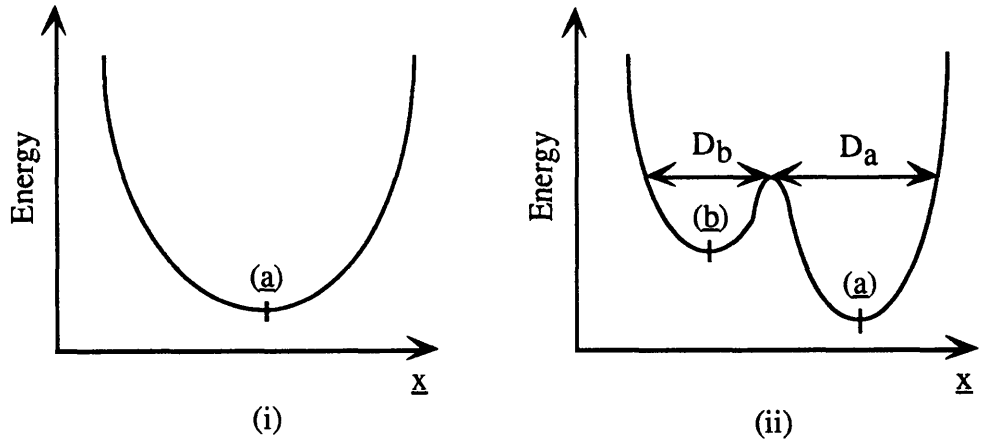

Figure 1.1: Nonlinear system with: (i) 1 global equilibrium, (ii) 2 local equilibria

System (ii) exhibits 2 coexistent equilibria: $\underline{x}=\underline{a}$, domain of attraction D_a and $\underline{x}=\underline{b}$, domain of attraction D_b. This is exactly what happens in the case of rotating stall when we are getting close to the peak of the compressor characteristic on its stable (right) side (see Figure I.2). Linear stability analysis [3,7,8] predicts that the peak of the characteristic is the linearly predicted stall inception point (S.I.P.). On the stable (right) side of the characteristic, 2 equilibria $\underline{a}$ and $\underline{b}$ exist. Both are linearly stable. The first equilibrium called $\underline{a}$ exists as axisymmetric mass flow, while the second, $\underline{b}$, is a non-axisymmetric wave of axial velocity traveling around the annulus of the compressor. The latter is the rotating stall equilibrium. We would like the compressor to operate axisymmetrically since the rotating stall (non-axisymmetric) equilibrium can lead to violent and destructive limit cycle-type oscillations. Therefore, we would like the state vector $\underline{x}$ to always stay around the equilibrium $\underline{x}=\underline{a}$, i.e. inside its domain of attraction D_a.

Assume that the system operates initially at $\underline{x}=\underline{a}$. As long as only perturbations whose magnitude is smaller than the radius of D_a are applied to the system, its trajectory will stay inside D_a and eventually go back to $\underline{x}=\underline{a}$. If a perturbation whose magnitude is bigger than the radius of D_a is introduced the trajectory of the system will exit D_a and enter D_b and eventually tend to $\underline{x}=\underline{b}$ which means for our compression system that the compressor will enter rotating stall. We have thus shown that the system can access rotating stall from a linearly stable and axisymmetric operating point ($\underline{x}=\underline{a}$) if perturbations are large enough and thus before the peak of the characteristic, which constitutes the linearly predicted stall inception point (S.I.P.). Some experimental data [5] exhibit exactly this kind of behavior. Noise itself can then be enough to make the system jump from an axisymmetric equilibrium into rotating stall before the S.I.P.

1.2. Principles of Lyapunov Analysis

The references used in this section are [11,12]. The Lyapunov function generalizes the concept of total energy of the system. The Lyapunov theorem generalizes the idea that if the total energy of a mechanical system is continuously dissipated, then the system, whether linear or nonlinear, must eventually settle down to an equilibrium point. One point that is fundamental and will help understanding the final results is that we will always try to choose a function V that makes sense physically, i.e. which can be interpreted as an energy.

A Lyapunov analysis does not require the knowledge of the solutions (trajectories) of the system. This point becomes critical when we want to analyze nonlinear systems whose trajectories are usually difficult to compute. The method will then prove to be particularly effective. A key principle of the Lyapunov analysis method is that it detects stability of a system through properties of a Lyapunov function $V(\underline{x})$ where $\underline{x}$ is the state of the system. This function is not unique and failure of one function to meet the stability conditions does not mean that a true Lyapunov function does not exist. Moreover there is no general and simple way to find a suitable Lyapunov function. This last remark constitutes the main weakness of the method.

The Lyapunov analysis can be performed in 2 steps.

→ <u>step #1</u>: Find a Lyapunov function that verifies:

$$\left.\begin{array}{l}\text{(i) } V(\underline{0}) = 0 \\ \text{(ii) } V(\underline{x} \neq \underline{0}) > 0\end{array}\right\} \Rightarrow \begin{array}{l}\text{V is positive definite} \\ \text{at least locally around } \underline{0}.\end{array}$$

$$\text{(iii) } \dot{V} < 0 \text{ in some region around } \underline{0}.$$

→ <u>step #2</u>: Apply Lyapunov's theorem for asymptotic stability:

If $\dot{V} < 0$ in some region Ω around $\underline{0}$ then $\underline{x}=\underline{0}$ is **asymptotically stable.**

From step #1, we know that the Lyapunov function $V(\underline{x})$ is positive definite and has a unique minimum at $\underline{x}=\underline{0}$. We can visualize V in the simple case where the dimension of $\underline{x}$ is 2. Then $V(\underline{x})$ corresponds to a surface which looks like a cup (Figure 1.2). The lowest point of the cup is located at the origin.

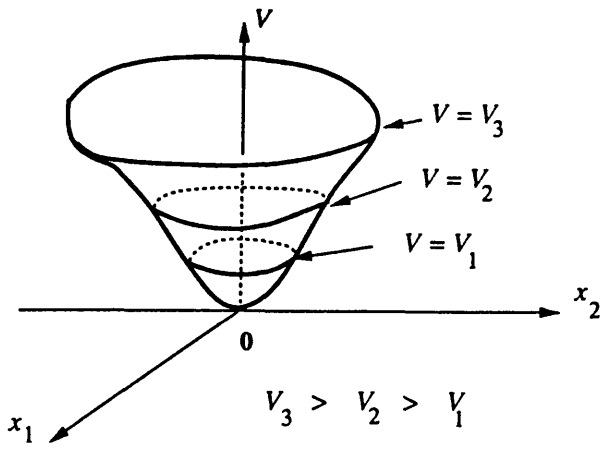

Figure 1.2 : Typical shape of a positive definite function $V(x_1,x_2)$.

A second geometrical representation can be made as follows. The level curves $V(x_1,x_2)=V_\alpha$ represent a set of closed contours surrounding the origin, with each contour corresponding to a positive value of V_α. These contours are horizontal sections of the cup, projected on the (x_1,x_2) plane (Figure 1.2). Note that the contours do not intersect, because $V(x_1,x_2)$ is uniquely defined given (x_1,x_2) (Figure 1.3).

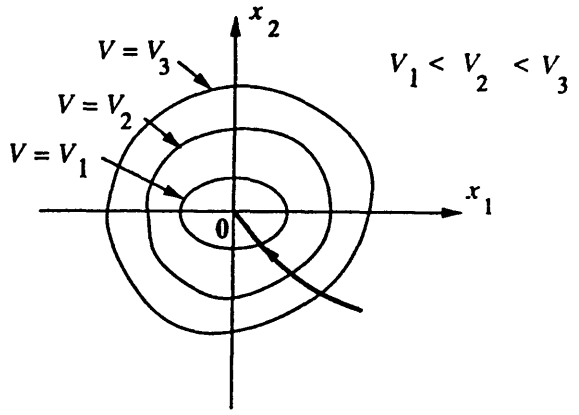

Figure 1.3 : Projection of 3 contour curves on the (x_1, x_2) plane and an example trajectory.

From step #2, we know that $\dot{V}(\underline{x})$ is negative for all points in the region Ω. This means that all trajectories in Ω cross the closed contour surfaces from the outside to the inside towards successively smaller values of $V(\underline{x})$, and eventually converge at the equilibrium point, i.e. at the origin (Figure 1.3). Projected on the $V(\underline{x})$ surface and starting on this cup close enough to the origin, the trajectory of the system will always slide down to the origin (Figure 1.4).

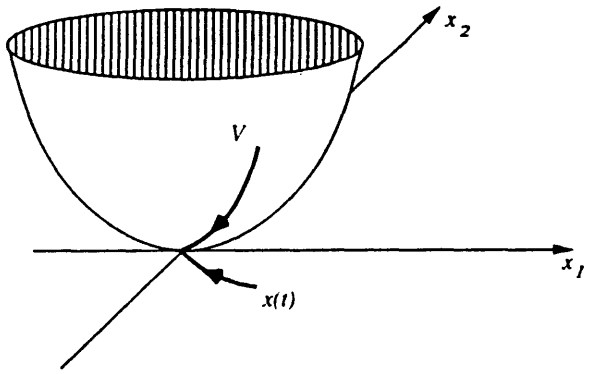

Figure 1.4 : Example of a trajectory projected on the $V(\underline{x})$ surface.

For now, we have only discussed asymptotic stability, which is the stability property we would like to show for the axisymmetric equilibrium of our compression system. In the same fashion, the notions of simple Lyapunov stability and instability can also been defined:

Lyapunov stability theorem:

> If V is positive definite at least locally around $\underline{0}$ and if $\dot{V} \leq 0$ in some region Ω around $\underline{0}$ then $\underline{x}=\underline{0}$ is **Lyapunov stable**.

Lyapunov instability theorem:

> If V is positive definite at least locally around $\underline{0}$ and if $\dot{V} > 0$ in some region Ω around $\underline{0}$ then $\underline{x}=\underline{0}$ is **unstable**.

Note that Lyapunov stability is weaker than asymptotic stability because it does not require that the trajectory necessarily returns to $\underline{0}$. It can, instead, oscillate around the origin (Figure 1.5(a)). In the case of instability, the trajectory escapes from the origin (Figure 1.5(c)).

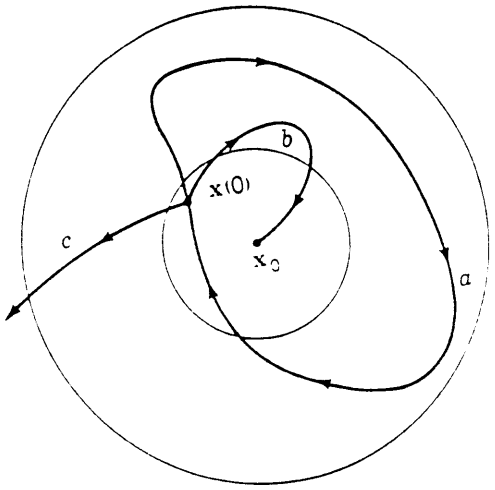

Figure 1.5 : State-space trajectories indicating (a) Lyapunov stability, (b) asymptotic stability, (c) instability.

As a final step in the presentation of the principles of a Lyapunov analysis, we need to discuss estimation of the domain of attraction of a nonlinear equilibrium using the Lyapunov function V. The domain of attraction (D.A.) of an equilibrium $\underline{x}=\underline{0}$ is defined as the largest set of points such that trajectories initiated at these points eventually converge to the origin. The size of D.A. measures how far from the origin a trajectory can start and still converge to 0 as $t\rightarrow\infty$.

One way to determine the domain of attraction would be to discretize a bigger and bigger domain around the origin and test each of its boundary points as follows: does the trajectory starting at this point eventually converge to the origin? But this procedure requires the knowledge of the trajectories (i.e. solutions) of the system. Therefore it is of interest to use the Lyapunov analysis, which does not require the solutions of the system to give an estimate of the domain of attraction.

Assume that the equilibrium $\underline{x}=\underline{0}$ is asymptotically stable in a region Ω around $\underline{0}$.
By definition, $\dot{V} < 0$ in Ω. Define D_c as the region inside the biggest contour curve $V(\underline{x}) = c$ that we can fit inside Ω. An example of such Ω and D_c are shown on Figure 1.6. Now consider a trajectory starting at $\underline{x}_0$ inside D_c. Then: $V(\underline{x}_0) \leq c$. $\underline{x}_0$ is also inside Ω and thus $\dot{V} < 0$ along this trajectory. $V(\underline{x})$ will always stay less than c and consequently the trajectory will never exit D_c and Ω. It will eventually converge to $\underline{0}$ as a result from the asymptotic stability property.

We have then shown that any trajectory starting in D_c will converge to the origin which means that D_c can be thought of as a domain of attraction of $\underline{x}=\underline{0}$. We must now give some motivation why D_c is the best estimate of D.A. we can get using the Lyapunov function V.

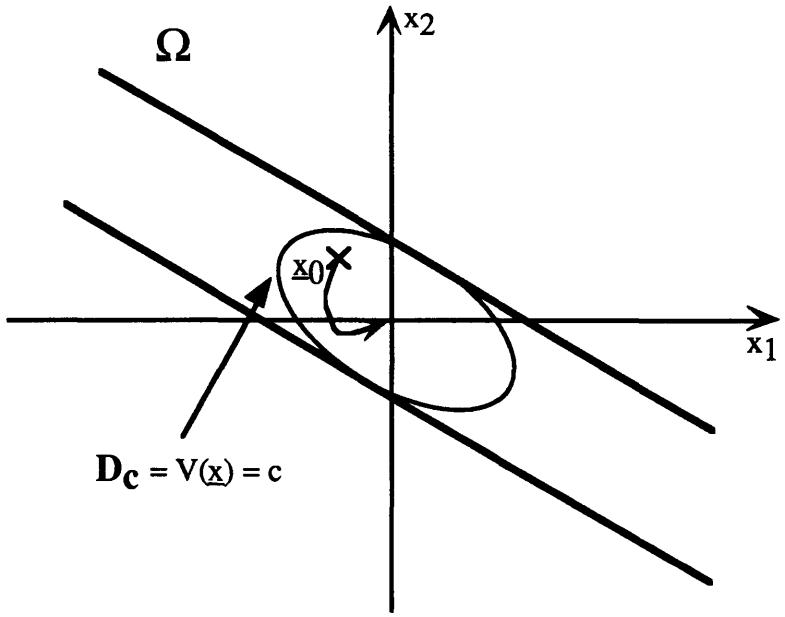

Figure 1.6: Construction of D_c given Ω

Assume that we have found a better estimate D of the domain of attraction of $\underline{x}=\underline{0}$. It is bigger than D_c and must verify the property that all trajectories starting inside D eventually converge to the origin. Let's use the example of Figure 1.7. D is shown to be a little bigger than D_c.

Consider a trajectory starting at $\underline{x}_0$ inside D (Figure 1.7). $c \le V(\underline{x}_0) \le d$. $\underline{x}_0$ lies inside Ω, so $\dot{V}(\underline{x}_0) < 0$. Consequently, $V(\underline{x})$ will decrease along this trajectory, at least at first, and we can guarantee that the trajectory will not exit the contour $V(\underline{x}) = d$. But it is not enough to guarantee that the trajectory will not exit Ω since this contour curve is not fully included in Ω (D_c was the biggest contour to be fully included in Ω). The trajectory can exit Ω while staying inside the contour curve $V(\underline{x}) = d$. When the trajectory exits Ω, $\dot{V} > 0$ and we loose the asymptotic stability property. An example of such a trajectory is shown on Figure 1.7. We have thus found a $\underline{x}_0$ such that the trajectory starting at $\underline{x}_0$ does not necessarily converge to the origin. D cannot be an estimate of the domain of attraction of $\underline{x}=\underline{0}$. Consequently, D_c is the best estimate we can get using the Lyapunov function V.

Note that a different Lyapunov function, if it could be found, might have a larger Ω and thus a larger D.A.

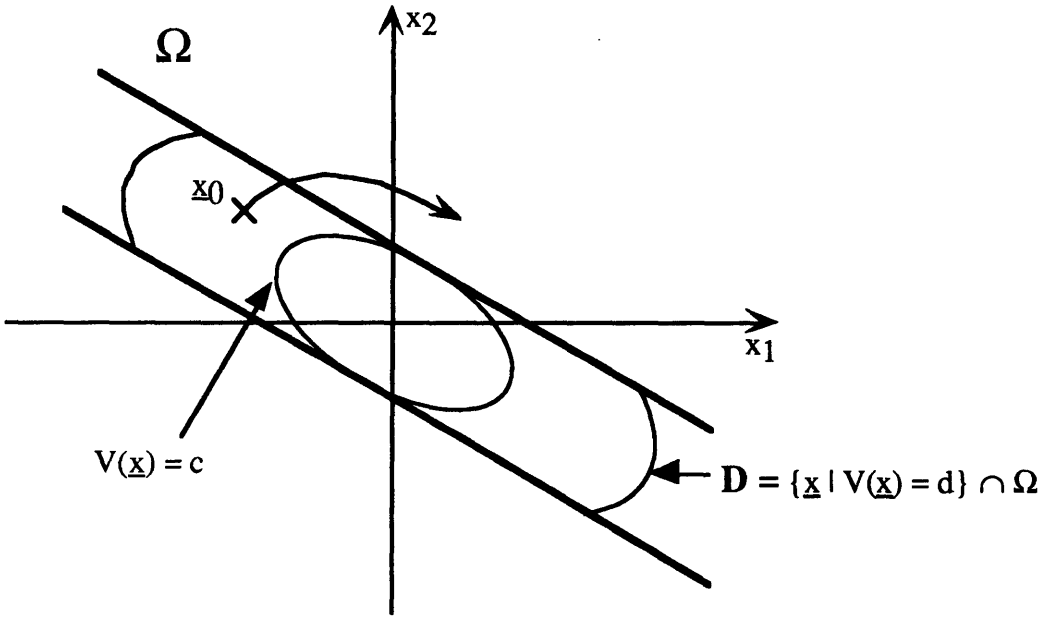

Figure 1.7: Attempt to find a better estimate for domain of attraction: D bigger than D_c

1.3 Lyapunov analysis of Surge

As a background for a future Lyapunov analysis of rotating stall, we briefly present Simon's work on the Lyapunov analysis of surge [13]. This will provide insight about the physical interpretation of a suitable Lyapunov function when we are dealing with compressor instabilities.

Surge is a one dimensional instability phenomenon.

The compression system is configured as follows:

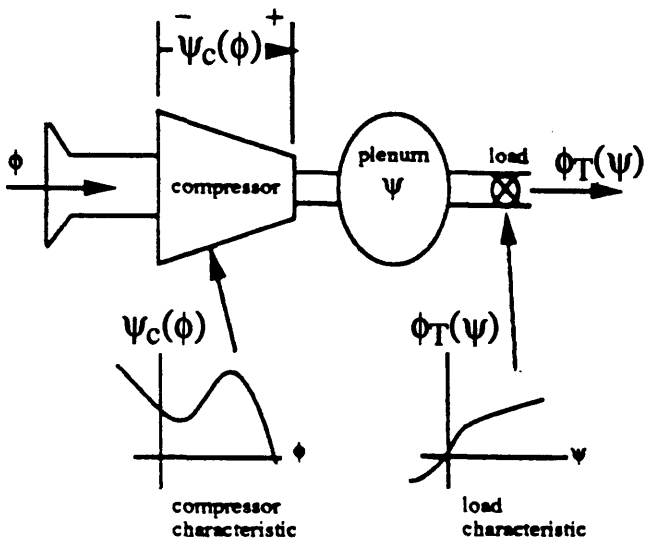

Figure 1.8: Basic compression system configuration [13]

2 state variables are necessary to characterize the system:

$\bar{\phi}$: non-dimensional flow rate through the compressor duct.

$\bar{\psi}$: non-dimensional pressure in the plenum.

The state-space formulation is then (see [13]): $\begin{cases} \dot{\bar{\phi}} = B\left[\psi_c(\bar{\phi}) - \bar{\psi}\right] \\ \dot{\bar{\psi}} = \frac{1}{B}\left[\bar{\phi} - \phi_T(\bar{\psi})\right] \end{cases}$.

If the state equations are transformed into a new local coordinate system in which the origin is located at an equilibrium operating point $(\bar{\phi}^*, \bar{\psi}^*)$ (see Figure I.2) as follows :

$$\begin{aligned} \tilde{\bar{\phi}} &= \bar{\phi} - \bar{\phi}^* \quad & \tilde{\psi}_c\left(\tilde{\bar{\phi}}\right) &= \psi_c\left(\bar{\phi}^* + \tilde{\bar{\phi}}\right) - \bar{\psi}^* \\ \tilde{\bar{\psi}} &= \bar{\psi} - \bar{\psi}^* \quad & \tilde{\phi}_T\left(\tilde{\bar{\psi}}\right) &= \phi_T\left(\bar{\psi}^* + \tilde{\bar{\psi}}\right) - \bar{\phi}^* \end{aligned}, \tag{1.2}$$

the system of equations becomes:

$$\begin{cases} \frac{d\tilde{\bar{\phi}}}{dt} = B\left[\tilde{\psi}_c\left(\tilde{\bar{\phi}}\right) - \tilde{\bar{\psi}}\right] \\ \frac{d\tilde{\bar{\psi}}}{dt} = \frac{1}{B}\left[\tilde{\bar{\phi}} - \tilde{\phi}_T\left(\tilde{\bar{\psi}}\right)\right] \end{cases} \tag{1.1}$$

The state variables in the local coordinate system are called incremental states. The values of these states are the deviations of the state from the equilibrium. They are not assumed to be infinitesimal.

Simon's choice for the Lyapunov function was: $$V\left(\tilde{\bar{\phi}},\tilde{\bar{\psi}}\right)=\frac{1}{2}\left(\frac{1}{B}\tilde{\bar{\phi}}^2+B\tilde{\bar{\psi}}^2\right). \qquad (1.3)$$

This function is called **incremental energy** and can be seen as the analog of the incremental energy of a mass-spring system where $\frac{1}{2}\frac{1}{B}\tilde{\bar{\phi}}^2$ corresponds to the **kinetic energy** term ($\tilde{\bar{\phi}}$, non-dimensional flow rate is the analog of a speed) and $\frac{1}{2}B\tilde{\bar{\psi}}^2$ corresponds to the **potential energy** term ($\tilde{\bar{\psi}}$ measures the degree of compression in the plenum, it is the analog of the compression of the spring).

V verifies all the properties required of a Lyapunov function:

V is positive definite globally around (0,0): $\begin{cases} V(0,0)=0 \\ V\left(\tilde{\bar{\phi}}\neq 0,\tilde{\bar{\psi}}\neq 0\right)>0 \end{cases}$.

Moreover, if we can find a region Ω around (0,0) where $\dot{V}<0$, Lyapunov's theorem for asymptotic stability will give that $\left(\tilde{\bar{\phi}},\tilde{\bar{\psi}}\right)=(0,0)$ or $\left(\bar{\phi},\bar{\psi}\right)=\left(\bar{\phi}^*,\bar{\psi}^*\right)$ is asymptotically stable. Therefore, the asymptotic stability of each operating point $\left(\bar{\phi}^*,\bar{\psi}^*\right)$ along the compressor characteristic will be determined by examining the sign of $\dot{V}\left(\tilde{\bar{\phi}},\tilde{\bar{\psi}}\right)$ around the origin for V as defined in (1.3):

$$\dot{V}\left(\tilde{\bar{\phi}},\tilde{\bar{\psi}}\right)=\frac{1}{B}\tilde{\bar{\phi}}\cdot\frac{d\tilde{\bar{\phi}}}{dt}+B\tilde{\bar{\psi}}\cdot\frac{d\tilde{\bar{\psi}}}{dt}$$

using (1.1): $$\dot{V}\left(\tilde{\bar{\phi}},\tilde{\bar{\psi}}\right)=\tilde{\bar{\phi}}\cdot\tilde{\psi}_c\left(\tilde{\bar{\phi}}\right)-\tilde{\bar{\psi}}\cdot\tilde{\phi}_T\left(\tilde{\bar{\psi}}\right) \qquad (1.4)$$

Both terms in $\dot{V}$ are products of incremental pressure and incremental flow rate and are thus power-like. $\dot{V}$ can then be seen as an **incremental power balance** between the incremental power production of the compressor, area (C) on Figure 1.9 counted positively, and the incremental power dissipation of the throttle, area (T) on Figure 1.9

counted negatively. This makes sense physically since the conclusion we can drawn from the sign of the power balance $\dot{V}$ is consistent with the idea that if the throttle dissipates more power than the compressor creates the system will be stable and if the compressor creates more power than the throttle is able to dissipate the system will be unstable [14].

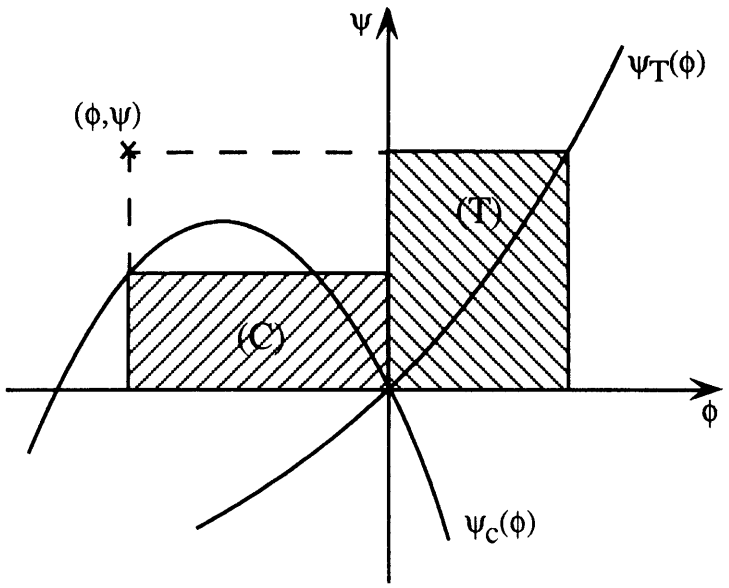

Figure 1.9: $\dot{V}$ as the balance between area (C): incremental power production of the compressor and area (T): incremental power dissipation of the throttle.

Simon showed that for all operating points $\left(\overline{\phi}^*, \overline{\psi}^*\right)$ along the characteristic, a region Ω around $\left(\tilde{\phi}, \tilde{\psi}\right) = (0,0)$ where $\dot{V} < 0$ can be created using close-coupled control. Moreover in the next chapter, a generalized form of this Lyapunov function (generated to be applied to rotating stall but also valid for surge) will be show that $\dot{V} < 0$ in some region Ω around the origin if $\left(\overline{\phi}^*, \overline{\psi}^*\right)$ is chosen on the stable (right) side of the characteristic. The size of Ω will also be addressed.

This choice of Lyapunov function $V\left(\tilde{\phi}, \tilde{\psi}\right) = \frac{1}{2}\left(\frac{1}{B}\tilde{\phi}^2 + B\tilde{\psi}^2\right)$ has proven to be suitable. It is also particularly pertinent since it stays very close to the notion of energy: V can be seen

as an incremental energy and $\dot{V}$ as an incremental power balance. Our purpose in the Lyapunov analysis of rotating stall will be to find a Lyapunov function that generalizes the one we have for surge, in order to keep the physical meaning of V and $\dot{V}$.

Chapter 2

Lyapunov based Nonlinear Stability Analysis applied to Nonlinear Model of Rotating Stall without Unsteady Losses

2.1 Nonlinear Model of Rotating Stall without Unsteady Losses

The basic state-space representation of rotating stall we are about to present is derived from the Moore-Greitzer model [9,10]. Rotating stall is a two-dimensional instability phenomenon that can occur in compression systems at low flow coefficient.

For surge analysis, the flow through the compressor was assumed to be axisymmetric and a single non-dimensional measure of flow was necessary: $\bar{\phi}$, mean flow coefficient in the inlet duct. $\bar{\phi}$, along with $\overline{\psi}$, the non-dimensional pressure in the plenum, determines the state of the system.

For rotating stall analysis, the flowfield is assumed to be non-axisymmetric. The non-axisymmetry can be taken into account by introducing a perturbation $\delta\phi(\eta,\theta,t)$ continuously distributed around the annulus. The total flow coefficient is then: $\phi(\eta,\theta,t) = \bar{\phi} + \delta\phi(\eta,\theta,t)$ where η is the non-dimensional axial position in the compressor, θ the circumferential angle around the annulus and t is time non-dimensionalized by the rotor revolution period.

One additional variable must be introduced in order to set up the system of equations. The upstream flowfield, being two-dimensional now, admits both axial and circumferential

velocity perturbations. Rather than introduce a circumferential velocity variable, we define the perturbation velocity potential $\delta\Phi$, such that:

$$\frac{\partial\delta\Phi}{\partial\eta} = \delta\phi \text{ and } \frac{\partial\delta\Phi}{\partial\theta} = \delta(\text{circ.vel.}) \qquad (2.1)$$

For the upstream flowfield we assume no incoming vorticity (clean inlet conditions) and thus the flow in this region is potential:

$$\nabla^2\delta\Phi = 0 \qquad \text{for } \eta \le 0$$

The following equations determine the dynamics of the system (see [9,10]):

$$\begin{cases} m\dfrac{\partial(\delta\Phi)}{\partial t} + l_c\dfrac{\partial\overline{\phi}}{\partial t} + \mu\dfrac{\partial(\delta\phi)}{\partial t} + \lambda\dfrac{\partial(\delta\phi)}{\partial\theta} = \psi_c\left(\overline{\phi} + \delta\phi(0,\theta,t)\right) - \overline{\psi} & (2.2a) \\ \dfrac{\partial\overline{\psi}}{\partial t} = \dfrac{1}{4l_cB^2}\left(\overline{\phi} - \phi_T(\overline{\psi})\right) & (2.2b) \end{cases}$$

At this point, the system is characterized by $\overline{\psi}$ and $\phi(\eta,\theta,t) = \overline{\phi} + \delta\phi(\eta,\theta,t)$ where $\delta\phi$ is a continuous function of θ, $\theta \in [0;2\pi]$ ($\delta\Phi$ is related to $\delta\phi$ by Equation (2.1)). We have to deal with an infinite number of states.

To come up with a finite state-space representation of Equations (2.2) in a matrix form, it is necessary to perform a spatial discretization in θ of the circumference of the annulus. We keep (2N+1) points equally spaced around the annulus to describe the perturbation $\delta\phi$. Then (2.2a) must be evaluated at 2N+1 different points, leading to a set of 2N+1 equations. This yields an overall system of 2N+2 equations. $\delta\phi$ and ϕ can be considered as vectors of length 2N+1. Their Discrete Fourier Transform is also of length 2N+1 which means that only the modes -N to +N are needed to reconstruct $\underline{\delta\phi}$ or $\underline{\phi}$. Thus, we will keep only modes -N to +N while taking the Discrete Fourier Transform (DFT) of (2.2a).

<u>Discretization in θ</u>:

$$\theta_k = \frac{2\pi k}{(2N+1)} \qquad \text{for } k \in [0,2N] \qquad (2.3)$$

$$\underline{\delta\phi} = \begin{bmatrix} \vdots \\ \delta\phi(\theta_k) \\ \vdots \end{bmatrix}_{k=2N}^{k=0} \qquad \underline{\phi} = \begin{bmatrix} \vdots \\ \overline{\phi} + \delta\phi(\theta_k) \\ \vdots \end{bmatrix}_{k=2N}^{k=0} \qquad (2.4)$$

A first step in the Fourier decomposition is to define the continuous Fourier Transform.

Fourier Transform (continuous form):

The upstream flow field being potential, a solution for the velocity potential is:

$$\delta\Phi(\eta,\theta,t) = \sum_{\substack{n=-\infty \\ n\neq 0}}^{n=+\infty} \hat{\Phi}_n(t)\cdot e^{in\theta}\cdot e^{|n|\eta} \qquad \text{for } \eta \le 0 \qquad (2.5)$$

where $\left\{\hat{\Phi}_n(t),\ n \in]-\infty;+\infty[\right\}$ are the Fourier coefficients associated to $\delta\Phi$.

Then using (2.1), we get:

$$\delta\phi(\eta,\theta,t) = \sum_{\substack{n=-\infty \\ n\neq 0}}^{n=+\infty} \hat{\phi}_n(t)\cdot e^{in\theta}\cdot e^{|n|\eta} \qquad \text{for } \eta \le 0 \qquad (2.6)$$

where $$\hat{\phi}_n(t) = \frac{1}{2\pi}\int_0^{2\pi}\delta\phi(0,\theta,t)\cdot e^{-in\theta}d\theta \qquad \text{for } \eta = 0 \qquad (2.7)$$

and $$\hat{\Phi}_n(t) = \frac{\hat{\phi}_n(t)}{|n|} \qquad (2.8)$$

The zeroth mode has been separated from the others but a simple equation will relate $\hat{\phi}_0(t)$ to $\overline{\phi}(t)$ in the discrete case.

This Fourier decomposition is valid for $\eta \le 0$ but in the first equation in (2.2), all functions are evaluated at $\eta = 0$, i.e. at the compressor face. Thus, from now on we will omit the variable η. Because of the assumptions on the upstream flow field, the partial-differential nature of the original system of equations (2.2) can be eliminated using Equation (2.8) and the dependence on the axial position η has been solved out of the system.

The next step is then to define a Matrix Discrete Fourier Transform, which we will use in our system representation.

Discrete Fourier Transform:

$$\hat{\phi}_n = \frac{1}{\sqrt{2N+1}}\sum_{k=0}^{2N}\phi(\theta_k)\cdot e^{-in\theta_k} \qquad \text{for } \eta = 0 \qquad (2.9)$$

$$\phi(\theta_k) = \frac{1}{\sqrt{2N+1}}\sum_{n=-N}^{+N}\hat{\phi}_n\cdot e^{+in\theta_k} \qquad \text{for } \eta = 0 \qquad (2.10)$$

Written in a matrix form, (2.9) and (2.10) become:

$$\underline{\hat{\phi}} = \begin{bmatrix} \vdots \\ \hat{\phi}_n \\ \vdots \end{bmatrix}_{n=+N}^{n=-N} = F \cdot \underline{\phi} \qquad \text{and} \qquad \underline{\phi} = F^{-1} \cdot \underline{\hat{\phi}} = F^{T} \cdot \underline{\hat{\phi}} \tag{2.11}$$

$$\text{where} \qquad F = \frac{1}{\sqrt{2N+1}} \begin{bmatrix} \cdots & \vdots & \cdots \\ & W_{2N+1}^{nk} & \\ & \vdots & \end{bmatrix}_{k=0 \quad k=2N}^{n=-N \quad n=+N} \qquad W_{2N+1} = e^{\frac{-2i\pi}{2N+1}} \tag{2.12}$$

The normalization factor $\frac{1}{\sqrt{2N+1}}$ has been chosen because it conveniently leads to $F^{-1} = F^{T}$ where $(\cdot)^{T}$ denotes the conjugate transposed of a matrix. Now, the zeroth mode is defined by:

$$\hat{\phi}_0(t) = \overline{\phi}(t) \cdot \sqrt{2N+1}.$$

Equation (2.8) still holds in the discrete case. The DFT is applied to $\underline{\phi}$ and not $\underline{\delta\phi}$. Then the vector $\underline{\hat{\phi}}$ of the Fourier coefficients includes also the zeroth mode and the DFT can be written in a compact form.

Discrete Fourier Transform of (2.2a):

2N+1 equations result from the D.F.T. of the group of 2N+1 equations (2.2a) for modes -N to +N. The terms involving $\underline{\delta\phi}$ (and $\underline{\delta\Phi}$) in (2.2a) contribute to the equations of all modes except 0 whereas the terms involving $\overline{\phi}$ and $\overline{\psi}$ contribute only to the equation for the zeroth mode.

$$\underline{n \neq 0} \qquad \left(\frac{m}{|n|} + \mu\right) \cdot \dot{\hat{\phi}}_n = -i\lambda n \cdot \hat{\phi}_n + \hat{\psi}_{c_n} \tag{2.13}$$

$$\underline{n=0} \qquad l_c \cdot \dot{\hat{\phi}}_0 = \hat{\psi}_{c0} - \overline{\psi} \cdot \sqrt{2N+1} \tag{2.14}$$

$$\text{Or in matrix form:} \qquad D_E \cdot \dot{\underline{\hat{\phi}}} = -D_A \cdot \underline{\hat{\phi}} + \underline{\hat{\psi}_c} - \begin{bmatrix} \underline{0} \\ \overline{\psi} \cdot \sqrt{2N+1} \\ \underline{0} \end{bmatrix} \leftarrow n = 0 \tag{2.15}$$

$$D_E = \begin{bmatrix} \ddots & & & & \\ & \frac{m}{|n|}+\mu & & (0) & \\ & & \ddots & & \\ & & & l_c & \ddots \\ & (0) & & & \frac{m}{|n|}+\mu \\ & & & & & \ddots \end{bmatrix}_{n=+N}^{n=-N} \leftarrow n = 0 \qquad (2.16)$$

$$D_A = \begin{bmatrix} \ddots & & (0) \\ & i\lambda n & \\ (0) & & \ddots \end{bmatrix}_{n=+N}^{n=-N} \qquad (2.17)$$

Using Equations (2.11), (2.15) can be written in terms of $\underline{\phi}$ as follows:

$$E \cdot \dot{\underline{\phi}} = -A \cdot \underline{\phi} + \underline{\psi_c} - \begin{bmatrix} \vdots \\ \overline{\psi} \\ \vdots \end{bmatrix} \qquad (2.18)$$

where $E = F^T \cdot D_E \cdot F$ and $A = F^T \cdot D_A \cdot F$ (2.19)

It will presently be useful to note that A has all its eigenvalues on the $j\omega$ axis. When applying A, each mode is rotated by $\pi/2$ and multiplied by $(\lambda|n|)$. This is best seen if we consider a <u>real</u> decomposition of A:

$$A = G^T \cdot D_A^G \cdot G \qquad (2.20)$$

$$D_A^G = \begin{bmatrix} 0 & & (0) \\ & \begin{bmatrix} 0 & 1\lambda \\ -1\lambda & 0 \end{bmatrix} & \\ & & \ddots \\ (0) & & \begin{bmatrix} 0 & N\lambda \\ -N\lambda & 0 \end{bmatrix} \end{bmatrix} \begin{matrix} n = 0 \\ n = 1 \\ \\ \\ n = N \end{matrix} \qquad (2.21)$$

$$G = \sqrt{\frac{2}{2N+1}} \cdot \begin{bmatrix} \cdots & \frac{1}{\sqrt{2}} & \cdots \\ \cdots & \cos\left(1 \cdot \frac{2\pi}{2N+1} \cdot k\right) & \cdots \\ \cdots & \sin\left(1 \cdot \frac{2\pi}{2N+1} \cdot k\right) & \cdots \\ & \vdots & \\ \cdots & \cos\left(N \cdot \frac{2\pi}{2N+1} \cdot k\right) & \cdots \\ \cdots & \sin\left(N \cdot \frac{2\pi}{2N+1} \cdot k\right) & \cdots \end{bmatrix} \begin{matrix} n=0 \\ \\ n=1 \\ \\ \\ \\ n=N \end{matrix} \qquad (2.22)$$

$$k=0 \qquad\qquad k=2N$$

To prove that $A\underline{\phi}$ is orthogonal to $\underline{\phi}$, we form their dot-product

$$\underline{\phi}^T \cdot A \cdot \underline{\phi} = \left(G \cdot \underline{\phi}\right)^T \cdot D_A^G \cdot \left(G \cdot \underline{\phi}\right).$$

Because of the structure of D_A^G, $\quad \underline{\phi}^T \cdot A \cdot \underline{\phi} = \sum_{n=1}^{N} \begin{bmatrix} a_n & b_n \end{bmatrix} \cdot \begin{bmatrix} 0 & n\lambda \\ -n\lambda & 0 \end{bmatrix} \cdot \begin{bmatrix} a_n \\ b_n \end{bmatrix}$

where $\quad G \cdot \underline{\phi} = \begin{bmatrix} a_0 \\ a_1 \\ b_1 \\ \vdots \\ a_N \\ b_N \end{bmatrix} \begin{matrix} n=0 \\ n=1 \\ \\ \\ n=N \end{matrix}$

for all n: $\quad \begin{bmatrix} a_n & b_n \end{bmatrix} \cdot \begin{bmatrix} 0 & n\lambda \\ -n\lambda & 0 \end{bmatrix} \cdot \begin{bmatrix} a_n \\ b_n \end{bmatrix} = a_n \cdot n\lambda \cdot b_n - b_n \cdot n\lambda \cdot a_n = 0$

Therefore for all $\underline{\phi}$, $A\underline{\phi}$ is orthogonal to $\underline{\phi}$ and $\quad \underline{\phi}^T \cdot A \cdot \underline{\phi} = 0 \qquad (2.23)$

A real decomposition of E can also be performed:

$$E = G^T \cdot D_E^G \cdot G \qquad (2.24)$$

with: $$D_E^G = \begin{bmatrix} l_c & & & (0) \\ & \begin{bmatrix} \frac{m}{1}+\mu & 0 \\ 0 & \frac{m}{1}+\mu \end{bmatrix} & & \\ & & \ddots & \\ (0) & & & \begin{bmatrix} \frac{m}{N}+\mu & 0 \\ 0 & \frac{m}{N}+\mu \end{bmatrix} \end{bmatrix} \begin{matrix} n=0 \\ n=1 \\ \\ \\ n=N \end{matrix} \qquad (2.25)$$

Summary of the state-space representation of rotating stall:

$\underline{T}$ creates a distributed (vector) representation of a zeroth mode disturbance from its scalar equivalent.

$\underline{S}^T$ is a row vector that extracts $\bar{\phi}$ from ϕ.

$$\underline{T}=\begin{bmatrix}\vdots\\1\\\vdots\end{bmatrix} \qquad \underline{S}^T=\frac{1}{M}[\cdots \quad 1 \quad \cdots] \qquad M=2N+1 \qquad (2.26)$$

Then, recalling (2.2b), a state-space representation of rotating stall can be written as:

$$\begin{aligned} E\cdot\dot{\underline{\phi}} &= -A\cdot\underline{\phi}+\underline{\psi_c}(\underline{\phi})-\underline{T}\cdot\bar{\psi} \\ \dot{\bar{\psi}} &= \frac{1}{4l_cB^2}\left(\underline{S}^T\cdot\underline{\phi}-\phi_T(\bar{\psi})\right) \end{aligned} \qquad (2.27)$$

The system is of order 2N+2 with 2N+2 equations and 2N+2 unknowns or states: $\bar{\psi}$ and the 2N+1 inputs in $\underline{\phi}$. If $\underline{\phi}$ is a uniform vector (the flow coefficient is constant around the annulus), the system can be reduced to a second order system: for $n\neq 0$ $\hat{\phi}_n=0$ and Equations (2.13) become $(\hat{\psi}_c)_n=0$ and thus can be dropped. The problem is axisymmetric. The states are $\bar{\phi}$ and $\bar{\psi}$ and we are left with the equations of surge. Therefore, the state-space representation of (2.27) is suitable for the analysis of both surge and rotating stall.

2.2 Lyapunov analysis of Rotating Stall

Using the state-space representation of rotating stall of (2.27) and knowing Simon's Lyapunov function for surge (1.3), we are trying now to find a suitable Lyapunov function for rotating stall. Although any positive definite function based on the system state is a candidate Lyapunov function, careful choice of the form will lead to a much more elegant and physically meaningful formulation of the problem. Thus, our purpose is to find for rotating stall a Lyapunov function that generalizes the one for surge in order to be able to keep and exploit the physical interpretation of V and $\dot{V}$ presented in Section 1.3.

As in Section 1.3, the first step in the Lyapunov analysis is to transform the state equations into a new local coordinate system in which the origin is located at an equilibrium point $(\bar{\phi}^*, \bar{\Psi}^*)$. The transformation equations are analogous to those in (1.2):

$$\begin{aligned} \tilde{\underline{\phi}} &= \underline{\phi} - \underline{T}\cdot\bar{\phi}^* & \tilde{\underline{\Psi}}_c\left(\tilde{\underline{\phi}}\right) &= \underline{\Psi}_c\left(\underline{T}\cdot\bar{\phi}^* + \tilde{\underline{\phi}}\right) - \underline{T}\cdot\bar{\Psi}^* \\ \tilde{\bar{\Psi}} &= \bar{\Psi} - \bar{\Psi}^* & \tilde{\phi}_T\left(\tilde{\bar{\Psi}}\right) &= \phi_T\left(\bar{\Psi}^* + \tilde{\bar{\Psi}}\right) - \bar{\phi}^* \end{aligned} \tag{2.28}$$

Again the state variables in the local coordinate system are called incremental states. They measure the deviation of the states from the equilibrium and are <u>not</u> assumed to be infinitesimal. The state-space representation becomes:

$$\boxed{\begin{aligned} E\cdot\dot{\tilde{\underline{\phi}}} &= -A\cdot\tilde{\underline{\phi}} + \tilde{\underline{\Psi}}_c\left(\tilde{\underline{\phi}}\right) - \underline{T}\cdot\tilde{\bar{\Psi}} \\ \dot{\tilde{\bar{\Psi}}} &= \frac{1}{4l_cB^2}\left(\underline{S}^T\cdot\tilde{\underline{\phi}} - \tilde{\phi}_T\left(\tilde{\bar{\Psi}}\right)\right) \end{aligned}} \tag{2.29}$$

Now consider the function

$$V\left(\tilde{\underline{\phi}}, \tilde{\bar{\Psi}}\right) = \frac{1}{2M}\tilde{\underline{\phi}}^T\cdot E\cdot\tilde{\underline{\phi}} + 2B^2l_c\,\tilde{\bar{\Psi}}^2 \tag{2.30}$$

where M=2N+1. From here on, all states and variables are evaluated about the new origin. It is straightforward to show the $V\left(\tilde{\underline{\phi}}, \tilde{\bar{\Psi}}\right)$ is positive definite globally around ($\underline{0}$,0):

Using (2.24),
$$V\left(\tilde{\underline{\phi}}, \tilde{\bar{\Psi}}\right) = \frac{1}{2M}\tilde{\underline{\phi}}^T\cdot\left(G^T\cdot D_E^G\cdot G\right)\cdot\tilde{\underline{\phi}} + 2B^2l_c\,\tilde{\bar{\Psi}}^2$$

$$V\left(\tilde{\underline{\phi}}, \tilde{\bar{\Psi}}\right) = \frac{1}{2M}\left(G\tilde{\underline{\phi}}\right)^T\cdot D_E^G\cdot\left(G\tilde{\underline{\phi}}\right) + 2B^2l_c\,\tilde{\bar{\Psi}}^2$$

Let $\tilde{\underline{x}} = \begin{bmatrix} G\tilde{\underline{\phi}} \\ \tilde{\bar{\Psi}} \end{bmatrix}$, then
$$V(\tilde{\underline{x}}) = \frac{1}{2}\tilde{\underline{x}}^T\cdot\underbrace{\begin{bmatrix} \frac{1}{M}D_E^G & 0 \\ 0 & 4B^2l_c \end{bmatrix}}_{D}\cdot\tilde{\underline{x}}$$

D_E^G is a diagonal matrix with strictly positive elements on the diagonal (see (2.25)). It is positive definite, thus D is also positive definite. Consequently, $V(\tilde{\underline{x}}) > 0$ for all $\tilde{\underline{x}} \neq \underline{0}$. V is positive definite globally around the origin. It will be a suitable Lyapunov function if we can find a region Ω around the origin in which $\dot{V} < 0$ for a given operating point $(\bar{\phi}^*, \bar{\Psi}^*)$.

Derivation of $\dot{V}$:

$$\dot{V}\left(\underline{\tilde{\phi}},\tilde{\bar{\psi}}\right)=\frac{1}{M}\underline{\tilde{\phi}}^{T}\cdot E\cdot\dot{\underline{\tilde{\phi}}}+4B^{2}l_{c}\,\tilde{\bar{\psi}}\cdot\dot{\tilde{\bar{\psi}}}$$

Using (2.27) $$\dot{V}\left(\underline{\tilde{\phi}},\tilde{\bar{\psi}}\right)=-\frac{1}{M}\underline{\tilde{\phi}}^{T}\cdot A\cdot\underline{\tilde{\phi}}+\frac{1}{M}\underline{\tilde{\phi}}^{T}\cdot\underline{\tilde{\psi}}_{c}\left(\underline{\tilde{\phi}}\right)-\frac{1}{M}\underline{\tilde{\phi}}^{T}\cdot\underline{T}\cdot\tilde{\bar{\psi}}+\tilde{\bar{\psi}}\cdot\tilde{\bar{\phi}}-\tilde{\bar{\psi}}\cdot\tilde{\phi}_{T}\left(\tilde{\bar{\psi}}\right)$$

This expression can be simplified. According to (2.23), the first term is 0. Then, using the fact that $\underline{S}^{T}=\frac{1}{M}\underline{T}^{T}$ we get: $\frac{1}{M}\underline{\tilde{\phi}}^{T}\cdot\underline{T}\cdot\tilde{\bar{\psi}}=\tilde{\bar{\psi}}\cdot\frac{1}{M}\underline{T}^{T}\cdot\underline{\tilde{\phi}}=\tilde{\bar{\psi}}\cdot\left(\underline{S}^{T}\cdot\underline{\tilde{\phi}}\right)=\tilde{\bar{\psi}}\cdot\tilde{\bar{\phi}}$ and the second and fourth terms cancel each other.

The resulting relationship is:

$$\boxed{\dot{V}\left(\underline{\tilde{\phi}},\tilde{\bar{\psi}}\right)=\frac{1}{M}\underline{\tilde{\phi}}^{T}\cdot\underline{\tilde{\psi}}_{c}\left(\underline{\tilde{\phi}}\right)-\tilde{\bar{\psi}}\cdot\tilde{\phi}_{T}\left(\tilde{\bar{\psi}}\right)} \qquad (2.31)$$

Note that if $\underline{\tilde{\phi}}$ is uniform, (2.31) becomes (1.4). The present expression for $\dot{V}$ is the generalization of the one for surge to the case where $\underline{\tilde{\phi}}$ varies around the annulus. Therefore, the physical interpretations of $\dot{V}$ and V are still valid. $\dot{V}$ represents again an incremental power balance between the incremental power production of the compressor which is now averaged around the annulus and the incremental power dissipation of the throttle. Taken to the 2D continuum limit (i.e. M→∞), (2.31) becomes:

$$\dot{V}=\frac{1}{2\pi}\int_{0}^{2\pi}\tilde{\phi}(\theta)\cdot\tilde{\psi}_{c}\left(\tilde{\phi}(\theta)\right)d\theta-\tilde{\bar{\psi}}\cdot\tilde{\phi}_{T}\left(\tilde{\bar{\psi}}\right) \qquad (2.32)$$

This measure of compression system stability was originally proposed by Gysling [15].

V can be seen as the incremental energy of a mass-spring system where the kinetic energy term is: $\frac{1}{2M}\underline{\tilde{\phi}}^{T}\cdot E\cdot\underline{\tilde{\phi}}$ and the potential energy term: $2B^{2}l_{c}\,\tilde{\bar{\psi}}^{2}$.

As defined by (2.30), V seems well-adapted to the analysis of rotating stall. It accounts for all perturbations that might exist in the compressor but also makes sense physically.

As (2.31) shows, $\dot{V}$ is the sum of two functions, where the first one depends only on $\underline{\tilde{\phi}}$ and the second one depends only on $\tilde{\bar{\psi}}$. The dependence of $\dot{V}$ on $\underline{\tilde{\phi}}$ and $\tilde{\bar{\psi}}$ can be studied separately, using the following definitions:

$$\dot{V}\left(\underline{\tilde{\phi}},\tilde{\bar{\psi}}\right)=\frac{1}{M}\sum_{k=0}^{2N} f\left(\tilde{\phi}_k\right)+g\left(\tilde{\bar{\psi}}\right) \qquad (2.33)$$

with $f\left(\tilde{\phi}_k\right)=\tilde{\phi}_k\cdot\tilde{\psi}_c\left(\tilde{\phi}_k\right)$ for each location k around the annulus

and $g\left(\tilde{\bar{\psi}}\right)=\tilde{\bar{\psi}}\cdot\tilde{\phi}_T\left(\tilde{\bar{\psi}}\right)$

1) Study of: $\left.\dot{V}\right|_{\underline{\tilde{\phi}}=\underline{0}}\left(\tilde{\bar{\psi}}\right)=g\left(\tilde{\bar{\psi}}\right)=\left(-\tilde{\bar{\psi}}\right)\cdot\tilde{\phi}_T\left(\tilde{\bar{\psi}}\right)$

The shape of $g\left(\tilde{\bar{\psi}}\right)$ can be easily deduced from a sketch of $\tilde{\phi}_T\left(\tilde{\bar{\psi}}\right)$ as shown on Figure 2.1. For low pressure ratios, $\psi_T(\phi)$ is usually taken to be a quadratic function of ϕ:

$$\psi_T(\phi)=\tfrac{1}{2}K_t\phi^2$$

Consequently, $\tilde{\psi}_T\left(\tilde{\phi}\right)$ and also its inverse $\tilde{\phi}_T\left(\tilde{\bar{\psi}}\right)$ are always in the first and third quadrants. Note that $g\left(\tilde{\bar{\psi}}\right)$ is always negative, as it is the product of two functions of opposite signs. Thus, $g\left(\tilde{\bar{\psi}}\right)=0$ only for $\tilde{\bar{\psi}}=0$. Note also that the function has zero slope at $\tilde{\bar{\psi}}=0$.

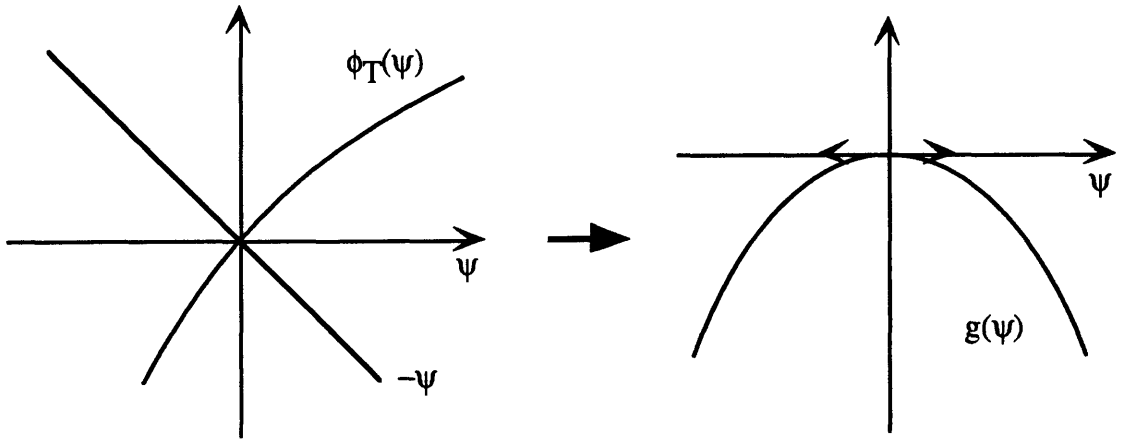

Figure 2.1: Shape of $g(\phi)$

Now, since $\dot{V}$ is a function of separated variables $\underline{\tilde{\phi}}$ and $\tilde{\bar{\psi}}$, and since $g(\tilde{\bar{\psi}})$ is maximum at $\tilde{\bar{\psi}} = 0$ and strictly stabilizing elsewhere, studying $\dot{V}$ along the axis $\tilde{\bar{\psi}} = 0$ as a function of $\underline{\tilde{\phi}}$ will give the worst case for the sign of $\dot{V}$, i.e. the most positive $\dot{V}$. This idea is confirmed by examining Figures 2.2 and 2.3.

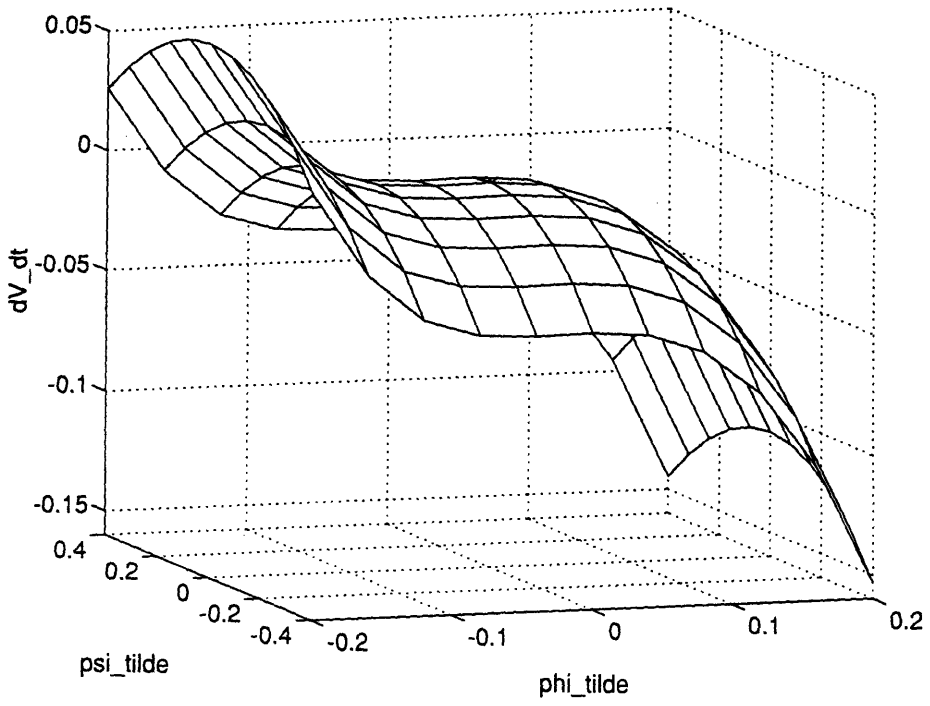

The example of $\dot{V}$ function shown on Figure 2.2 illustrates the separation of variables $\underline{\tilde{\phi}}$ and $\tilde{\bar{\psi}}$. For clarity of the plot, N=0. The perturbation is evaluated at only one point around the annulus and $\underline{\tilde{\phi}}$ becomes $\tilde{\phi}$. Along each axis $\tilde{\bar{\psi}} = \text{constant}$ we find the shape of $f(\tilde{\phi}_k)$ and along each axis $\tilde{\phi} = \text{constant}$ the shape of $g(\tilde{\bar{\psi}})$. The operating point (0,0) is marked with a cross. Note that the highest curve $\dot{V}\Big|_{\tilde{\bar{\psi}} = \text{constant}}(\underline{\tilde{\phi}})$ is obtained for $\tilde{\bar{\psi}} = 0$, as expected.

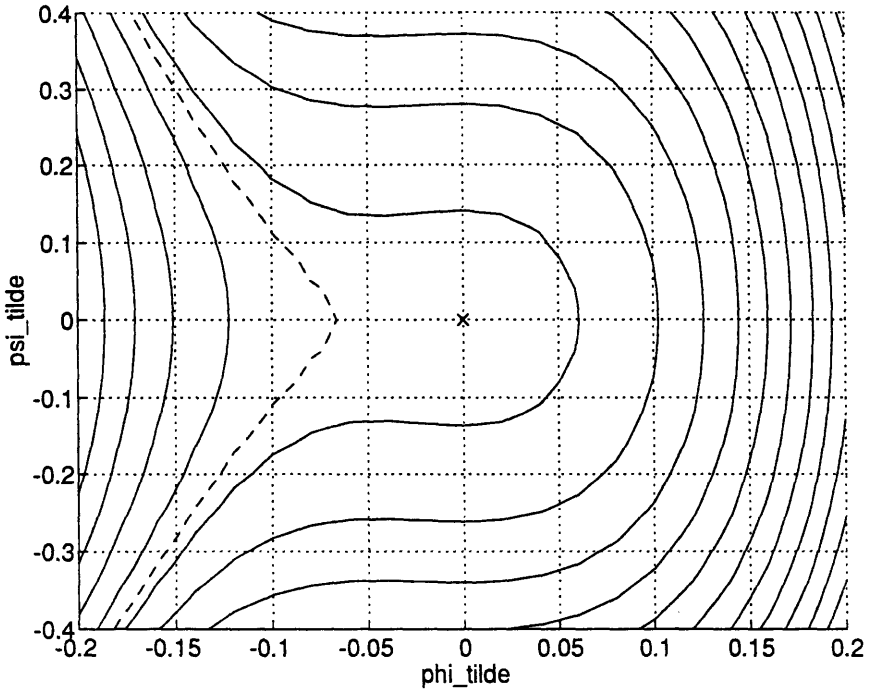

Figure 2.3: Contour curves of $\dot{V}(\underline{\tilde{\phi}}, \tilde{\psi})$ for N=0, $\dot{V} = 0$: '--'

Figure 2.3 shows several contour curves $\dot{V} = \text{constant}$ of the same function as in Figure 2.2. The contour curve we are most specifically interested in is $\dot{V} = 0$, which is the dotted line on Figure 2.3. On its left $\dot{V} > 0$ and on its right $\dot{V} < 0$. The distance between this curve and the equilibrium point is minimum for $\tilde{\psi} = 0$ which again means that restricting the study of $\dot{V}$ to the axis $\tilde{\psi} = 0$ will give the worst case for the sign of $\dot{V}$.

In conclusion, the stability of the system can be addressed by the study of the sign of $\dot{V}\Big|_{\tilde{\psi}=0}(\underline{\tilde{\phi}})$.

2) Study of: $\dot{V}\Big|_{\tilde{\Psi}=0}\left(\underline{\tilde{\phi}}\right)=\frac{1}{M}\sum_{k=0}^{2N} f\left(\tilde{\phi}_k\right)_{\underline{\ }}$ $\quad f\left(\tilde{\phi}\right)=\tilde{\phi}\cdot\tilde{\psi}_c\left(\tilde{\phi}\right)$

The shape of $f\left(\tilde{\phi}\right)$ can also be easily deduced, this time using the shape of $\tilde{\psi}_c\left(\tilde{\phi}\right)$, i.e. from the compressor characteristic. Figure 2.4 is an example characteristic shape and is quite general near the peak of the characteristic. If the operating point $\left(\overline{\phi}^*,\overline{\psi}^*\right)$ is taken on the stable (right) side of the characteristic, $\tilde{\psi}_c\left(\tilde{\phi}\right)=0$ for $\tilde{\phi}=0$ and $\tilde{\phi}=-d<0$. Then, $f\left(\tilde{\phi}\right)=0$ also for $\tilde{\phi}=0$ and $\tilde{\phi}=-d<0$. The "f" function will invariably have a local maximum that goes through the origin, be negative for values of $\tilde{\phi}$ greater than 0 and become positive for values of $\tilde{\phi}$ below -d.

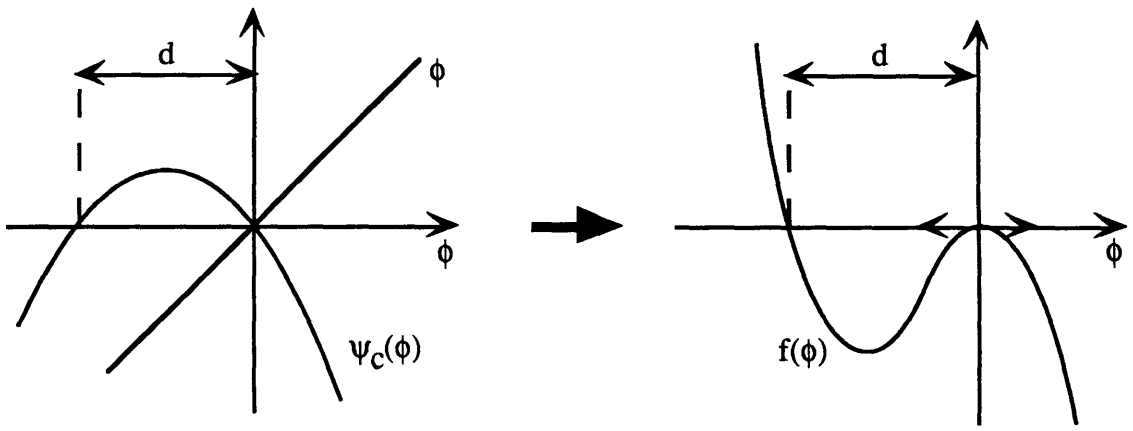

Figure 2.4: Shape of f(ϕ)

Understanding the shape of the "f" function for a given characteristic is fundamental since $\dot{V}\Big|_{\tilde{\Psi}=0}\left(\underline{\tilde{\phi}}\right)$ is calculated by mapping the velocity perturbation onto f, as shown by the bold line on Figure 2.5, and taking the average of $f\left(\tilde{\phi}\right)$ around the annulus. This is true whether the perturbation is discrete ($\underline{\tilde{\phi}}$) as in Equation (2.31) or continuous ($\tilde{\phi}(\theta)$) as in Equation (2.32) and Figure 2.5.

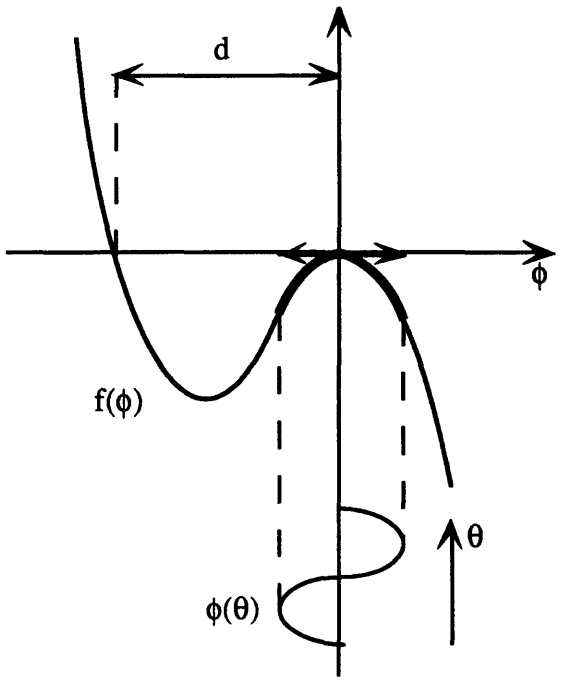

Figure 2.5: Mapping velocity perturbations onto f

As seen on Figure 2.5, the perturbation $\tilde{\phi}(\theta)$ is mapped about the equilibrium point, i.e. about 0 in the local coordinate system. Based on the shape of f for stable equilibria, if the minimum of the perturbation is strictly greater than -d, it will be entirely mapped on the region where $f\left(\tilde{\phi}\right) \le 0$. Consequently, $\dot{V}\Big|_{\tilde{\Psi}=0}\left(\underline{\tilde{\phi}}\right)$ will also be negative as well as $\dot{V}\left(\underline{\tilde{\phi}},\tilde{\Psi}\right)$ for all $\tilde{\Psi}$ since $g\left(\tilde{\Psi}\right) \le 0$ for all $\tilde{\Psi}$. Stated mathematically we have:

1) <u>for a continuous perturbation</u>:

$$\min_{0\le\theta\le 2\pi}\left[\tilde{\phi}(\theta)\right] > -d \quad \Rightarrow \quad \dot{V} \le 0 \tag{2.34}$$

where the equality holds only when $\tilde{\phi}(\theta) = 0 \ \ \forall\theta$

2) <u>for a discrete perturbation</u>:

$$\min_{0\le k\le 2N}\left[\tilde{\phi}_k\right] > -d \ \Rightarrow \ \dot{V} \le 0 \quad \text{or} \quad \underline{x} \in \Omega \ \Rightarrow \ \dot{V} \le 0 \tag{2.35}$$

where the equality holds only when $\underline{x} = \begin{bmatrix} 0 \\ \tilde{\Psi} \end{bmatrix}$. $\underline{x} = \begin{bmatrix} \tilde{\phi} \\ \tilde{\Psi} \end{bmatrix}$ is the state of the system and $\Omega =]-d;+\infty[^{2N+1} \times \mathbf{R}$. (2.36)

It is critical to note at this point that the shape of $\tilde{\phi}(\theta)$ has not been restricted in any way except its minimum.

(2.36) defines a region Ω around the origin in which $\dot{V} < 0$. This is the well-known condition for local asymptotic stability of the equilibrium point [12]. In the case of a discrete perturbation where $\tilde{\phi}(\theta)$ is evaluated at only 2 points around the annulus: θ_1 and θ_2, Ω is easily visualized as the quarter of plane in Figure 2.6 where the shaded lines show the directions where the boundary of Ω is at ∞. The component of Ω along the $\tilde{\psi}$ axis is not shown on this plot for clarity, and since it includes the whole $\tilde{\psi}$ axis. This very simple representation of Ω does not correspond to any reality for the system since $\underline{\tilde{\phi}}$ is always a vector of odd dimension 2N+1 (N is the number of modes we keep to describe the system) but it is useful to illustrate Equation (2.36) and will be useful in the next section to show how the domain of attraction is constructed.

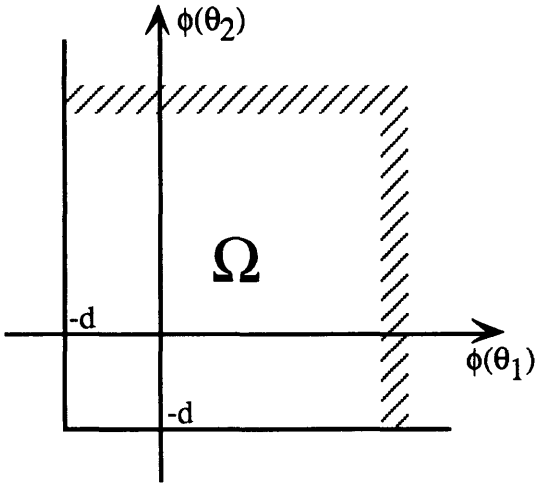

Figure 2.6: Visualization of Ω in a simple 2D case

In conclusion, we have found a Lyapunov function that is suitable for the stability analysis of rotating stall. It is a 2D generalization of Simon's Lyapunov function for surge [13]. Moreover, the flow coefficient d gives a measure of the size of Ω as the operating point proceeds from the stable (right) side of the characteristic towards the peak.

2.3 Domain of Attraction

Linear stability analysis of rotating stall [3,7,8] have already proven that operating points on the right side of the compressor characteristic $\psi_c(\phi)$ are linearly stable and that those on the left side are linearly unstable. The neutral stability point is located at the peak of the characteristic. In Section 1.1 we mentioned that the system can access rotating stall from a linearly stable operating point if perturbations are large enough, i.e. if they exceed the size of its domain of attraction at this point. Therefore, it is necessary to know how stable a linearly stable operating point is from a nonlinear perspective and this can be measured by the size of the domain of attraction.

Our purpose is then to use the Lyapunov analysis of rotating stall of Section 2.2 to estimate the domain of attraction (D.A.) and its size for any given linearly stable operating point. We will present plots of the size of D.A. as the operating point moves along the compressor characteristic. Intuitively, the size of D.A. will be finite (and non zero) for any operating point on the linearly stable (right) part of the compressor characteristic and is going to decrease as the operating point moves to the left towards the unstable part of the characteristic until it reaches 0 exactly at the neutral stability point, i.e. the peak of the characteristic.

Recalling the notations and definitions of Section 1.2, an estimate of the domain of attraction is given by the biggest contour curve $D_C = \{\underline{x} \mid V(\underline{x}) = c\}$ that we can fit inside Ω where V is defined by Equation (2.30) and Ω by Equation (2.36). D_C is an hyper-ellipsoid of dimension 2N+2. The constant c measures the size of the D.A. We want to fit D_C inside Ω as tightly as possible. Again, there is no need to look at the $\tilde{\bar{\psi}}$ axis in this problem since Ω is infinite along this direction (there D_C will always fit inside Ω) and we can restrict D_C and Ω to the $\underline{\tilde{\phi}}$ directions. Then, as shown on Figure 2.7, fitting D_C inside Ω can be quickly done by using C_C instead of D_C where C_C is the hypersphere of center the origin and radius the major axis of D_C.

A diagonalized form of E and thus V is already given in Equation (2.16). The major axis of D_c called m_c is then:

$$m_c = \sqrt{\frac{2Mc}{\min\left(l_c, \frac{m}{N} + \mu\right)}}$$

From Figure 2.7, the biggest C_c we can fit inside Ω is such that $m_c = d$ which means that:

$$c = \frac{d^2}{2M} \cdot \min\left(l_c, \frac{m}{N} + \mu\right) \qquad (2.37)$$

The min function in Equation (2.37) indicates that the size of D.A. may be limited by either surge (l_c) or rotating stall ($\frac{m}{N} + \mu$) considerations.

If N is large (and we want it to be large to include a lot of modes and represent accurately the dynamics of the system), c will be small compared to d. Moreover, c has no units, whereas d is known to be a flow coefficient. Thus, even though the rigorous definition of the size of the domain of attraction is c, we will use d from now on, keeping in mind that d and c are related by Equation (2.37).

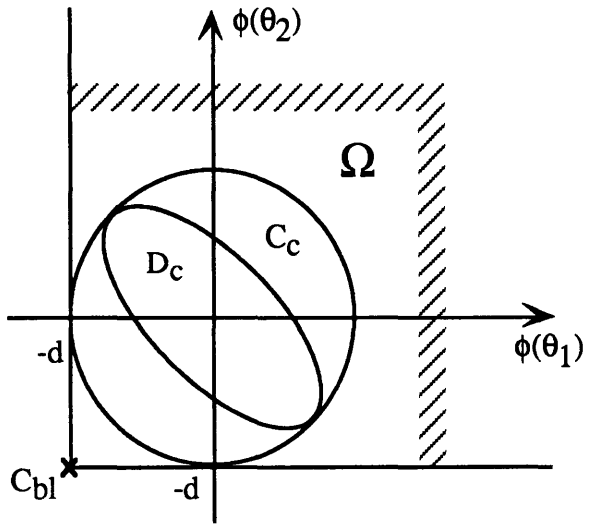

Figure 2.7: Construction of $D_c = \{\underline{x} \mid V(\underline{x}) = c\}$

Is it possible to improve the present definition of the size of D.A.? One might wonder why the eigenvectors of E were not used to try to fit D_c more tightly inside Ω without using C_c. This would have increased c, but the size of D.A. will always be related to d in a way

similar to (2.37). One might also wonder if it is possible to find Ω such that (2.35) becomes: $\underline{x} \in \Omega \Leftrightarrow \dot{V} \leq 0$.

In other words, Ω as defined by (2.36) is only subset of the region where $\dot{V} < 0$. Can it be extended to the whole region of negative $\dot{V}$?

Going back to the last section and to the mapping of a discrete velocity perturbation $\underline{\tilde{\phi}}$ onto the f function of Figure 2.5, if part of $\underline{\tilde{\phi}}$ is mapped on the region where f is positive ($\tilde{\phi} < -d$) but only for a small fraction of the annulus, the result $\dot{V}\Big|_{\underline{\tilde{\Psi}} = 0}\left(\underline{\tilde{\phi}}\right)$ can still be negative. Ω could then be extended towards smaller flow coefficients but to what extent ? This question can only be answered by specifying both the shape of the f function, i.e. of the characteristic $\tilde{\psi}_c$, and the shape of the perturbation $\tilde{\phi}$ and then calculating $\dot{V}\Big|_{\underline{\tilde{\Psi}} = 0}\left(\underline{\tilde{\phi}}\right) = \frac{1}{M}\sum_{k=0}^{2N} f\left(\tilde{\phi}_k\right)$. The dimension of $\underline{\tilde{\phi}}$ is 2N+1 where N is typically at least 5. Thus, exploring all possible shapes for $\underline{\tilde{\phi}}$ is not straightforward. The number of perturbations to be tested before reaching the boundary of $\dot{V}$ cannot be reduced by using the principle of superposition because f is nonlinear. This number stays very large and extending Ω to the whole region of negative $\dot{V}$ would require a lot of computation and has not been done in this thesis. However, the "bottom-left" corner C_{bl} defined by $\underline{\tilde{\phi}} = \begin{bmatrix} \vdots \\ -d \\ \vdots \end{bmatrix}$ is a tight boundary of Ω (C_{bl} is marked by a cross on Figure 2.7). If any of its entries -d is replaced by -d-ε (ε>0), $\dot{V}\Big|_{\underline{\tilde{\Psi}} = 0}\left(\underline{\tilde{\phi}}\right)$ becomes strictly positive. So even if Ω can be deformed towards smaller flow coefficients, this corner is fixed. Thus, it may be possible to fit a bigger ellipsoid D_C inside Ω but d will still be a valid measure of the size of Ω and of the domain of attraction. Chapter 3 will also show a good agreement between d, size of the domain of attraction resulting from the Lyapunov analysis of Section 2.2, and another flow coefficient d, size of the domain of attraction resulting from application of the Absolute

Stability Theory. This will validate the use of Ω as defined in (2.36) as a good approximation of the entire region $\dot{V} < 0$.

In conclusion, it is relevant to use the distance d along the $\tilde{\phi}$ axis from the origin to the next zero of the function $\tilde{\psi}_c(\tilde{\phi})$ as a measure of the size of the domain of attraction of a linearly stable operating point.

2.4 Applications of Lyapunov Analysis of Rotating Stall: Stall Inception Behavior and Nonlinear Compressor Characteristic

In the preceding section we defined a parameter d which indicates the size of the domain of attraction around a given stable operating point near stall. This measure provides a quantitative way to compare the stability of various compressors, and allows experimental stall inception behavior to be linked to the compressor characteristic nonlinear shape. The reference used in this section is [16].

To illustrate this, consider the following scenario which is a common test procedure (see Figure I.2). A compressor is put into operation at a stable operating point. The throttle is then closed quasi-steadily, moving the operating point towards stall. During this process, the slope of the characteristic $d\psi_c/d\phi$ at the operating point will monotonically approach zero.

According to the linearized theory (see, for instance, [3]) the damping ratio of rotating stall perturbation waves is directly proportional to $d\psi_c/d\phi$, and thus during our hypothetical experiment, the system will begin to resonate. Random excitations which exist in the compressor environment will excite the rotating stall modes, and waves will begin to appear in the compressor. The size of these waves depends on both the excitation level and

on the damping ratio of the rotating stall modes, that is on $d\psi_c/d\phi$. Unsteadiness in the compressor also tends to increase as the peak of the compressor characteristic is approached, so one might expect the excitation level to also rise during such an experiment. When a disturbance wave becomes large enough that it is outside the domain of attraction for the current operating point, the compressor will go unstable.

Based on this discussion, a compressor is more likely to stall if d is small for a given value of $d\psi_c/d\phi$. Thus, plotting d as a function of $d\psi_c/d\phi$ allows the stall flow coefficient to be assessed as shown graphically in Figure 2.8. It also indicates the damping ratio at which one can expect the system to go into rotating stall, which directly influences the size of the "pre-stall" waves which exist prior to stall inception.

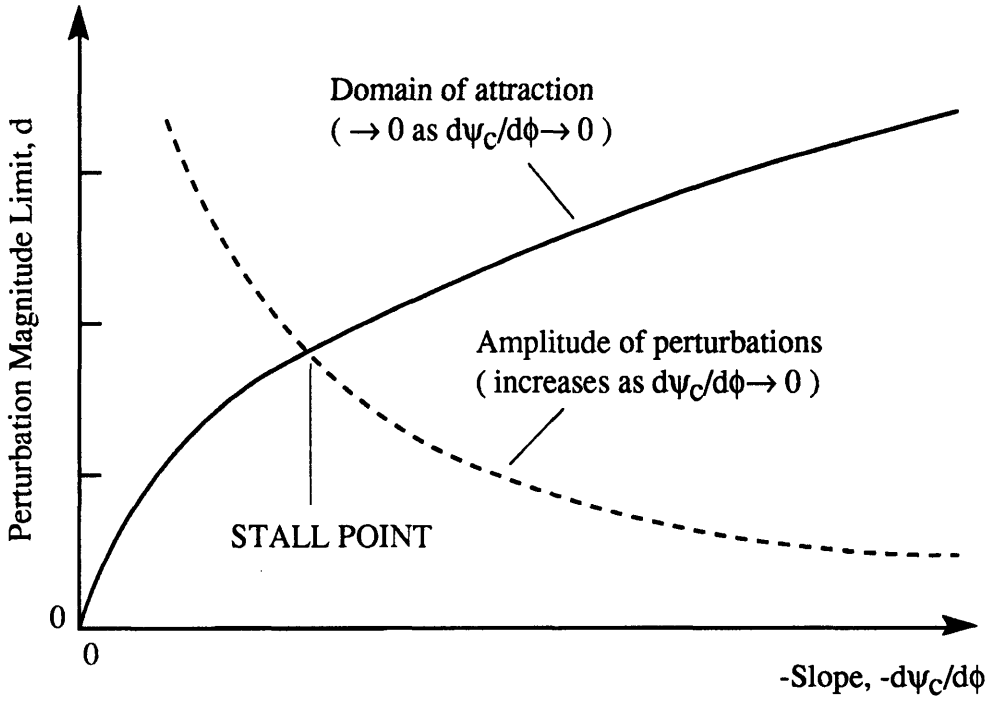

Figure 2.8: Importance of both the size of the domain of attraction and the compressor slope in determining the stall point

Figure 2.10 shows d vs. $d\psi_c/d\phi$ for three example compressors whose characteristics are presented analytically in Table 2.1 and graphically in Figure 2.9.

Table 2.1 - Compressor Characteristics

C1:

$$\psi_C(\phi) = \begin{cases} 1.9753\cdot\phi^2 - 0.098765\cdot\phi + 0.051235 \ ; & \phi \le 0.025 \\ -12.776\cdot\phi^3 + 6.3946\cdot\phi^2 - 0.29577\cdot\phi + 0.053597 \ ; & 0.025 < \phi \le 0.30 \\ -5.5363\cdot\phi^4 + 7.7202\cdot\phi^3 - 4.2045\cdot\phi^2 + 1.1276\cdot\phi + 0.071953 \ ; & \phi > 0.30 \end{cases}$$

C2:

$$\psi_C(\phi) = \begin{cases} 12.117\cdot\phi^2 - 2.4235\cdot\phi + 0.22117 \ ; & \phi \le 0.1 \\ -49.624\cdot\phi^3 + 39.509\cdot\phi^2 - 6.4130\cdot\phi + 0.39584 \ ; & 0.1 < \phi \le 0.40 \\ -10.0695\cdot\phi^2 + 9.4301\cdot\phi - 1.1848 \ ; & \phi > 0.40 \end{cases}$$

C3:

$$\psi_C(\phi) = \begin{cases} 4\cdot\phi^2 - 2\cdot\phi + 0.5 \ ; & \phi \le 0.25 \\ -143.14\cdot\phi^3 + 143.04\cdot\phi^2 - 44.683\cdot\phi + 4.7172 \ ; & 0.25 < \phi \le 0.405 \\ -13.365\cdot\phi^2 + 11.574\cdot\phi - 1.9206 \ ; & 0.405 < \phi \le 0.4638 \\ -5.4283\cdot\phi^2 + 4.2112\cdot\phi - 0.21325 \ ; & \phi > 0.4638 \end{cases}$$

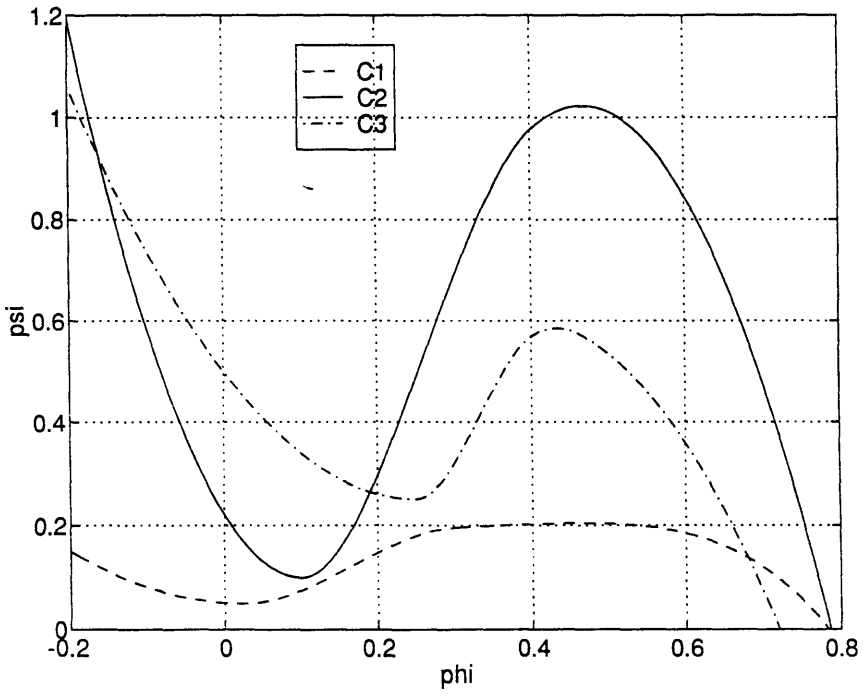

Figure 2.9: Compressor characteristics $\psi_c(\phi)$

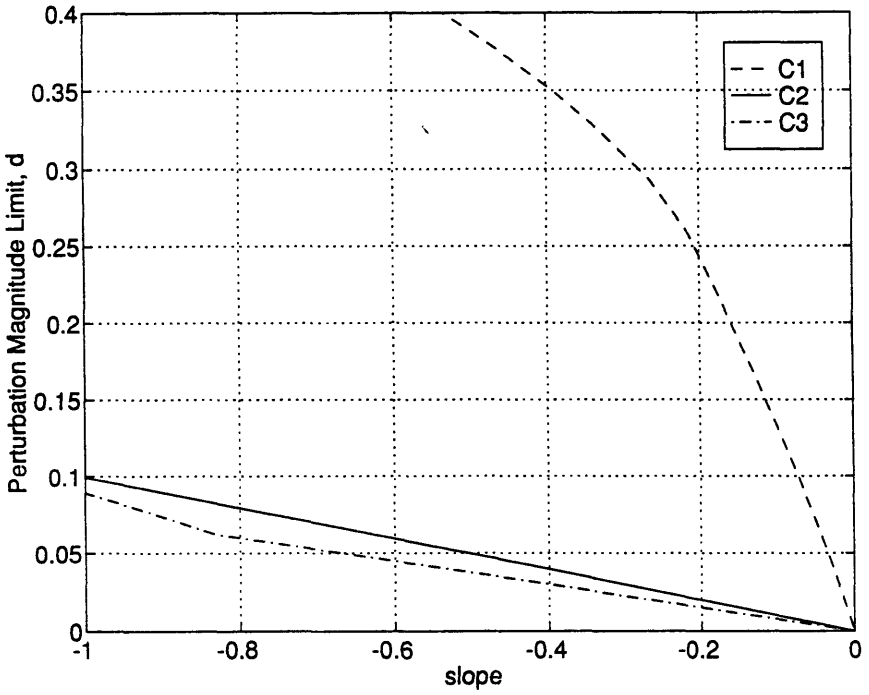

Figure 2.10: Domain of attraction variation with level of linear stability as measured by the compressor characteristic slope.

Figure 2.10 clearly shows that in compressor C1 we expect strong resonance to occur prior to stall inception, because only under such highly resonant conditions will the domain of attraction be violated. On the other hand, compressors C2 and C3 tend to go unstable more easily, and thus require only mild resonance for stall inception. This is consistent with both the experimentally observed and simulated behaviors presented in [16]. In conclusion, the shape of the compressor characteristic determines, to a large extent, the character of stall inception.

Clearly, compressors which go unstable well before they are linearly unstable are more difficult to control, especially if one limits oneself to linear controllers. Detection of pre-stall waves, an important area of current research, is also more difficult in such compressors. Thus it is of interest to understand the conditions under which the domain of attraction of a compressor will be small when measured against $d\psi_c/d\phi$. Figures 2.11 and 2.12 show two parametric studies which provide some insight into the trends.

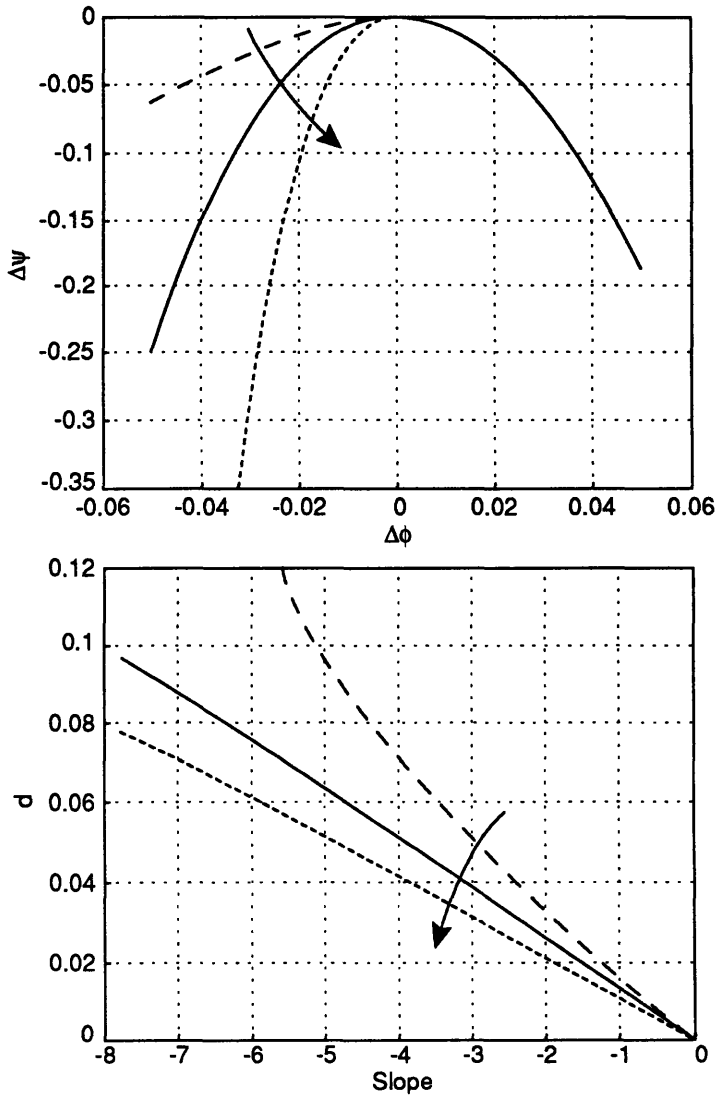

Figures 2.11: Effect of the unstable part of the compressor characteristic on the domain of attraction

Figures 2.11 shows 3 compressors whose stable (which also implies measurable) characteristics are identical, but which have different unstable characteristics. A plot of d vs. $d\psi_c/d\phi$ for these compressors reveals that, for a given stable characteristic, the steeper the unstable characteristic, the more difficult one can expect both detection and control of rotating stall to be.

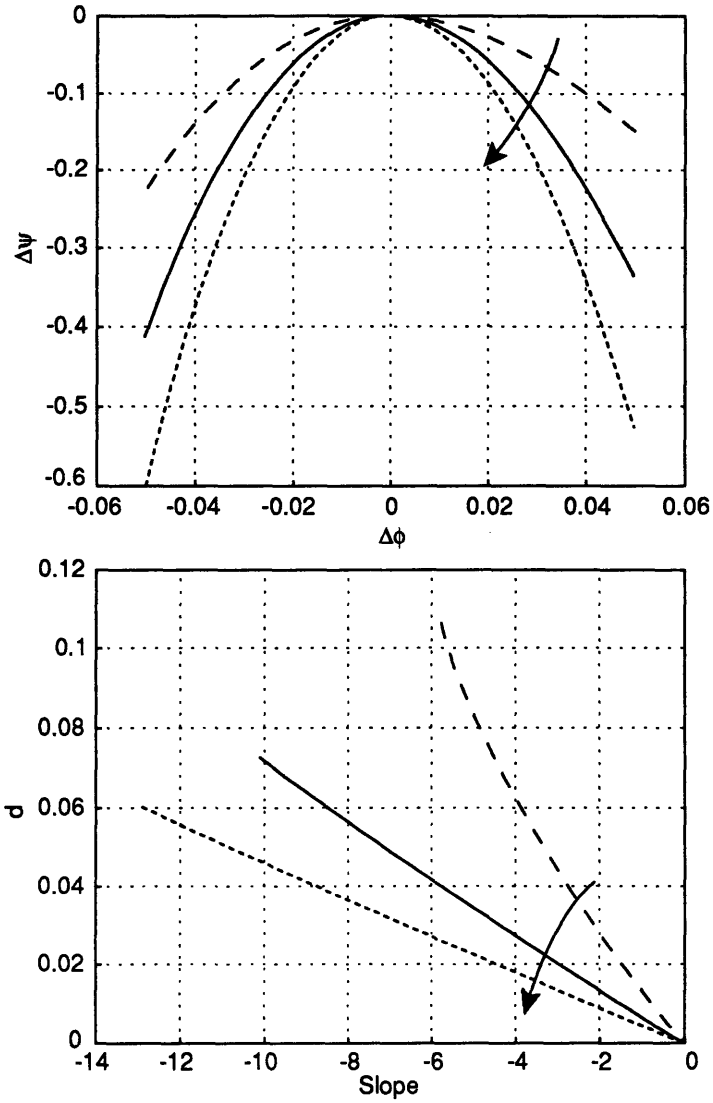

Figures 2.12: Effect of the narrowness of the peak of the compressor characteristic on the domain of attraction

Figures 2.12 shows the effect of the "narrowness" of the characteristic peak on domains of attraction. Here we see that wide peaks are more benign from a detection and control perspective than narrow peaks. Unfortunately the latter may be more prevalent in high-speed compressor applications, where rotating stall control is of highest interest.

This delineation of compressor behavior provides an explanation for two experimentally observed phenomena, both of which are inexplicable using linearized arguments: 1) some compressors exhibit large traveling waves prior to stall, while others stall while traveling waves are still relatively small, 2) the experimentally determined damping ratios of pre-stall waves do not generally go to zero before stall inception occurs.

2.5 1D Lyapunov analysis and nonlinear control of rotating stall

The purpose of this section is to interpret the results of [5] using a 1D Lyapunov analysis. In this paper, the authors explain how they 'stabilized' a compressor which is operating right at the peak of the compressor characteristic. The idea was to use a simple nonlinear control to increase the size of the domain of attraction of the operating points close to the peak on the stable (right) side of the characteristic and thus improve the operability near the peak and reduce the necessary stall margin. They used a 1D axisymmetric actuation with limited 2D sensing and low bandwidth requirements. The nonlinear control modifies the throttle characteristic through the following relationship $K_t = K_{t_0} + k \cdot A^2$ where A is the amplitude of the first mode, $\left|\hat{\phi}_1\right|$. Note that this control law cannot extend the stable flow range of the compressor, since it does not change the eigenvalues of the system. However, it will allow to safe operation of the compressor right at the peak of the characteristic, which is highly desirable because the pressure rise is then maximum.

To understand the operation of this control law, consider the following scenario:
Starting at an operating point right at the peak of the characteristic and without any control, the system stalls. If we assume that the B parameter is very small, the operating point leaves the peak and moves along the throttle characteristic as shown on Figure 2.13. The perturbation $\delta\tilde{\phi}(\theta)$ is then a growing perturbation wave. If we assume also that the motion of the operating point is quasi-steady, at each point along the throttle characteristic the

perturbation wave is characterized by the fact that when mapped onto the compressor characteristic $\tilde{\psi}_c(\tilde{\phi})$ about the mean flow coefficient (0 in the local coordinate system), it gives back the initial pressure rise (again 0 in the local coordinate system). The operating point stops moving when the system reaches its fully developed stall.

Now consider the effect of the above nonlinear control, as visualized in Figure 2.13:

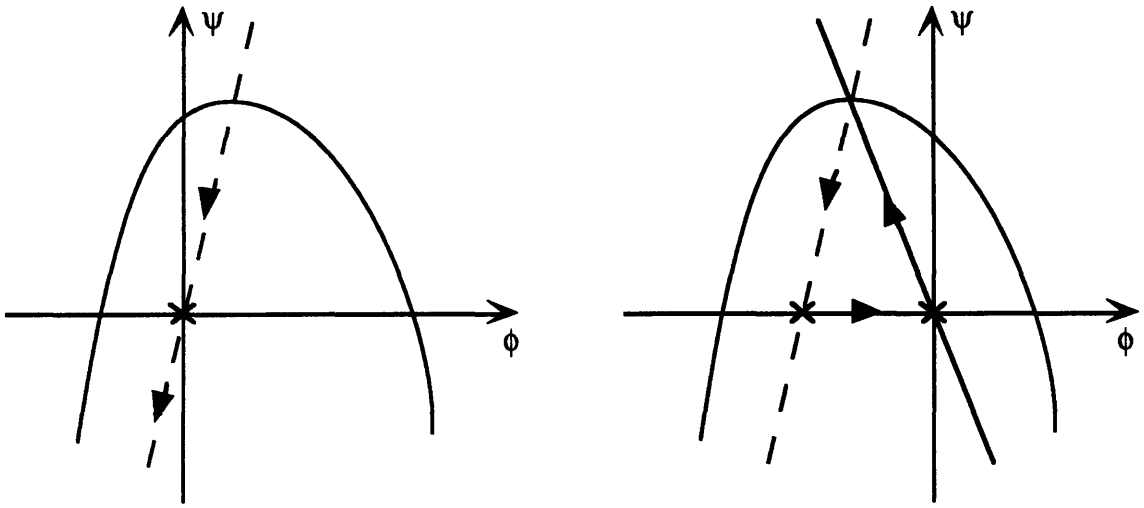

Unstable system Stabilized system

Figure 2.13: Effect of the nonlinear control on the operability at the peak

As soon as the system begins to stall and the amplitude of the perturbation wave is finite (non zero), the controller opens the throttle quasi instantaneously. This results in a sudden increase of the flow coefficient $\tilde{\phi}$ while the pressure rise $\tilde{\bar{\psi}}$ stays identical. The operating point is moved to the right and the real throttle characteristic (dotted line on Figure 2.13) is replaced by an apparent throttle characteristic (solid line on Figure 2.13). The perturbation $\delta\tilde{\phi}(\theta)$ stays the same. When it is mapped onto $\tilde{\psi}_c(\tilde{\phi})$ about the new operating point, we get a larger pressure rise. $\tilde{\bar{\psi}}$ increases and the operating point tends to go back to the peak and thus is stable. Concommitantly, the amplitude of the perturbation wave also decreases. If the control is rapid enough to react to any small increase in the amplitude of the

perturbation wave, the operating point will stay close to the peak. The arrows on Figure 2.13 show to the path taken by the operating point.

The last paragraph constitutes a simple explanation of the stabilization of rotating stall at the peak of the characteristic using the proposed nonlinear control. We now derive the same conclusion from a 1D Lyapunov analysis. This is particularly pertinent since the trajectory taken by the operating point is known to be initially the real throttle line and then the apparent throttle line.

From Definition 3.8 of [11], if $V(\underline{x})$ is at least locally positive definite about the origin (equilibrium point), has continuous partial derivatives and if its time derivative $\dot{V}(\underline{x})$ evaluated along any state trajectory is strictly negative, then V is a Lyapunov function and the origin is asymptotically stable.

We will start with the same V function as in Equation (2.30) but here the approach of the Lyapunov analysis is different than in Section 2.2. In that section, the operating point was fixed at the origin and the sign of $\dot{V}$ was studied about the origin as a function of the unknown perturbation $\underline{\delta\tilde{\phi}}$. Here, the mean flow is moving from the origin (which corresponds to the peak) along the throttle characteristic and the perturbation is assumed to be a known function of the location of the mean flow $(\overline{\phi},\overline{\psi})$. $V(\underline{x})$ and $\dot{V}(\underline{x})$ are then evaluated along trajectories corresponding to both the real and the apparent closed-loop throttle lines, as functions of the position of the mean flow. We check first that $V(\underline{x})$ is positive definite about the origin. The sign of $\dot{V}(\underline{x})$ will then allow us to conclude the stability of the system, i.e. whether V is a proper Lyapunov function.

Some assumptions are made for simplicity of this 1D Lyapunov analysis:

1) the compressor characteristic is a third order polynomial:
$\tilde{\psi}_c(\tilde{\phi}) = \alpha\,\tilde{\phi}^3 + \beta\,\tilde{\phi}^2$ in the local coordinate system about the peak.

Here we will use $\alpha = 300$ and $\beta = -75$.

2) the throttle characteristic in the local coordinate system is:

$\tilde{\psi}_T(\tilde{\phi}) = \frac{K_t}{2}\,\tilde{\phi}^2 + Q\,\tilde{\phi}$. where Q is the slope of the throttle characteristic at the peak.

Here we will use Kt = 6 and Q = 8.

3) the perturbation wave is assumed here to take the simple form

$\delta\tilde{\phi}(\theta) = A\sin(\theta)$. This is relevant if the perturbation is small and if the compressor stalls by instability of the first mode.

If $\left(\tilde{\bar{\phi}}_0, \tilde{\bar{\psi}}_0\right)$ denotes the position along the throttle characteristic, the "state" of the system is then:

$$\begin{vmatrix} \tilde{\phi}(\theta) = \tilde{\bar{\phi}}_0 + A\sin(\theta)\ ,\ \theta \in [0;2\pi] \\ \tilde{\bar{\psi}}_0 \end{vmatrix} \qquad (2.38)$$

The perturbation wave is defined by: $\frac{1}{2\pi}\int_0^{2\pi} \tilde{\psi}_c\left(\tilde{\phi}(\theta)\right) d\theta = \tilde{\bar{\psi}}_0 = \frac{K_t}{2}\,\tilde{\bar{\phi}}_0^{\,2} + Q\,\tilde{\bar{\phi}}_0 \qquad (2.39)$

since, as we have said, the perturbation wave will be approximately quasi-steady.

Using (2.38), the definition of the compressor characteristic and:

$$\begin{aligned} &\tfrac{1}{2\pi}\int_0^{2\pi}\sin\theta\, d\theta = 0 \qquad \tfrac{1}{2\pi}\int_0^{2\pi}(\sin\theta)^3\, d\theta = 0 \\ &\tfrac{1}{2\pi}\int_0^{2\pi}(\sin\theta)^2\, d\theta = \tfrac{1}{2} \qquad \tfrac{1}{2\pi}\int_0^{2\pi}(\sin\theta)^4\, d\theta = \tfrac{3}{8} \end{aligned} \qquad (2.40)$$

Equation (2.39) introduces a relationship between A and $\tilde{\bar{\phi}}_0$ as follows:

$$\left(\tfrac{3}{2}\alpha\,\tilde{\bar{\phi}}_0 + \tfrac{\beta}{2}\right)A^2 + \left(\alpha\,\tilde{\bar{\phi}}_0^{\,3} + \left(\beta - \frac{K_t}{2}\right)\tilde{\bar{\phi}}_0^{\,2} - Q\,\tilde{\bar{\phi}}_0\right) = 0 \qquad (2.41)$$

Equation (2.41) determines A^2 and therefore the size of the perturbation wave as a function of $\tilde{\bar{\phi}}_0$. Knowing A^2 is enough since the sign of the limit cycle is indifferent.

<u>Calculation of $V\left(\tilde{\bar{\phi}}_0, \tilde{\bar{\psi}}_0\right)$ and $\dot{V}\left(\tilde{\bar{\phi}}_0, \tilde{\bar{\psi}}_0\right)$ as $\left(\tilde{\bar{\phi}}_0, \tilde{\bar{\psi}}_0\right)$ moves along a trajectory</u>:

From Definition (2.30) and Equation (2.19),

$$V\left(\underline{\tilde{\phi}}, \tilde{\bar{\psi}}\right) = \frac{1}{2M}\left(F\underline{\tilde{\phi}}\right)^T \cdot D_E \cdot \left(F\underline{\tilde{\phi}}\right) + 2B^2 l_c\,\tilde{\bar{\psi}}^2 \qquad (2.42)$$

Here, the perturbation $\delta\tilde{\phi}(\theta)$ is continuous. So we should use a continuous form of Equation (2.42). But because of the simple form of $\delta\tilde{\phi}(\theta)$ (first mode only), the expression for $V\left(\bar{\tilde{\phi}}_0, \bar{\tilde{\psi}}_0\right)$ turns out to be very simple since:

$$D_E = \begin{bmatrix} \ddots & & & \\ \frac{m}{|n|}+\mu & (0) & & \\ & \ddots & & \\ & & l_c & \\ & & & \ddots \\ (0) & & \frac{m}{|n|}+\mu & \\ & & & \ddots \end{bmatrix} \begin{matrix} n \to -\infty \\ \\ n = 0 \\ \\ n \to +\infty \end{matrix}$$

$$\begin{matrix} n \to -\infty & & n \to +\infty \end{matrix}$$

and, for our case $F\left(\tilde{\phi}\right) = \begin{bmatrix} (0) \\ \frac{1}{2}iA \\ \bar{\tilde{\phi}}_0 \\ -\frac{1}{2}iA \\ (0) \end{bmatrix} \begin{matrix} n \to -\infty \\ n = -1 \\ n = 0 \\ n = 1 \\ n \to +\infty \end{matrix}$

We get:
$$V\left(\bar{\tilde{\phi}}_0, \bar{\tilde{\psi}}_0\right) = \tfrac{1}{4}(m+\mu)\,A^2 + \tfrac{1}{2}l_c\bar{\tilde{\phi}}_0^{\,2} + 2B^2 l_c \bar{\tilde{\psi}}_0^{\,2} \qquad (2.43)$$

where A^2 is related to $\bar{\tilde{\phi}}_0$ by Equation (2.41).

For all $\left(\bar{\tilde{\phi}}_0, \bar{\tilde{\psi}}_0\right) \neq (0,0)$ along the trajectory, $V\left(\bar{\tilde{\phi}}_0, \bar{\tilde{\psi}}_0\right) > 0$. Thus, V is globally positive definite in this 1D space. We now have to study the sign of $\dot{V}\left(\bar{\tilde{\phi}}_0, \bar{\tilde{\psi}}_0\right)$ along the real and apparent throttle lines.

$\dot{V}\left(\bar{\tilde{\phi}}_0, \bar{\tilde{\psi}}_0\right)$ is given by Equation (2.32) for a continuous perturbation:

$$\dot{V}\left(\bar{\tilde{\phi}}_0, \bar{\tilde{\psi}}_0\right) = \frac{1}{2\pi}\int_0^{2\pi} \tilde{\phi}(\theta)\cdot\tilde{\psi}_c\left(\tilde{\phi}(\theta)\right)d\theta - \bar{\tilde{\psi}}_0 \cdot \tilde{\phi}_T\left(\bar{\tilde{\psi}}_0\right) \qquad (2.44)$$

Using (2.38), (2.40) and the definition of the compressor characteristic, this expression can be simplified to:

$$\dot{V}\left(\bar{\tilde{\phi}}_0, \bar{\tilde{\psi}}_0\right) = \alpha\bar{\tilde{\phi}}_0^{\,4} + \beta\bar{\tilde{\phi}}_0^{\,3} + \tfrac{1}{2}A^2\left(\tfrac{3}{4}\alpha A^2 + 6\alpha\bar{\tilde{\phi}}_0^{\,2} + 3\beta\bar{\tilde{\phi}}_0\right) - \bar{\tilde{\phi}}_0\bar{\tilde{\psi}}_0 \qquad (2.45)$$

Figures 2.14 show the system in the configuration of the real throttle and the corresponding function $\dot{V}\left(\tilde{\bar{\phi}}_0, \tilde{\bar{\psi}}_0\right)$ along the trajectory. As expected, $\dot{V}\left(\tilde{\bar{\phi}}_0, \tilde{\bar{\psi}}_0\right)$ is always positive and the peak is an unstable operating point in the absence of any control. Now, suppose that, as a consequence of the nonlinear control $K_t = K_{t_0} + k \cdot A^2$, the real throttle line is moved to an apparent throttle line whose characteristic is taken to be $\tilde{\psi}_T\left(\tilde{\phi}\right) = Q\,\tilde{\phi}$. 2 configurations are studied: Q = -60 and Q = -20. The results are shown in Figures 2.15 and 2.16 respectively. These configurations differ by the position of the apparent throttle characteristic with respect to the mid-line of the compressor characteristic (dotted line on the plots). Our conjecture was that the system would be stabilized if the throttle line was moved to the right of the mid-line because then the mapping of the perturbation $\delta\tilde{\phi}(\theta)$ onto the f function is favorable to a negative $\dot{V}$ as shown on Figure 2.17.

Because $\left(\tilde{\bar{\phi}}_0, \tilde{\bar{\psi}}_0\right)$ is a quasi-steady operating point, the expression for $\dot{V}\left(\tilde{\bar{\phi}}_0, \tilde{\bar{\psi}}_0\right)$ in Equation (2.44) can be simplified if written in the local set of axis about $\left(\tilde{\bar{\phi}}_0, \tilde{\bar{\psi}}_0\right)$:

Using:
$$\tilde{\tilde{\phi}}(\theta) = \delta\tilde{\phi}(\theta) = \tilde{\phi}(\theta) - \tilde{\bar{\phi}}_0 \qquad \tilde{\tilde{\psi}}_c\left(\delta\tilde{\phi}(\theta)\right) = \tilde{\psi}_c\left(\tilde{\bar{\phi}}_0 + \delta\tilde{\phi}(\theta)\right) - \tilde{\bar{\psi}}_0$$
$$\tilde{\tilde{\psi}} = \tilde{\psi} - \tilde{\bar{\psi}}_0 \qquad \tilde{\tilde{\phi}}_T\left(\tilde{\tilde{\psi}}\right) = \tilde{\phi}_T\left(\tilde{\bar{\psi}}_0 + \tilde{\tilde{\psi}}\right) - \tilde{\bar{\phi}}_0$$

we get:

$$\dot{V}\left(\tilde{\bar{\phi}}_0, \tilde{\bar{\psi}}_0\right) = \frac{1}{2\pi}\int_0^{2\pi}\left(\tilde{\bar{\phi}}_0 + \delta\tilde{\phi}(\theta)\right)\cdot\left(\tilde{\bar{\psi}}_0 + \tilde{\tilde{\psi}}_c\left(\delta\tilde{\phi}(\theta)\right)\right)d\theta - \tilde{\bar{\psi}}_0 \cdot \tilde{\bar{\phi}}_0$$

$$\dot{V}\left(\tilde{\bar{\phi}}_0, \tilde{\bar{\psi}}_0\right) = \tilde{\bar{\phi}}_0 \cdot \frac{1}{2\pi}\int_0^{2\pi}\tilde{\tilde{\psi}}_c\left(\delta\tilde{\phi}(\theta)\right)d\theta + \frac{1}{2\pi}\int_0^{2\pi}\delta\tilde{\phi}(\theta)\,d\theta\cdot\tilde{\bar{\psi}}_0 + \frac{1}{2\pi}\int_0^{2\pi}\delta\tilde{\phi}(\theta)\cdot\tilde{\tilde{\psi}}_c\left(\delta\tilde{\phi}(\theta)\right)d\theta$$

But by definition of the perturbation wave, $\frac{1}{2\pi}\int_0^{2\pi}\tilde{\tilde{\psi}}_c\left(\delta\tilde{\phi}(\theta)\right)d\theta = 0$ in the local coordinate system. Also, the assumed form of the perturbation gives: $\frac{1}{2\pi}\int_0^{2\pi}\delta\tilde{\phi}(\theta)\,d\theta = 0$.

Therefore, for all operating points $\left(\tilde{\bar{\phi}}_0, \tilde{\bar{\psi}}_0\right)$ along the throttle characteristic,

$$\dot{V}\left(\tilde{\bar{\phi}}_0, \tilde{\bar{\psi}}_0\right) = \frac{1}{2\pi}\int_0^{2\pi}\delta\tilde{\phi}(\theta)\cdot\tilde{\tilde{\psi}}_c\left(\delta\tilde{\phi}(\theta)\right)d\theta,$$

which implies that the perturbation $\delta\tilde{\phi}(\theta)$ is mapped onto an "f" function (as in Section 2.2), where f is now constructed in the local coordinate system about $\left(\tilde{\tilde{\phi}}_0, \tilde{\tilde{\psi}}_0\right)$.

It is clear in Figure 2.17 that when the throttle line crosses the $\tilde{\tilde{\psi}} = 0$ axis on the left of the mid-line of the compressor characteristic, the f function exhibits a strong positive bump between $\tilde{\tilde{\phi}} = 0$ and $\tilde{\tilde{\phi}} = +c$. It is bigger in magnitude and width than the negative bump between $\tilde{\tilde{\phi}} = -d$ and $\tilde{\tilde{\phi}} = 0$ as shown on Figure 2.17(a). Consequently when the symmetric perturbation $\delta\tilde{\phi}(\theta) = A\sin(\theta)$ is mapped onto f, $\frac{1}{2\pi}\int_0^{2\pi} \delta\tilde{\phi}(\theta)\cdot\tilde{\tilde{\psi}}_c\left(\delta\tilde{\phi}(\theta)\right) d\theta$ and thus $\dot{V}\left(\tilde{\tilde{\phi}}_0, \tilde{\tilde{\psi}}_0\right)$ is positive. In the opposite case, when the throttle line crosses the $\tilde{\tilde{\psi}} = 0$ axis on the right of the mid-line, the contribution of the negative bump is dominant and $\dot{V}\left(\tilde{\tilde{\phi}}_0, \tilde{\tilde{\psi}}_0\right)$ is negative, see Figure 2.17(b). Therefore, we expect the system to be stabilized when the throttle line is moved to the right of the compressor characteristic mid-line.

Figures 2.15 show that moving the throttle characteristic to a straight line of slope Q = -60 is not enough to stabilize the system at the peak. $\dot{V}\left(\tilde{\tilde{\phi}}_0, \tilde{\tilde{\psi}}_0\right)$ is still positive along the trajectory. If the slope is Q = -20 as on Figures 2.16, the throttle line is on the right of the mid-line of the compressor characteristic. Then, $\dot{V}\left(\tilde{\tilde{\phi}}_0, \tilde{\tilde{\psi}}_0\right)$ is negative close to the peak and becomes positive again if the deviation from the peak is too big. The region over which $\dot{V}$ is negative constitutes the domain of attraction of the operating point. The size of the domain of attraction of the peak is now finite whereas it used to be zero without any control.

Note that the stabilization of the system does not occur exactly when the apparent throttle line is the mid-line of the compressor characteristic because we use here a very simple

model for the limit cycle: $A\sin(\theta)$ with only a first order content. Also note that the effect of B is not modeled by this analysis.

The 1D Lyapunov analysis proves again that the system operating at the peak can be stabilized by moving the throttle line to the right.

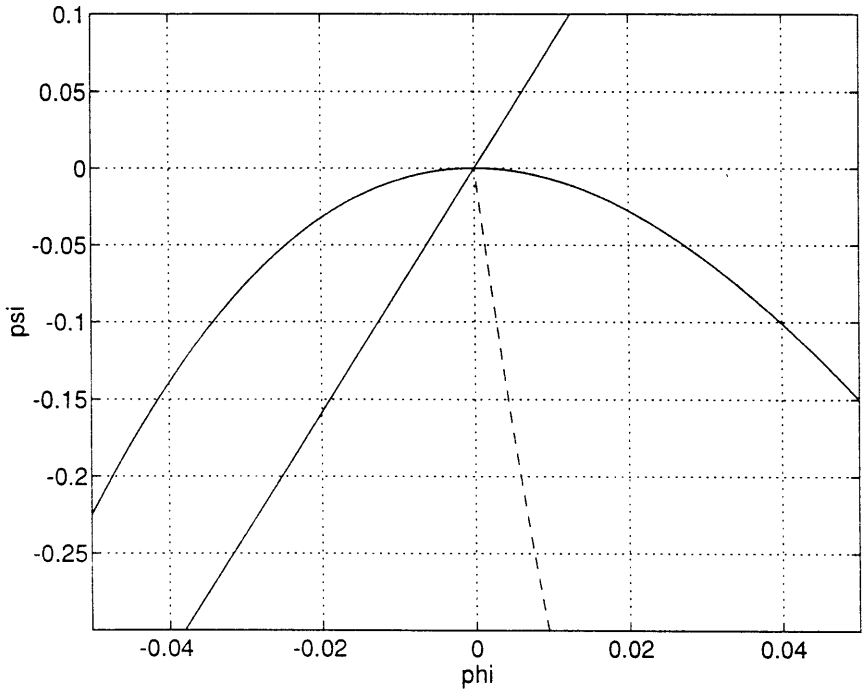

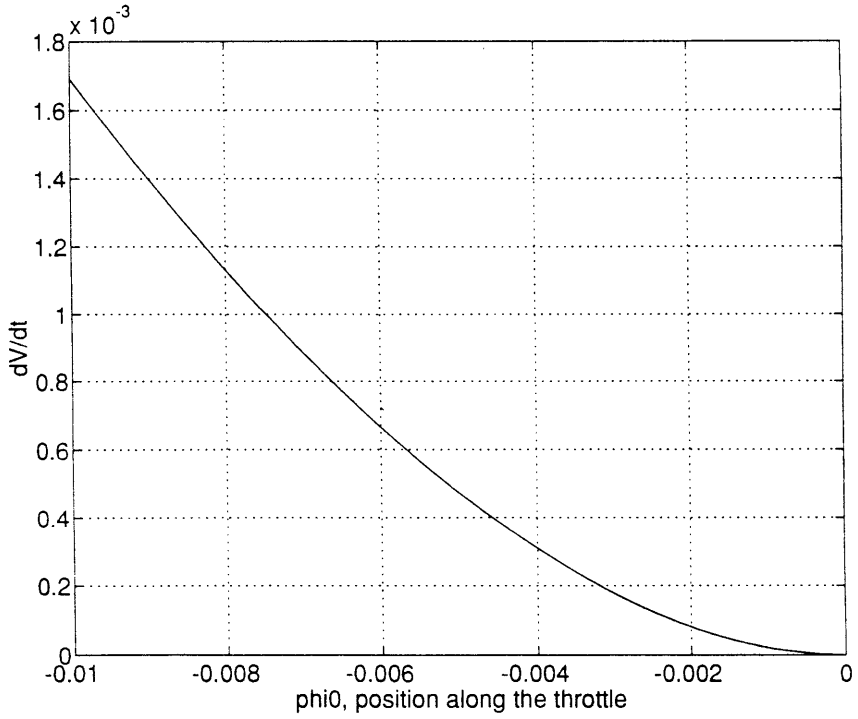

Figures 2.14: Configuration of the real throttle

$$\tilde{\psi}_T\left(\tilde{\phi}\right) = \frac{K_t}{2}\,\tilde{\phi}^2 + Q\,\tilde{\phi},\ K_t = 6,\ Q = 8.$$

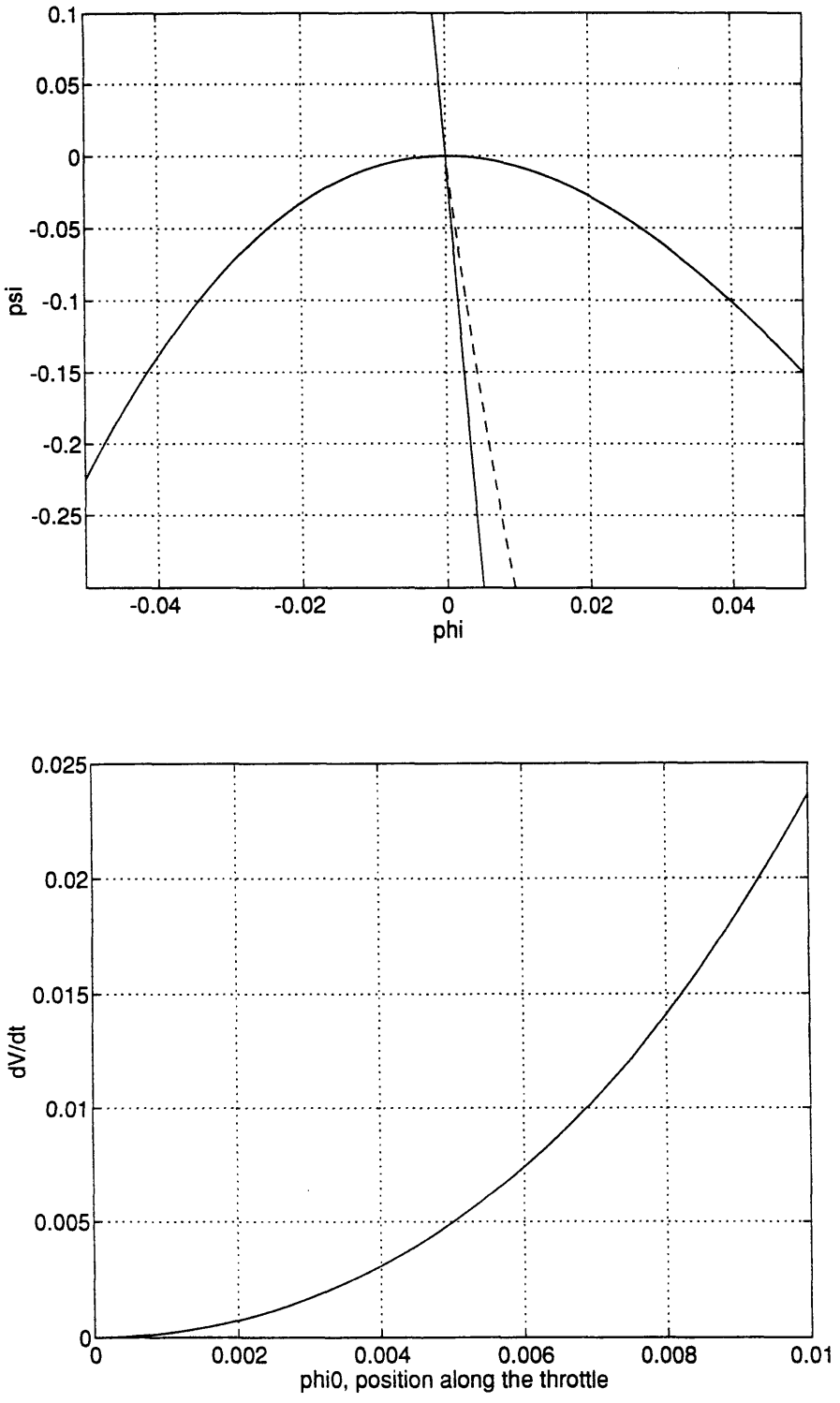

Figures 2.15: Configuration of the apparent throttle $\tilde{\psi}_T(\tilde{\phi}) = Q\,\tilde{\phi}$, Q = -60.

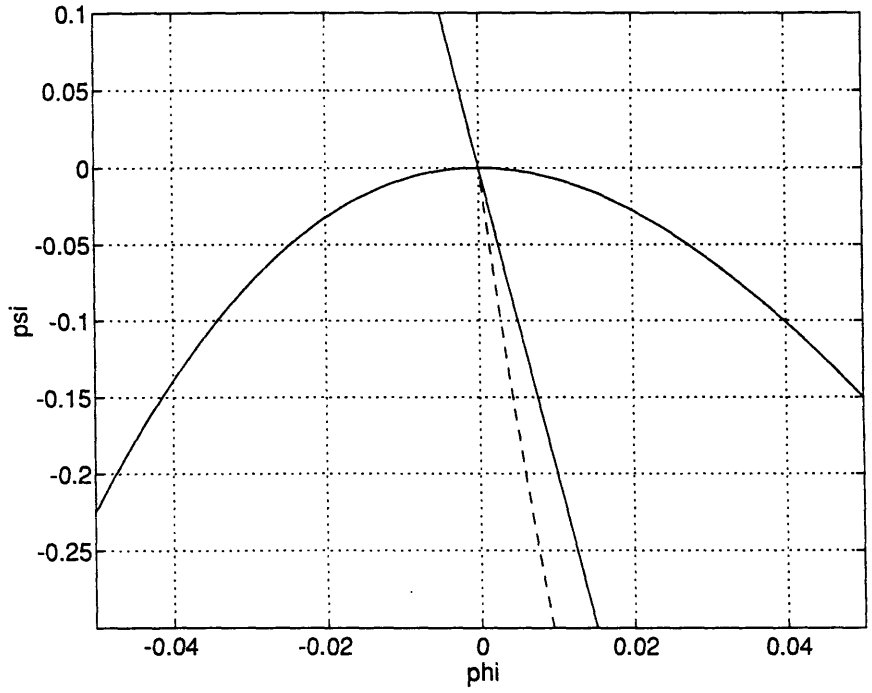

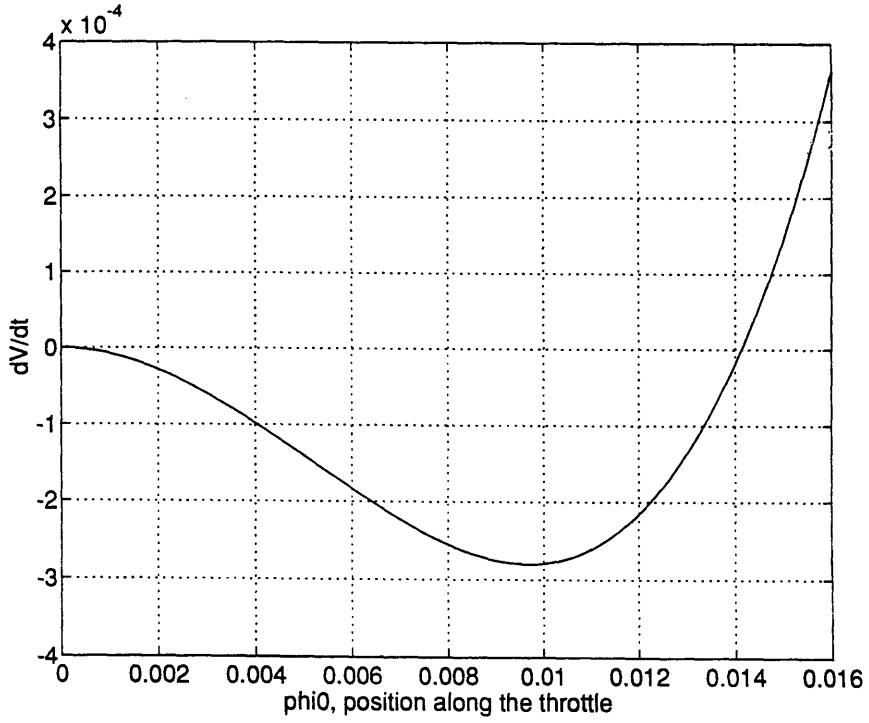

Figures 2.16: Configuration of the apparent throttle $\tilde{\psi}_T(\tilde{\phi}) = Q\,\tilde{\phi}$, Q = -20.

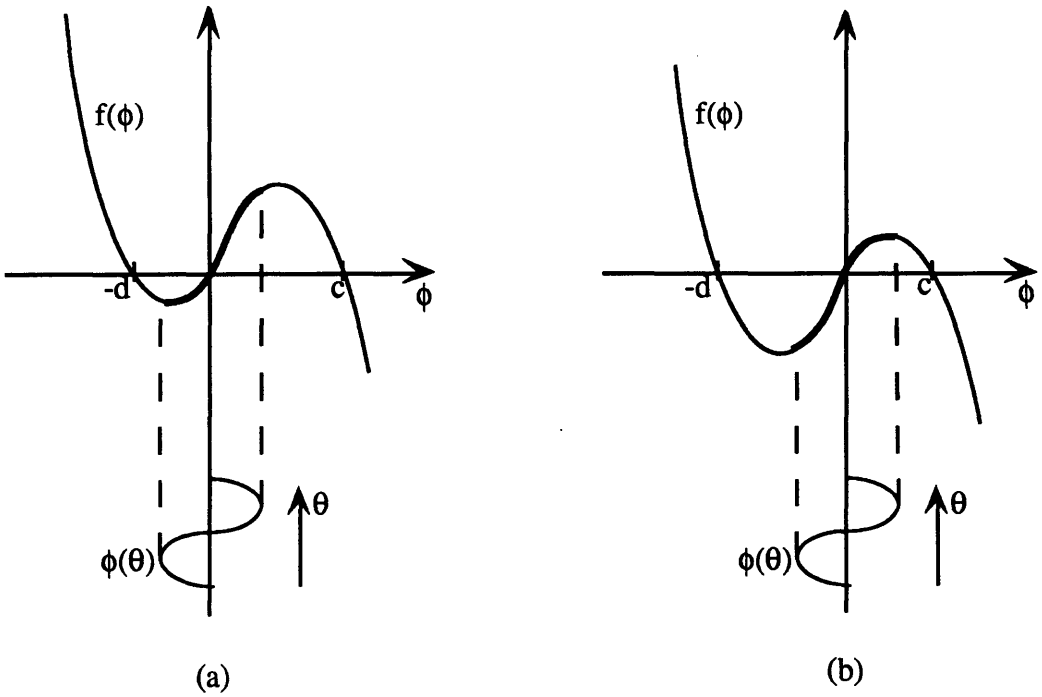

Figure 2.17: Mapping velocity perturbations onto f:

(a) Throttle characteristic on the left of compressor characteristic mid-line.

(b) Throttle characteristic on the right of compressor characteristic mid-line.

Chapter 3

Absolute Stability based Nonlinear Stability Analysis applied to Nonlinear Model of Rotating Stall with Unsteady Losses

3.1 Nonlinear Model of Rotating Stall with Unsteady Losses

The purpose of the elaboration of a second nonlinear model of rotating stall is to improve the state-space representation of Chapter 2 by including the effects of unsteady losses. As explained in [10,17], in Section 2.1 the assumption is made that the axisymmetric compressor characteristic $\psi_c(\phi)$ is quasi-steady and is not altered by the presence of unsteadiness in the flow. However, if an abrupt change in the axisymmetric mass flow is applied to the engine, the compressor naturally requires a finite time to adjust to the new flow condition. Up to now this fluid dynamic lag has not been taken into account in the compressor model. The assumption of quasi-steadiness will be increasingly inaccurate with increasing mode number because the higher modes "see" more rapid flow unsteadiness. If the steady state compressor characteristic $\psi_c(\phi)$ is decomposed into:

$$\psi_c(\phi) = \psi_i(\phi) - L_{ss}(\phi) \qquad (3.1)$$

where $\psi_i(\phi)$ is the ideal characteristic of the compressor assumed isentropic and $L_{ss}(\phi)$ represents the viscous losses of the compressor when it operates in steady state, the effect of unsteady losses is incorporated by letting the pressure rise of the compressor be given by:

$$\psi(\phi) = \psi_i(\phi) - L(\phi) \qquad (3.2)$$

In general, the loss $L(\phi)$ will be subject to unsteadiness so that the actual compressor characteristic ψ will vary and be different from ψ_C.

The rotors and stators have different dynamic characteristics in unsteady flow. Therefore, the rotor loss L_r should be distinguished from the stator loss L_S. The proportion of the contribution of each is determined by the reactions of the compressor blading R_r and R_S.

$$\begin{aligned} L_{ss} &= L_{ss}^{(r)} + L_{ss}^{(s)} \qquad & L &= L_r + L_s \\ L_{ss}^{(r)} &= R_r \cdot L_{ss} \qquad & L_r &= R_r \cdot L \qquad \text{with:} \quad R_r + R_s = 1 \\ L_{ss}^{(s)} &= R_s \cdot L_{ss} \qquad & L_s &= R_s \cdot L \end{aligned}$$

Then, Equations (3.1) and (3.2) become:

1) Pressure rise delivered by the compressor in steady state:

$$\psi_c(\phi) = \psi_i(\phi) - L_{ss}^{(r)}(\phi) - L_{ss}^{(s)}(\phi) \tag{3.3}$$

2) Unsteady pressure rise delivered by the compressor:

$$\psi(\phi) = \psi_i(\phi) - L_r(\phi) - L_s(\phi) \tag{3.4}$$

The unsteadiness is modeled by a first-order lag:

rotor:
$$\tau\left(\frac{\partial L_r}{\partial t} + \frac{\partial L_r}{\partial \theta}\right) = L_{ss}^{(r)} - L_r \tag{3.5}$$

stator:
$$\tau\,\frac{\partial L_s}{\partial t} = L_{ss}^{(s)} - L_s \tag{3.6}$$

t is the nondimensional time as in Chapter 2. The time constant τ is the same for rotors and stators. It should have a value approximately equivalent to the time necessary for a fluid particle to convect through a blade row and is usually of order 0.1.

Our starting point is again the Moore-Greitzer model and the system of equations presented in (2.2). Replacing the steady state form of the pressure rise delivered by the compressor by its unsteady form, we have:

$$\begin{cases} m\dfrac{\partial(\delta\Phi)}{\partial t} + l_c\dfrac{\partial\overline{\phi}}{\partial t} + \mu\dfrac{\partial(\delta\phi)}{\partial t} + \lambda\dfrac{\partial(\delta\phi)}{\partial\theta} = \left(\psi_i - L_r - L_s\right)\left(\overline{\phi} + \delta\phi(0,\theta,t)\right) - \overline{\psi} \\ \dfrac{\partial\overline{\psi}}{\partial t} = \dfrac{1}{4l_cB^2}\left(\overline{\phi} - \phi_T(\overline{\psi})\right) \end{cases} \tag{3.7}$$

The approach is the same as in Section 2.1. The same spatial discretization in θ is performed around the annulus and only the modes -N to +N are kept while taking the DFT of the first group of 2N+1 equations in (3.7).

All losses are functions of ϕ and like ϕ are evaluated at 2N+1 locations around the annulus of the compressor. Through the discretization they become vectors of length 2N+1 to which we can apply the DFT definition in (2.9) and (2.10).

$$L_{\bullet}(\theta_k) = \frac{1}{\sqrt{2N+1}} \sum_{n=-N}^{+N} \hat{L}_{\bullet_n} \cdot e^{+in\theta_k} \qquad \text{or} \qquad \underline{\hat{L}}_{\bullet} = F \cdot \underline{L}_{\bullet}$$

$$L_{ss}^{(\bullet)}(\theta_k) = \frac{1}{\sqrt{2N+1}} \sum_{n=-N}^{+N} \hat{L}_{ss\,n}^{(\bullet)} \cdot e^{+in\theta_k} \qquad \underline{\hat{L}}_{ss}^{(\bullet)} = F \cdot \underline{L}_{ss}^{(\bullet)}$$

Equations (3.5) and (3.6) are evaluated at each one of the 2N+1 locations around the annulus. Taking the DFT of these 2 groups of 2N+1 equations we get:

$\forall\, n \in [-N;+N]$, rotor:
$$\tau\, \dot{\hat{L}}_{r_n} = \hat{L}_{ss\,n}^{(r)} - (1 + in\tau)\hat{L}_{r_n} \qquad (3.8)$$

stator:
$$\tau\, \dot{\hat{L}}_{s_n} = \hat{L}_{ss\,n}^{(s)} - \hat{L}_{s_n} \qquad (3.9)$$

Before taking the DFT of (3.7) it is useful to separate linear and nonlinear parts in ψ_i and $L_{ss}^{(r)}$, $L_{ss}^{(s)}$. The nonlinear system modeling the dynamics of rotating stall will then be represented as a feedback connection between a linear dynamical system and a nonlinear element regrouping all nonlinear contributions from ψ_i and $L_{ss}^{(r)}$, $L_{ss}^{(s)}$.

$$\begin{aligned} \psi_i(\phi) &= c_i + d_i\,\phi + h_i(\phi) & \underline{\psi}_i(\underline{\phi}) &= c_i\underline{T} + d_i\underline{\phi} + \underline{h}_i(\underline{\phi}) \\ L_{ss}^{(r)}(\phi) &= c_r + d_r\,\phi + h_r(\phi) \quad \Rightarrow & \underline{L}_{ss}^{(r)}(\underline{\phi}) &= c_r\underline{T} + d_r\underline{\phi} + \underline{h}_r(\underline{\phi}) \\ L_{ss}^{(s)}(\phi) &= c_s + d_s\,\phi + h_s(\phi) & \underline{L}_{ss}^{(s)}(\underline{\phi}) &= c_s\underline{T} + d_s\underline{\phi} + \underline{h}_s(\underline{\phi}) \end{aligned} \qquad (3.10)$$

h_i, h_r and h_s are the nonlinear part of ψ_i, $L_{ss}^{(r)}$ and $L_{ss}^{(s)}$ respectively.

Moreover, we know that the first step in the nonlinear stability analysis of an operating point $(\overline{\phi}^*, \overline{\psi}^*)$ is to express all variables in a new local coordinate system in which the origin is located at $(\overline{\phi}^*, \overline{\psi}^*)$. Doing this now will save one step in the next section.

The transformations equations are:

$$\tilde{\underline{\phi}} = \underline{\phi} - \underline{T}\cdot\overline{\phi}^* \qquad \tilde{\underline{p}}\left(\tilde{\underline{\phi}}\right) = \underline{p}\left(\underline{T}\cdot\overline{\phi}^* + \tilde{\underline{\phi}}\right) - \underline{T}\cdot\overline{\psi}^*$$
$$\tilde{\overline{\psi}} = \overline{\psi} - \overline{\psi}^* \qquad \tilde{\phi}_T\left(\tilde{\overline{\psi}}\right) = \phi_T\left(\overline{\psi}^* + \tilde{\overline{\psi}}\right) - \overline{\phi}^*$$

where p can be ψ_i, $L_{ss}^{(r)}$, $L_{ss}^{(s)}$, L_r or L_s.

In the local coordinate system, Equations (3.10) become:

$$\begin{aligned}
\tilde{\underline{\psi}}_i\left(\tilde{\underline{\phi}}\right) &= C_i\underline{T} + D_i\tilde{\underline{\phi}} + \tilde{\underline{H}}_i\left(\tilde{\underline{\phi}}\right) \\
\tilde{\underline{L}}_{ss}^{(r)}\left(\tilde{\underline{\phi}}\right) &= C_r\underline{T} + D_r\tilde{\underline{\phi}} + \tilde{\underline{H}}_r\left(\tilde{\underline{\phi}}\right) \qquad (3.11)\\
\tilde{\underline{L}}_{ss}^{(s)}\left(\tilde{\underline{\phi}}\right) &= C_s\underline{T} + D_s\tilde{\underline{\phi}} + \tilde{\underline{H}}_s\left(\tilde{\underline{\phi}}\right)
\end{aligned}$$

C_i, C_r and C_s are scalars which give the value taken by $\tilde{\psi}_i$, $\tilde{L}_{ss}^{(r)}$ and $\tilde{L}_{ss}^{(s)}$ for $\tilde{\phi} = 0$.

D_i, D_r and D_s are scalars which give the slope of $\tilde{\psi}_i$, $\tilde{L}_{ss}^{(r)}$ and $\tilde{L}_{ss}^{(s)}$ for $\tilde{\phi} = 0$.

$\tilde{H}_i$, $\tilde{H}_r$ and $\tilde{H}_s$ are the nonlinear part of $\tilde{\psi}_i$, $\tilde{L}_{ss}^{(r)}$ and $\tilde{L}_{ss}^{(s)}$.

From Equation (3.3) written in the local coordinate system, we can get a relationship between C_i, C_r and C_s as follows:

$$\psi_c(\phi) = \psi_i(\phi) - L_{ss}^{(r)}(\phi) - L_{ss}^{(s)}(\phi)$$
$$\Downarrow$$
$$\tilde{\psi}_c\left(\tilde{\phi}\right) + \overline{\psi}^* = \tilde{\psi}_i\left(\tilde{\phi}\right) + \overline{\psi}^* - \tilde{L}_{ss}^{(r)}\left(\tilde{\phi}\right) - \overline{\psi}^* - \tilde{L}_{ss}^{(s)}\left(\tilde{\phi}\right) - \overline{\psi}^*$$
$$\tilde{\psi}_c\left(\tilde{\phi}\right) = \tilde{\psi}_i\left(\tilde{\phi}\right) - \tilde{L}_{ss}^{(r)}\left(\tilde{\phi}\right) - \tilde{L}_{ss}^{(s)}\left(\tilde{\phi}\right) - 2\overline{\psi}^*$$

Evaluated at $\tilde{\phi} = 0$, the last expression gives:

$$C_i - C_r - C_s - 2\overline{\psi}^* = 0.$$

In the same fashion, $\psi_i(\phi) - L_r(\phi) - L_s(\phi) - \overline{\psi}$ in Equation (3.7) becomes, after the change of coordinate system:

$$\tilde{\psi}_i\left(\tilde{\phi}\right) - \tilde{L}_r\left(\tilde{\phi}\right) - \tilde{L}_s\left(\tilde{\phi}\right) - \tilde{\overline{\psi}} - 2\overline{\psi}^*.$$

Using (3.11) Equations (3.8) and (3.9) become in the local coordinate system:

$\forall\, n \in [-N;+N]$ rotor:
$$\tau\,\dot{\hat{\tilde{L}}}_{r_n} = C_r\hat{T}_n + D_r\hat{\tilde{\phi}}_n + \hat{\tilde{H}}_{r_n} - (1 + in\tau)\hat{\tilde{L}}_{r_n} \qquad (3.12)$$

stator:
$$\tau\,\dot{\hat{\tilde{L}}}_{s_n} = C_s\hat{T}_n + D_s\hat{\tilde{\phi}}_n + \hat{\tilde{H}}_{s_n} - \hat{\tilde{L}}_{s_n} \qquad (3.13)$$

where $\hat{T}_n$ is the "modal" form of T. Here, we have used the fact that $\hat{T}_n \neq 0$ only for n≠0 and consequently, $n\,\hat{T}_n = 0$ for all n.

Equations (3.12) and (3.13) can be separated into linear and nonlinear parts:
Defining $\underline{\tilde{L}}_\bullet^{\,i}$ and $\underline{\tilde{L}}_\bullet^{\,e}$ such that: $\underline{\tilde{L}}_\bullet = C_\bullet \underline{T} + \underline{\tilde{L}}_\bullet^{\,i} + \underline{\tilde{L}}_\bullet^{\,e}$ where the superscript "i" stands for internal (to the feedback loop) or linear part and the superscript "e" for external or nonlinear part and where:

$\forall\, n \in [-N;+N]$	rotor:	$\tau\,\dot{\hat{\tilde{L}}}_{r_n}^{i} = D_r\hat{\tilde{\phi}}_n - (1+in\tau)\hat{\tilde{L}}_{r_n}^{i}$	(3.14)
		$\tau\,\dot{\hat{\tilde{L}}}_{r_n}^{e} = \hat{\tilde{H}}_{r_n} - (1+in\tau)\hat{\tilde{L}}_{r_n}^{e}$	(3.15)
	stator:	$\tau\,\dot{\hat{\tilde{L}}}_{s_n}^{i} = D_s\hat{\tilde{\phi}}_n - \hat{\tilde{L}}_{s_n}^{i}$	(3.16)
		$\tau\,\dot{\hat{\tilde{L}}}_{s_n}^{e} = \hat{\tilde{H}}_{s_n} - \hat{\tilde{L}}_{s_n}^{e}$	(3.17)

guarantees that Equations (3.12) and (3.13) are satisfied. However, this is not obvious for the rotor and needs to be verified.

$$\tau\,\dot{\hat{\tilde{L}}}_{r_n} = \tau\,\dot{\hat{\tilde{L}}}_{r_n}^{i} + \tau\,\dot{\hat{\tilde{L}}}_{r_n}^{e} = D_r\hat{\tilde{\phi}}_n + \hat{\tilde{H}}_{r_n} - (1+in\tau)\hat{\tilde{L}}_{r_n}^{i} - (1+in\tau)\hat{\tilde{L}}_{r_n}^{e}$$

$$\tau\,\dot{\hat{\tilde{L}}}_{r_n} = D_r\hat{\tilde{\phi}}_n + \hat{\tilde{H}}_{r_n} - (1+in\tau)\hat{\tilde{L}}_{r_n} + (1+in\tau)C_r\hat{T}_n$$

$$\tau\,\dot{\hat{\tilde{L}}}_{r_n} = C_r\hat{T}_n + D_r\hat{\tilde{\phi}}_n + \hat{\tilde{H}}_{r_n} - (1+in\tau)\hat{\tilde{L}}_{r_n}$$

The last equality uses again that $n\,\hat{T}_n = 0$ for all n and proves that (3.12) is satisfied.

Taking the DFT of the first group of 2N+1 equations in (3.7) written in the local coordinate system, we get 2N+1 equations (one for each mode) which are analogous to Equations (2.13) and (2.14)

$$\underline{n\neq 0} \qquad \left(\frac{m}{|n|}+\mu\right)\cdot\dot{\hat{\tilde{\phi}}}_n = (D_i - i\lambda n)\cdot\hat{\tilde{\phi}}_n - \hat{\tilde{L}}_{r_n}^{i} - \hat{\tilde{L}}_{s_n}^{i} - \hat{\tilde{L}}_{r_n}^{e} - \hat{\tilde{L}}_{s_n}^{e} + \hat{\tilde{H}}_{i_n}$$

$$\underline{n=0} \qquad l_c\cdot\dot{\hat{\tilde{\phi}}}_0 = D_i\,\hat{\tilde{\phi}}_0 - \bar{\tilde{\psi}}\cdot\sqrt{2N+1} - \hat{\tilde{L}}_{r0}^{i} - \hat{\tilde{L}}_{s0}^{i} - \hat{\tilde{L}}_{r0}^{e} - \hat{\tilde{L}}_{s0}^{e}$$
$$+\left(C_i - C_r - C_s - 2\bar{\psi}^*\right)\cdot\sqrt{2N+1} + \hat{\tilde{H}}_{i0}$$

Calling $d_n = \begin{cases} \frac{m}{|n|} + \mu, & \text{for } n \neq 0 \\ l_c, & \text{for } n = 0 \end{cases}$ the (n+N+1)th element on the diagonal of the matrix D_E

and recalling that $C_i - C_r - C_s - 2\overline{\psi}^* = 0$, we are left with:

$$\underline{n\neq 0} \qquad d_n \cdot \dot{\hat{\tilde{\phi}}}_n = (D_i - i\lambda n)\cdot \hat{\tilde{\phi}}_n - \hat{\tilde{L}}^i_{rn} - \hat{\tilde{L}}^i_{sn} - \hat{\tilde{L}}^e_{rn} - \hat{\tilde{L}}^e_{sn} + \hat{\tilde{H}}_{in} \tag{3.18}$$

$$\underline{n=0} \qquad d_0 \cdot \dot{\hat{\tilde{\phi}}}_0 = D_i\, \hat{\tilde{\phi}}_0 - \overline{\tilde{\psi}} \cdot \sqrt{2N+1} - \hat{\tilde{L}}^i_{r0} - \hat{\tilde{L}}^i_{s0} - \hat{\tilde{L}}^e_{r0} - \hat{\tilde{L}}^e_{s0} + \hat{\tilde{H}}_{i0} \tag{3.19}$$

The last equation is coupled with:

$$\dot{\overline{\tilde{\psi}}} = \frac{1}{4B^2 l_c}\left(\frac{1}{\sqrt{2N+1}}\hat{\tilde{\phi}}_0 - \tilde{\phi}_T\left(\overline{\tilde{\psi}}\right)\right) \tag{3.20}$$

Therefore, 4(2N+1) equations and 4(2N+1) unknowns have been introduced to model the dynamics of rotating stall with unsteady losses, bringing the dimension of the system to 10N+6. The 10N+6 unknowns are the entries of $\underline{\tilde{\phi}}$, $\underline{\tilde{L}}^i_r$, $\underline{\tilde{L}}^e_r$, $\underline{\tilde{L}}^i_s$, $\underline{\tilde{L}}^e_s$ and $\overline{\tilde{\psi}}$. The 10N+6 equations are (3.14) to (3.20). Considering that N is usually at least 5, the number of states has to be reduced in some way. We are going to perform a model reduction mode by mode to eliminate all 4(2N+1) states associated to the losses thus returning to a system of dimension 2N+2. However, in the meanwhile the location of the eigenvalues of the linear system will have been modified to take into account the effect of unsteady losses.

Mode by mode model reduction, Part I: $n \neq 0$

Five states are associated to such a mode. Its dynamics are given by:

$$\underbrace{\begin{bmatrix} \dot{\hat{\tilde{\phi}}}_n \\ \dot{\hat{\tilde{L}}}^i_{rn} \\ \dot{\hat{\tilde{L}}}^i_{sn} \\ \dot{\hat{\tilde{L}}}^e_{rn} \\ \dot{\hat{\tilde{L}}}^e_{sn} \end{bmatrix}}_{\dot{\underline{X}}} = \underbrace{\begin{bmatrix} \frac{D_i - i\lambda n}{d_n} & \frac{-1}{d_n} & \frac{-1}{d_n} & \frac{-1}{d_n} & \frac{-1}{d_n} \\ \frac{D_r}{\tau} & \frac{-1}{\tau} - in & 0 & 0 & 0 \\ \frac{D_s}{\tau} & 0 & \frac{-1}{\tau} & 0 & 0 \\ 0 & 0 & 0 & \frac{-1}{\tau} - in & 0 \\ 0 & 0 & 0 & 0 & \frac{-1}{\tau} \end{bmatrix}}_{A} \underbrace{\begin{bmatrix} \hat{\tilde{\phi}}_n \\ \hat{\tilde{L}}^i_{rn} \\ \hat{\tilde{L}}^i_{sn} \\ \hat{\tilde{L}}^e_{rn} \\ \hat{\tilde{L}}^e_{sn} \end{bmatrix}}_{\underline{X}} + \underbrace{\begin{bmatrix} \frac{\hat{\tilde{H}}_{in}}{d_n} \\ 0 \\ 0 \\ \frac{\hat{\tilde{H}}_{rn}}{\tau} \\ \frac{\hat{\tilde{H}}_{sn}}{\tau} \end{bmatrix}}_{\underline{U}} \quad \text{or} \quad \dot{\underline{X}} = A\underline{X} + \underline{U} \tag{3.21}$$

The matrix A is diagonalized through the change of variables $\underline{X} = V\underline{Z}$, V is the matrix of right eigenvectors of A where $\Lambda = WAV$ is the diagonal matrix of eigenvalues of A and $W = V^{-1}$ is the matrix of left eigenvectors of A.

Multiplying (3.21) on the left by W, we get:

$$\dot{\underline{Z}} = \Lambda\underline{Z} + W\underline{U} \tag{3.22}$$

If τ is small, the coupling between the equations of (3.21) is not strong and $\underline{Z}$ is close to $\underline{X}$ as defined by (3.21). Consequently, the first state in $\underline{Z}$, which we will call z_1, stays close to $\hat{\tilde{\phi}}_n$. The 4 other states, which we will call $\underline{z}$, are close to the losses $\hat{\tilde{L}}^i_{rn}$, $\hat{\tilde{L}}^i_{sn}$, $\hat{\tilde{L}}^e_{rn}$ and $\hat{\tilde{L}}^e_{sn}$ whose "uncoupled" dynamics are very fast: the absolute value of $\frac{-1}{\tau}$, the real part of their eigenvalues, is large if τ is small and is the dominant term in the eigenvalue (see Equations (3.14) to (3.17)). Therefore, $\underline{z}$ contains the fast high frequency states and its steady-state is reached very quickly. It is valid to assume that $\dot{\underline{z}} = 0$ to perform the model reduction.

Separating z_1 from $\underline{z}$, Equation (3.22) can be written:

$$\begin{bmatrix} \dot{z}_1 \\ \dot{\underline{z}} \end{bmatrix} = \begin{bmatrix} \lambda_1 & (0) \\ (0) & \begin{bmatrix} \lambda_2 & & (0) \\ & \lambda_3 & \\ & & \lambda_4 \\ (0) & & & \lambda_5 \end{bmatrix} \end{bmatrix} \begin{bmatrix} z_1 \\ \underline{z} \end{bmatrix} + \begin{bmatrix} \underline{w}_1^T \\ \begin{bmatrix} \underline{w}_2^T \\ \underline{w}_3^T \\ \underline{w}_4^T \\ \underline{w}_5^T \end{bmatrix} \end{bmatrix} \underline{U} \tag{3.23}$$

We want to keep only:

$$\dot{z}_1 = \lambda_1 z_1 + \underline{w}_1^T \cdot \underline{U} \tag{3.24}$$

$\underline{z}$ is eliminated as follows:

$$\dot{\underline{z}} \cong 0 \quad \Rightarrow \quad \underline{z} \cong -\begin{bmatrix} \underline{w}_2^T/\lambda_2 \\ \underline{w}_3^T/\lambda_3 \\ \underline{w}_4^T/\lambda_4 \\ \underline{w}_5^T/\lambda_5 \end{bmatrix} \underline{U} \tag{3.25}$$

$\hat{\tilde{\phi}}_n$ can be recovered from $\underline{Z}$ through:

$$\hat{\tilde{\phi}}_n = v_{11} z_1 + \begin{bmatrix} v_{12} & v_{13} & v_{14} & v_{15} \end{bmatrix} \cdot \underline{z} \tag{3.26}$$

where $\begin{bmatrix} v_{11} & v_{12} & v_{13} & v_{14} & v_{15} \end{bmatrix}$ is the first row of the matrix V.

Combining (3.25) and (3.26), we get:

$$\hat{\tilde{\phi}}_n = v_{11} z_1 - \underbrace{\left[\frac{v_{12}\underline{w}_2^T}{\lambda_2} \quad \frac{v_{13}\underline{w}_3^T}{\lambda_3} \quad \frac{v_{14}\underline{w}_4^T}{\lambda_4} \quad \frac{v_{15}\underline{w}_5^T}{\lambda_5} \right]}_{\text{usually} \approx 0} \cdot \underline{U}$$

The contribution of $\underline{U}$ in $\hat{\tilde{\phi}}_n$ is usually negligible since λ_2, λ_3, λ_4 and λ_5 are close to the "uncoupled" eigenvalues of the losses and thus have a big magnitude.

Under this assumption, $\hat{\tilde{\phi}}_n$ can be reconstructed using:

$$\hat{\tilde{\phi}}_n = v_{11} z_1$$

Multiplying Equation (3.24) on the left by v_{11}, we get:

$$\dot{\hat{\tilde{\phi}}}_n = \lambda_1 \hat{\tilde{\phi}}_n + v_{11}\underline{w}_1^T \cdot \underline{U}$$

Using the definition of $\underline{U}$, the final result of the model reduction is:

$$\dot{\hat{\tilde{\phi}}}_n = \lambda_1 \hat{\tilde{\phi}}_n + \frac{v_{11}w_{11}}{d_n}\hat{\tilde{H}}_{i_n} + \frac{v_{11}w_{14}}{\tau}\hat{\tilde{H}}_{r_n} + \frac{v_{11}w_{15}}{\tau}\hat{\tilde{H}}_{s_n} \qquad (3.27)$$

where $\underline{w}_1^T = [w_{11} \;\; w_{12} \;\; w_{13} \;\; w_{14} \;\; w_{15}]$.

Equation (3.27) is true for all $n \neq 0$. For clarity, the index n is omitted on λ_1, v_{11}, w_{11}, w_{14} and w_{15} which are all functions of n.

The 4 high frequency modes associated with the unsteady losses have been eliminated. The nonlinear part of the ideal characteristic $\tilde{\psi}_i$ and the steady-state losses of rotor and stator $\tilde{L}_{ss}^{(r)}$ and $\tilde{L}_{ss}^{(s)}$ are still considered as a nonlinear feedback modifying the linear system. The effect of the combined introduction of the dynamics of the unsteady losses and their subsequent elimination by the model reduction has been to translate the eigenvalues of the linear system from initially $\frac{D_i - i\lambda n}{d_n}$ to λ_1 and to apply to the nonlinear feedback a complicated control power matrix (no longer the identity matrix). The model of rotating stall elaborated in this section will not be more complex than the one of Chapter 2 (same dimension) but will reflect the effect of unsteady losses through the modified control power matrix and eigenvalues of the linear system.

Mode by mode model reduction, Part II: n = 0

Six states are associated to the zeroth mode. Before writing its dynamics in a matrix form as in (3.21), the dynamics of $\tilde{\bar{\psi}}$ and the throttle characteristic must be linearized (this thesis deals with the study of the effects of the nonlinearity of the compressor characteristic only). By definition,

$$\psi_T(\phi) = \frac{K_t}{2}\phi^2 \quad \text{or} \quad \phi_T(\psi) = \sqrt{\frac{2\psi}{K_t}}$$

which becomes in the local coordinate system:

$$\tilde{\phi}_T\left(\tilde{\bar{\psi}}\right) = \sqrt{\frac{2\left(\bar{\psi}^* + \tilde{\bar{\psi}}\right)}{K_t}} - \bar{\phi}^* = \sqrt{\frac{2\bar{\psi}^*}{K_t}}\left(1 + \frac{\tilde{\bar{\psi}}}{\bar{\psi}^*}\right)^{\frac{1}{2}} - \bar{\phi}^*$$

Linearization of this equation gives:

$$\tilde{\phi}_T\left(\tilde{\bar{\psi}}\right) = \sqrt{\frac{2\bar{\psi}^*}{K_t}}\left(1 + \frac{\tilde{\bar{\psi}}}{2\bar{\psi}^*}\right) - \bar{\phi}^*$$

which is simplified into:

$$\tilde{\phi}_T\left(\tilde{\bar{\psi}}\right) = \sqrt{\frac{1}{2K_t\bar{\psi}^*}} \cdot \tilde{\bar{\psi}} \tag{3.28}$$

Using (3.28), (3.14) to (3.17), (3.19) and (3.20), the dynamics of the zeroth mode are also given in the form $\dot{\underline{X}} = A\underline{X} + \underline{U}$:

$$\underbrace{\begin{bmatrix} \dot{\hat{\tilde{\phi}}}_0 \\ \dot{\tilde{\bar{\psi}}} \\ \dot{\hat{\tilde{L}}}^i_{r0} \\ \dot{\hat{\tilde{L}}}^i_{s0} \\ \dot{\hat{\tilde{L}}}^e_{r0} \\ \dot{\hat{\tilde{L}}}^e_{s0} \end{bmatrix}}_{\dot{\underline{X}}} = \underbrace{\begin{bmatrix} \frac{D_i}{d_0} & \frac{-\sqrt{2N+1}}{d_0} & \frac{-1}{d_0} & \frac{-1}{d_0} & \frac{-1}{d_0} & \frac{-1}{d_0} \\ \frac{1}{4B^2 l_c \sqrt{2N+1}} & \frac{-1}{4B^2 l_c \sqrt{2K_t\bar{\psi}^*}} & 0 & 0 & 0 & 0 \\ \frac{D_r}{\tau} & 0 & \frac{-1}{\tau} & 0 & 0 & 0 \\ \frac{D_s}{\tau} & 0 & 0 & \frac{-1}{\tau} & 0 & 0 \\ 0 & 0 & 0 & 0 & \frac{-1}{\tau} & 0 \\ 0 & 0 & 0 & 0 & 0 & \frac{-1}{\tau} \end{bmatrix}}_{A} \underbrace{\begin{bmatrix} \hat{\tilde{\phi}}_0 \\ \tilde{\bar{\psi}} \\ \hat{\tilde{L}}^i_{r0} \\ \hat{\tilde{L}}^i_{s0} \\ \hat{\tilde{L}}^e_{r0} \\ \hat{\tilde{L}}^e_{s0} \end{bmatrix}}_{\underline{X}} + \underbrace{\begin{bmatrix} \frac{\hat{H}_{i0}}{d_0} \\ 0 \\ 0 \\ 0 \\ \frac{\hat{H}_{r0}}{\tau} \\ \frac{\hat{H}_{s0}}{\tau} \end{bmatrix}}_{\underline{U}} \tag{3.29}$$

The procedure of the model reduction is the same as before. If τ is small, the 2 first states in $\underline{Z}$, z_1 and z_2, are close to $\hat{\tilde{\phi}}_0$ and $\tilde{\tilde{\psi}}$. The 4 high frequency modes associated to the unsteady losses are eliminated. The notations used in the diagonalization of A are identical. Now, Equation (3.23) takes the form:

$$\begin{bmatrix} \dot{z}_1 \\ \dot{z}_2 \\ \dot{\underline{z}} \end{bmatrix} = \begin{bmatrix} \begin{bmatrix} \lambda_1 & 0 \\ 0 & \lambda_2 \end{bmatrix} & (0) \\ (0) & \begin{bmatrix} \lambda_3 & & (0) \\ & \lambda_4 & \\ (0) & & \lambda_5 \end{bmatrix} \end{bmatrix} \begin{bmatrix} z_1 \\ z_2 \\ \underline{z} \end{bmatrix} + \begin{bmatrix} \begin{bmatrix} \underline{w}_1^T \\ \underline{w}_2^T \end{bmatrix} \\ \begin{bmatrix} \underline{w}_3^T \\ \underline{w}_4^T \\ \underline{w}_5^T \\ \underline{w}_6^T \end{bmatrix} \end{bmatrix} \underline{U}$$

We want to keep only:

$$\begin{bmatrix} \dot{z}_1 \\ \dot{z}_2 \end{bmatrix} = \begin{bmatrix} \lambda_1 & 0 \\ 0 & \lambda_2 \end{bmatrix} \begin{bmatrix} z_1 \\ z_2 \end{bmatrix} + \begin{bmatrix} \underline{w}_1^T \\ \underline{w}_2^T \end{bmatrix} \cdot \underline{U} \tag{3.30}$$

using:

$$\dot{\underline{z}} \cong 0 \quad \Rightarrow \quad \underline{z} \cong -\begin{bmatrix} \underline{w}_3^T/\lambda_3 \\ \underline{w}_4^T/\lambda_4 \\ \underline{w}_5^T/\lambda_5 \\ \underline{w}_6^T/\lambda_6 \end{bmatrix} \underline{U} \tag{3.31}$$

$\begin{bmatrix} \hat{\tilde{\phi}}_0 \\ \tilde{\tilde{\psi}} \end{bmatrix}$ can be recovered from $\underline{Z}$ through:

$$\begin{bmatrix} \hat{\tilde{\phi}}_0 \\ \tilde{\tilde{\psi}} \end{bmatrix} = \underbrace{\begin{bmatrix} v_{11} & v_{12} \\ v_{21} & v_{22} \end{bmatrix}}_{V_{12}} \begin{bmatrix} z_1 \\ z_2 \end{bmatrix} + \begin{bmatrix} v_{13} & v_{14} & v_{15} & v_{16} \\ v_{23} & v_{24} & v_{25} & v_{26} \end{bmatrix} \cdot \underline{z}$$

Using (3.31),

$$\begin{bmatrix} \hat{\tilde{\phi}}_0 \\ \tilde{\tilde{\psi}} \end{bmatrix} = V_{12} \begin{bmatrix} z_1 \\ z_2 \end{bmatrix} - \underbrace{\begin{bmatrix} \frac{v_{13}\underline{w}_3^T}{\lambda_3} & \frac{v_{14}\underline{w}_4^T}{\lambda_4} & \frac{v_{15}\underline{w}_5^T}{\lambda_5} & \frac{v_{16}\underline{w}_6^T}{\lambda_6} \\ \frac{v_{23}\underline{w}_3^T}{\lambda_3} & \frac{v_{24}\underline{w}_4^T}{\lambda_4} & \frac{v_{25}\underline{w}_5^T}{\lambda_5} & \frac{v_{26}\underline{w}_6^T}{\lambda_6} \end{bmatrix}}_{\text{usually} \approx 0} \cdot \underline{U}$$

For the same reasons as before, the contribution of $\underline{U}$ in $\begin{bmatrix} \hat{\tilde{\phi}}_0 \\ \tilde{\tilde{\psi}} \end{bmatrix}$ is negligible.

Therefore, $\begin{bmatrix} \hat{\tilde{\phi}}_0 \\ \tilde{\tilde{\psi}} \end{bmatrix}$ can be approximated by:

$$\begin{bmatrix} \hat{\tilde{\phi}}_0 \\ \tilde{\tilde{\psi}} \end{bmatrix} = V_{12} \begin{bmatrix} z_1 \\ z_2 \end{bmatrix}.$$

Multiplying (3.30) on the left by V_{12} and using the definition of $\underline{U}$, we get:

$$\begin{bmatrix} \dot{\hat{\tilde{\phi}}}_0 \\ \dot{\hat{\tilde{\psi}}} \end{bmatrix} = \left\{ V_{12} \begin{bmatrix} \lambda_1 & 0 \\ 0 & \lambda_2 \end{bmatrix} V_{12}^{-1} \right\} \begin{bmatrix} \hat{\tilde{\phi}}_0 \\ \hat{\tilde{\psi}} \end{bmatrix} + \frac{1}{I_c} V_{12} \begin{bmatrix} w_{11} \\ w_{21} \end{bmatrix} \hat{\tilde{H}}_{i0} + \frac{1}{\tau} V_{12} \begin{bmatrix} w_{15} \\ w_{25} \end{bmatrix} \hat{\tilde{H}}_{r0} + \frac{1}{\tau} V_{12} \begin{bmatrix} w_{16} \\ w_{26} \end{bmatrix} \hat{\tilde{H}}_{s0}$$

Which is of the form: $$\begin{bmatrix} \dot{\hat{\tilde{\phi}}}_0 \\ \dot{\hat{\tilde{\psi}}} \end{bmatrix} = \underbrace{\begin{bmatrix} * & * \\ * & * \end{bmatrix}}_{\Lambda_a^0} \begin{bmatrix} \hat{\tilde{\phi}}_0 \\ \hat{\tilde{\psi}} \end{bmatrix} + \underbrace{\begin{bmatrix} * \\ * \end{bmatrix}}_{\Lambda_i^0} \hat{\tilde{H}}_{i0} + \underbrace{\begin{bmatrix} * \\ * \end{bmatrix}}_{\Lambda_r^0} \hat{\tilde{H}}_{r0} + \underbrace{\begin{bmatrix} * \\ * \end{bmatrix}}_{\Lambda_s^0} \hat{\tilde{H}}_{s0} \qquad (3.32)$$

Assembling of the state-space representation:

Defining, $$\underline{\hat{\tilde{X}}} = \begin{bmatrix} \vdots \\ \hat{\tilde{\phi}}_n \\ \vdots \\ \hat{\tilde{\phi}}_0 \\ \tilde{\psi} \\ \vdots \\ \hat{\tilde{\phi}}_n \\ \vdots \end{bmatrix} \begin{matrix} n = -N \\ \\ n = -1 \\ n = 0 \\ n = 0 \\ n = +1 \\ \\ n = +N \end{matrix}$$ and using (3.27) for all $n \neq 0$ and (3.32) for n=0,

$$\dot{\underline{\hat{\tilde{X}}}} = \Lambda_a \underline{\hat{\tilde{X}}} + \Lambda_i \underline{\hat{\tilde{H}}}_i + \Lambda_r \underline{\hat{\tilde{H}}}_r + \Lambda_s \underline{\hat{\tilde{H}}}_s \qquad (3.33)$$

with: $$\Lambda_a = \begin{bmatrix} \ddots & & & \\ & \lambda_1 & & (0) \\ & & \begin{bmatrix} ** \\ ** \end{bmatrix} \Lambda_a^0 & \\ & (0) & & \lambda_1 \ddots \end{bmatrix} \begin{matrix} n = -N \\ \\ n = -1 \\ n = 0 \\ n = 0 \\ n = +1 \\ \\ n = +N \end{matrix}$$ dimension(Λ_a)= (2N+2)(2N+2)

$$\Lambda_i = \begin{bmatrix} \ddots & & & \\ & \frac{v_{11} w_{11}}{d_n} & & (0) \\ & & \begin{bmatrix} * \\ * \end{bmatrix} \Lambda_i^0 & \\ & (0) & & \frac{v_{11} w_{11}}{d_n} \ddots \end{bmatrix}$$ dimension(Λ_i)= (2N+2)(2N+1)

$$\Lambda_r = \begin{bmatrix} \ddots & & \\ & \frac{v_{11}w_{14}}{\tau} & (0) \\ & & \ddots \\ & & \begin{bmatrix} * \\ * \end{bmatrix} \Lambda_r^0 \\ & & \ddots \\ & (0) & \frac{v_{11}w_{14}}{\tau} \\ & & \ddots \end{bmatrix} \qquad \text{dimension}(\Lambda_r) = (2N+2)(2N+1)$$

$$\Lambda_s = \begin{bmatrix} \ddots & & \\ & \frac{v_{11}w_{15}}{\tau} & (0) \\ & & \ddots \\ & & \begin{bmatrix} * \\ * \end{bmatrix} \Lambda_s^0 \\ & & \ddots \\ & (0) & \frac{v_{11}w_{15}}{\tau} \\ & & \ddots \end{bmatrix} \qquad \text{dimension}(\Lambda_s) = (2N+2)(2N+1)$$

If $\underline{\tilde{X}} = \begin{bmatrix} \tilde{\phi} \\ \tilde{\underline{\psi}} \\ \tilde{\bar{\psi}} \end{bmatrix}$, the matrix that transforms $\underline{\tilde{X}}$ into $\underline{\hat{\tilde{X}}}$ is basically the DFT matrix F as defined by (2.12), extended to take into account the extra state $\tilde{\bar{\psi}}$.

$$\underline{\hat{\tilde{X}}} = F_{ext}\underline{\tilde{X}} \qquad \text{with} \qquad F_{ext} = \begin{bmatrix} \begin{bmatrix} & F & \end{bmatrix} & \vdots & \\ & & n=-N \\ & (0) & \\ & \vdots & \\ & & n=0 \\ \cdots \quad (0) \quad \cdots & 1 & n=0\ (\tilde{\bar{\psi}}) \\ & \vdots & \\ & & n=+1 \\ \begin{bmatrix} & F & \end{bmatrix} & (0) & \\ & \vdots & \\ & & n=+N \end{bmatrix}$$

$$-N \le n \le +N$$

Like F, F_{ext} satisfies the property: $F_{ext}^{-1} = F_{ext}^{T}$.

Then, multiplying (3.33) on the left by F_{ext}^{T} and defining $\begin{cases} A = F_{ext}^{T}\Lambda_a F_{ext} \\ I = F_{ext}^{T}\Lambda_i F \\ R = F_{ext}^{T}\Lambda_r F \\ S = F_{ext}^{T}\Lambda_s F \end{cases}$ we have:

$$\dot{\underline{\tilde{X}}} = A\underline{\tilde{X}} + \begin{bmatrix} I & R & S \end{bmatrix} \begin{bmatrix} \underline{\tilde{H}}_i \\ \underline{\tilde{H}}_r \\ \underline{\tilde{H}}_s \end{bmatrix}$$

Finally, if we define

$$\underline{\tilde{Y}} = C\underline{\tilde{X}} = \begin{bmatrix} \underline{\tilde{\phi}} \\ \underline{\dot{\tilde{\phi}}} \\ \underline{\ddot{\tilde{\phi}}} \end{bmatrix}, \quad \text{where} \qquad C = \begin{bmatrix} I_{2N+1} & \underline{0} \\ I_{2N+1} & \underline{0} \\ I_{2N+1} & \underline{0} \end{bmatrix}$$

and I_{2N+1} is the identity matrix of dimension 2N+1,

and we also define

$$\underline{\tilde{\Psi}}\left(\underline{\tilde{Y}}\right) = \begin{bmatrix} \underline{\tilde{H}}_i\left(\underline{\tilde{\phi}}\right) \\ \underline{\tilde{H}}_r\left(\underline{\tilde{\phi}}\right) \\ \underline{\tilde{H}}_s\left(\underline{\tilde{\phi}}\right) \end{bmatrix}, \quad \text{so that} \quad \underline{\tilde{U}} = -\underline{\tilde{\Psi}}; \qquad \text{and} \qquad B = [-I \ -R \ -S],$$

a state-space representation of the system of dimension 2N+2 is:

$$\begin{cases} \dot{\underline{\tilde{X}}} = A\underline{\tilde{X}} + B\underline{\tilde{U}} \\ \underline{\tilde{Y}} = C\underline{\tilde{X}} \end{cases}$$

As shown in Figure 3.1, the full nonlinear system is represented as a negative feedback connection between a linear dynamical system and a nonlinear element which contains all nonlinearities due to the compressor characteristic.

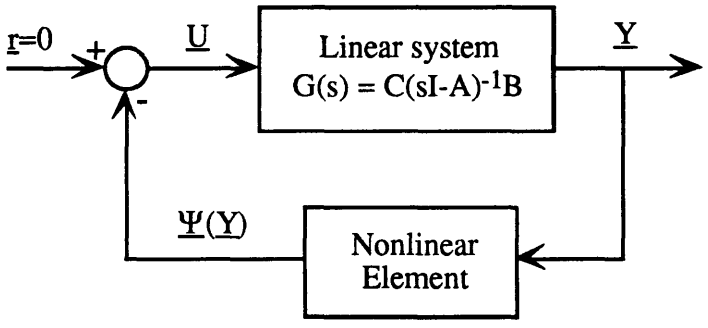

Figure 3.1: Representation of the system as a feedback connection of a linear system and a nonlinear element

Effect of unsteady losses on the location of the eigenvalues of the linear system:

As an example we are going to study the compressor C2 of Section 2.4 for different throttle settings K_t. The model parameters are found in [16] and shown on Table 3.1. The decomposition of the steady-state characteristic of C2 into ideal characteristic and steady-state losses of rotors and stators is calculated using data in [17] and presented in Table 3.2.

Table 3.1: Model parameters of compressor C2

U (speed at mean wheel radius)	72 m/s
R (wheel radius)	0.287 m
$\bar{\phi}$ at stall inception	0.463
K_T at stall inception	9.41
l_c	6.66
B	0.1
m	2
μ	1.2937
λ	0.6787
τ (nondim. convection time)	0.3
R_T (reaction of rotors)	0.738
R_S (reaction of stators)	0.262

Table 3.2: Decomposition of compressor C2 characteristic into ideal characteristic and steady-state losses for $0.42<\phi<0.6$

$$\psi_c(\phi) = 1.023 - 10.07(\phi - 0.46825)^2$$

$$\psi_i(\phi) = -3.3741 + 8.9947\phi - 7.4985\phi^2 + \frac{1.0114}{\phi}$$

$$L_{ss}^{(r)}(\phi) = -1.6156 - 0.32166\phi + 1.8978\phi^2 + \frac{0.74641}{\phi}$$

$$L_{ss}^{(s)}(\phi) = -0.57356 - 0.1142\phi + 0.6737\phi^2 + \frac{0.2650}{\phi}$$

Even if τ is not very small here (τ = 0.3), Figure 3.2 validates the use of the model reduction method since it shows that it is possible to sort the "coupled" eigenvalues and to

associate each separate group to a group of "uncoupled" eigenvalues. This is true for all K_t we will be using (from 9 to 10.6).

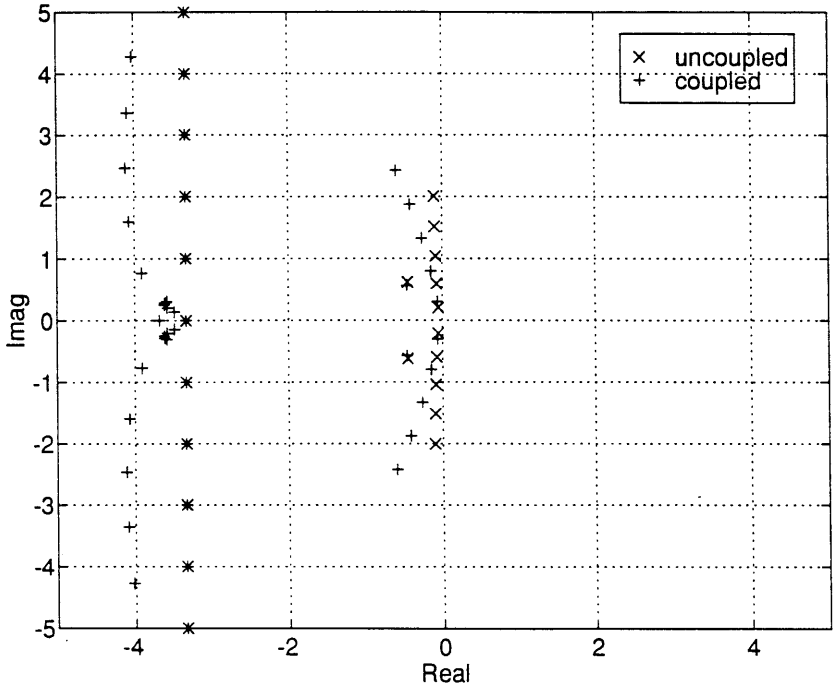

Figure 3.2: Location of eigenvalues of coupled and uncoupled dynamics for the full order system, $K_t = 9$.

Figures 3.3 to 3.5 illustrate the evolution of the location of the eigenvalues for the reduced order system as K_t increases from 9 to 9.93. All of them show that unsteady losses have a stabilizing effect on the system. The eigenvalues of the coupled dynamics are always on the left of those of the uncoupled dynamics and the stabilization gets bigger and bigger as the mode number increases. An explanation of these trends can be found in [17].

For $K_t = 9$ the linear analysis predicts that the system is stable, the operating point being on the stable (right) side of the compressor characteristic. This is confirmed by Figure 3.3 since all eigenvalues have a negative real part.

For $K_t = 9.333$, the operating point is exactly at the peak of the characteristic. The linear analysis without unsteady losses [7] predicts that all modes become unstable at this point.

This is again confirmed by Figure 3.4. All eigenvalues of the uncoupled dynamics are on the jω axis while the "coupled" eigenvalues are still all stable. Therefore, the introduction of unsteady losses in the model explains that a value of K_t larger than 9.333 is necessary to destabilize the system. Experimentally, the stall inception occurs at $K_t = 9.41$.

For $K_t = 9.515$ according to the linear analysis without unsteady losses, the system is unstable. All eigenvalues of the uncoupled dynamics are on the right half plane. Taking into account unsteady losses on the other hand, the system is exactly at the neutral stability point since the first mode crosses the jω axis. $K_t = 9.515$ sets a new limit for the stall inception point which is not violated by the experiment (see [16]). According to this analysis, the stall inception cannot occur for $K_t > 9.515$ otherwise there would exist a stable range of $K_t > 9.515$. However, it can occur before $K_t = 9.515$ if the domain of attraction gets smaller than the size of the perturbations encountered by the system.

Two other important values of K_t can be pointed out. At $K_t = 9.93$, the second coupled mode becomes unstable and at $K_t = 10.6$, the third coupled mode becomes unstable.

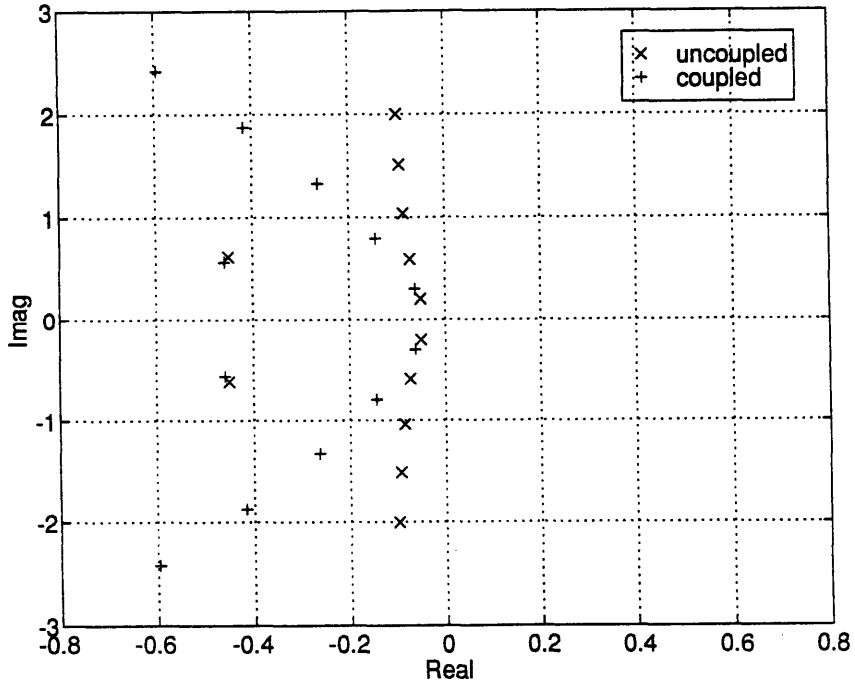

Figure 3.3: Location of eigenvalues of coupled and uncoupled dynamics for the reduced order system, $K_t = 9$.

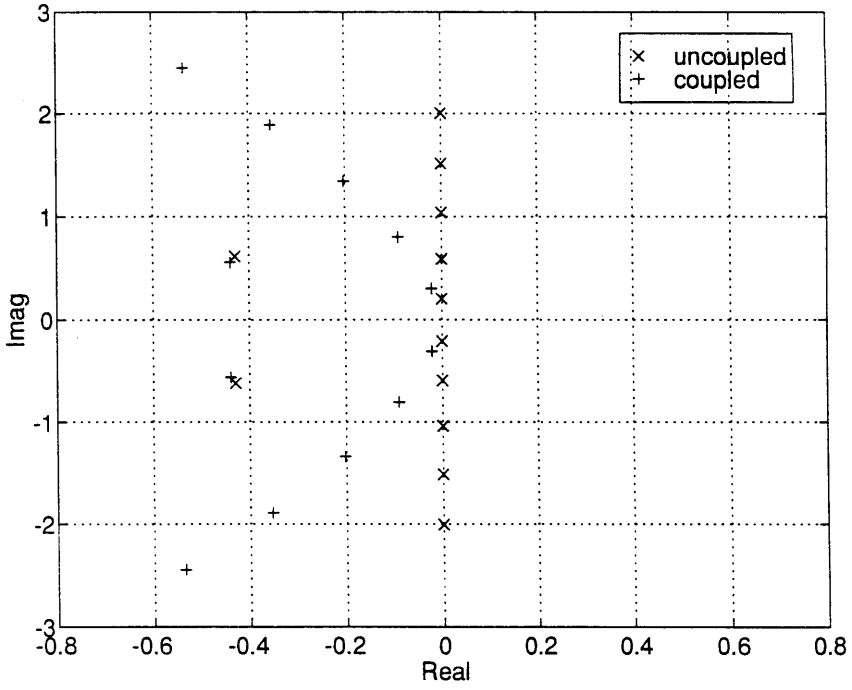

Figure 3.4: Location of eigenvalues of coupled and uncoupled dynamics for the reduced order system, $K_t = 9.333$.

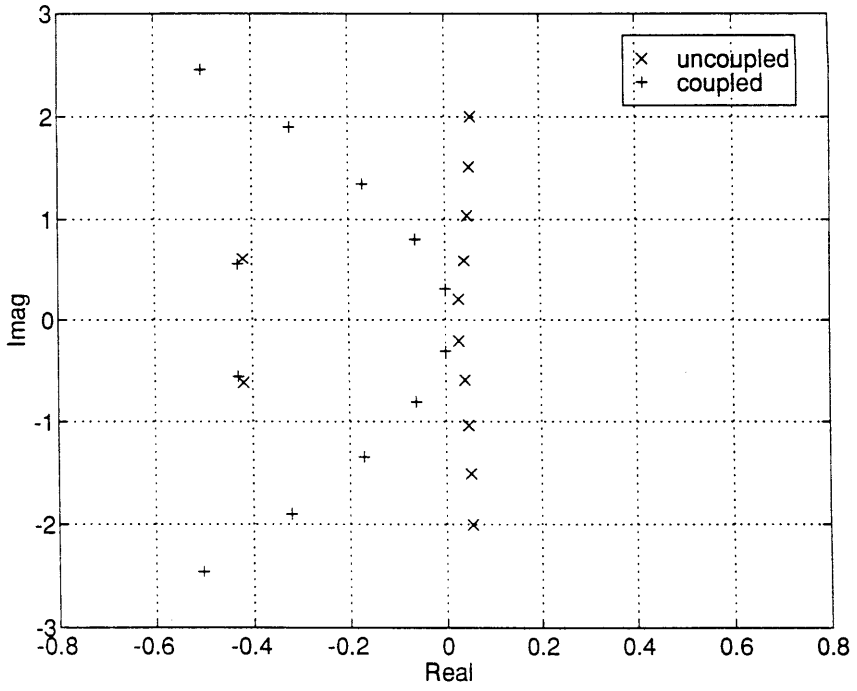

Figure 3.5: Location of eigenvalues of coupled and uncoupled dynamics for the reduced order system, $K_t = 9.515$.

In conclusion of this section, a new state-space representation of rotating stall has been elaborated. Its dimension is 2N+2. The nonlinear system is represented as a feedback connection of a linear dynamical system and a nonlinear element. This representation takes into account the effects of unsteady losses through the location of the eigenvalues of the linear system and a complex control power matrix B.

3.2 Motivations for using Absolute Stability Theory

Our purpose is now to perform a nonlinear stability analysis of the second nonlinear model of rotating stall presented in Section 3.1. The idea that comes naturally to mind is to try using the same approach as in Section 2.2. In that section it was possible to find a Lyapunov function V that made sense physically, and to interpret the sign of its derivative $\dot{V}$ while keeping the perturbation $\underline{\delta\tilde{\phi}}$ very general (it was not necessary to specify its form, i.e its modal content, to conclude on the sign of $\dot{V}$). However, both reasons that made the Lyapunov analysis successful are no longer present. The state-space representation was:

$$\begin{aligned} E\cdot\dot{\underline{\tilde{\phi}}} &= -A\cdot\underline{\tilde{\phi}} + \underline{\tilde{\psi}_c}\left(\underline{\tilde{\phi}}\right) - \underline{T}\cdot\tilde{\bar{\psi}} \\ \dot{\tilde{\bar{\psi}}} &= \frac{1}{4l_c B^2}\left(\underline{S}^T\cdot\underline{\tilde{\phi}} - \tilde{\phi}_T\left(\tilde{\bar{\psi}}\right)\right) \end{aligned} \tag{2.29}$$

To analyze the system, we had to deal with only one nonlinearity $\underline{\tilde{\psi}_c}\left(\underline{\tilde{\phi}}\right)$. The control power matrix in front of this nonlinearity, if treated as a feedback like in Section 3.1, was the identity matrix. The second property of this state-space representation was that A had all eigenvalues on the jω axis. Therefore, with V defined by (2.30), the term involving A canceled out in $\dot{V}$ and $\dot{V}$ took the simple form in (2.31), which had a very straightforward interpretation.

Now, the state-space representation is:

$$\dot{\underline{\tilde{X}}} = A\underline{\tilde{X}} + I\underline{\tilde{H}}_i + R\underline{\tilde{H}}_r + S\underline{\tilde{H}}_s$$

Note that the state $\tilde{\bar{\psi}}$ is included in $\underline{\tilde{X}}$ here. The nonlinearity of the compressor characteristic has been broken into 3 nonlinearities. The control power matrix in front of each one of them is complicated. All modes are actuated differently. A change of variables can make only one out of 3 actuation matrices be the identity. We get for example:

$$E'\dot{\underline{\tilde{X}}} = A'\underline{\tilde{X}} + \underline{\tilde{H}}_i + R'\underline{\tilde{H}}_r + S'\underline{\tilde{H}}_s.$$

Moreover, the eigenvalues of A' are no longer on the jω axis. If our purpose was to keep the same "incremental energy" definition of the Lyapunov function, $V(\underline{\tilde{X}}) = \frac{1}{2M}\underline{\tilde{X}}^T \cdot E' \cdot \underline{\tilde{X}}$, we would get for $\dot{V}$:

$$\dot{V}(\underline{\tilde{X}}) = \frac{1}{M}\underline{\tilde{X}}^T \cdot A' \cdot \underline{\tilde{X}} + \frac{1}{M}\underline{\tilde{X}}^T \cdot (\underline{\tilde{H}}_i + R'\underline{\tilde{H}}_i + S'\underline{\tilde{H}}_s)$$

The first term does not cancel out any more. Because the eigenvalues of A' are no longer on the jω axis and because of the presence of the actuation matrices R' and S', it is not possible to study the sign of $\dot{V}$ without specifying the modal content of $\underline{\tilde{X}}$. The analysis looses its generality and is no longer pertinent.

Consequently, we turn to another method which is derived from the Lyapunov analysis and is well-adapted to the current model of rotating stall: Absolute Stability theory. It applies to nonlinear systems seen as a feedback connection of a linear system and a nonlinear element which is exactly the case here and it provides a new way of dealing with nonlinearities and of finding a suitable Lyapunov function.

3.3 Absolute Stability based Nonlinear Stability Analysis

The reference on absolute stability theory used in this Section is [18]. Notions that are useful for the stability analysis are summarized below. Absolute stability theory applies to nonlinear systems seen as a feedback connection between a linear dynamical system and a nonlinear element such as in Figure 3.1. A state-space representation of the system is:

$$\begin{cases} \dot{\underline{X}} = A\underline{X} + B\underline{U} \\ \underline{Y} = C\underline{X} \\ \underline{U} = -\underline{\Psi}(t,\underline{Y}) \end{cases} \qquad \text{where } \underline{X} \in \mathbf{R}^n,\ \underline{U} \in \mathbf{R}^p,\ \underline{Y} \in \mathbf{R}^p.$$

As usual, the state equations are written in a local coordinate system, such that the origin is located at the equilibrium point whose stability is being studied.

Some assumptions are made which are all verified by the model.

1) [A,B] controllable

2) [A,C] observable

3) $\Psi:[0;+\infty[\times \mathbf{R}^p \rightarrow \mathbf{R}^p$ is a memoryless, possibly time-varying, nonlinearity which is piecewise continuous in t and locally Lipschitz in $\underline{Y}$. Here, Ψ does not depend on t, so the variable t is dropped.

4) The transfer function matrix of the linear system, $G(s) = C(sI - A)^{-1}B$ is a square strictly proper transfer function.

The nonlinearity $\Psi(.)$ is required to satisfy a sector condition globally or locally. In the monodimensional case, the sector condition can be visualized as follows:

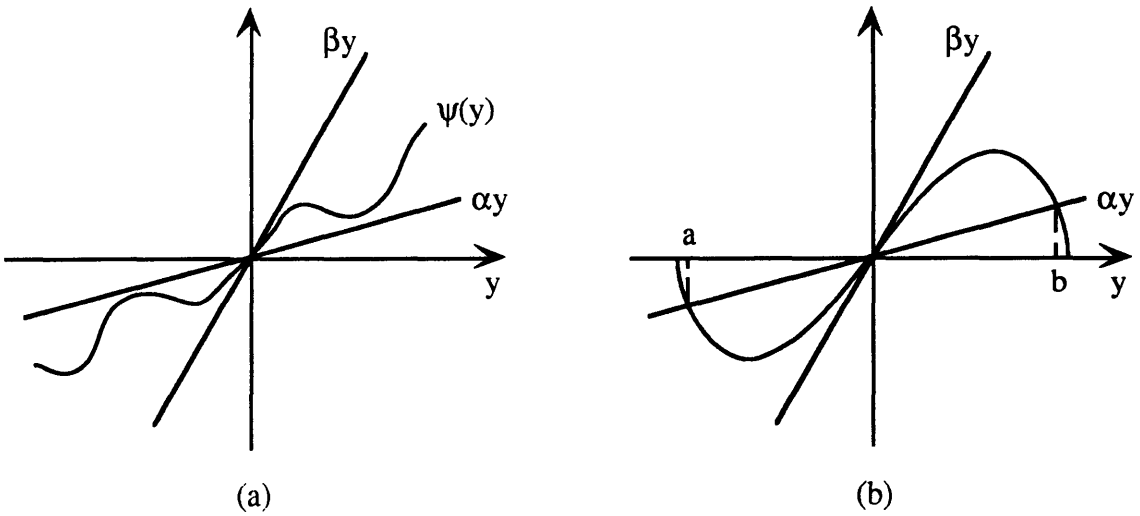

(a) (b)

Figure 3.6: Sector condition satisfied (a) globally, (b) locally over [a;b]

In the multidimensional case, the sector condition takes the form:

$$[\underline{\Psi}(\underline{Y}) - K_{min}\underline{Y}]^T \cdot [\underline{\Psi}(\underline{Y}) - K_{max}\underline{Y}] \leq 0, \forall \underline{Y} \in \Gamma \subset \mathbf{R}^p \qquad (3.34)$$

for some real matrices K_{min} and K_{max}, where $K = K_{max} - K_{min}$ is a symmetric positive definite matrix and the interior of Γ is connected and contains the origin. If $\Gamma = \mathbf{R}^p$, $\underline{\Psi}$ satisfies the sector condition globally.

The purpose of the analysis is to study the asymptotic stability of the origin not for a given nonlinearity but for the entire class of nonlinearities that satisfy a given sector condition. This preserves the generality of the analysis as the Lyapunov analysis did in Section 2.2.

Definition of absolute stability:

> The system is said to be absolutely stable if the origin is asymptotically stable for all nonlinearities satisfying the sector condition (3.34).
>
> The phrase "absolute stability" implies that the sector condition is satisfied globally and that the origin is globally asymptotically stable. Otherwise, the phrase "absolute stability with a finite domain" will be used.

The candidate for Lyapunov function is:

$$V = \underline{X}^T \cdot P \cdot \underline{X}, \quad P = P^T > 0$$

The question that must be addressed now is: is it possible to find P symmetric definite positive such that $\dot{V}(\underline{X}) < 0$ along all trajectories of the system for all nonlinearities that satisfy the sector condition (3.34)? A method to find such a P is given by the Multivariable Circle Criterion whose main steps are recalled here.

Assuming that the nonlinearity satisfies the sector condition (3.34), it is always possible through the loop transformation or pole shifting shown on Figure 3.7 to consider the case

where K_{min} is replaced by 0 and K_{max} by $K=K_{max}-K_{min}$ provided that the state-space representation of the system is modified as follows.

The system whose state-space representation is:

$$\begin{cases} \dot{\underline{X}} = A\underline{X} + B\underline{U} \\ \underline{Y} = C\underline{X} \\ \underline{U} = -\underline{\Psi}(\underline{Y}) \end{cases}$$

and whose nonlinearity satisfies: $\left[\underline{\Psi}(\underline{Y}) - K_{min}\underline{Y}\right]^T \cdot \left[\underline{\Psi}(\underline{Y}) - K_{max}\underline{Y}\right] \leq 0, \forall \underline{Y} \in \Gamma \subset \mathbf{R}^p$

is equivalent to the system whose state-space representation is:

$$\begin{cases} \dot{\underline{X}} = (A - BK_{min}C)\underline{X} + B\underline{U} \\ \underline{Y} = C\underline{X} \\ \underline{U} = -\underline{\Psi}_t(\underline{Y}) \end{cases} \quad \text{with} \quad \underline{\Psi}_t(\underline{Y}) = \underline{\Psi}(\underline{Y}) - K_{min}\underline{Y} \qquad (3.35)$$

and whose nonlinearity satisfies:

$$\left[\underline{\Psi}_t(\underline{Y})\right]^T \cdot \left[\underline{\Psi}_t(\underline{Y}) - K\ \underline{Y}\right] \leq 0, \forall \underline{Y} \in \Gamma \subset \mathbf{R}^p \text{ with } K = K_{max} - K_{min} = K^T > 0 \qquad (3.36)$$

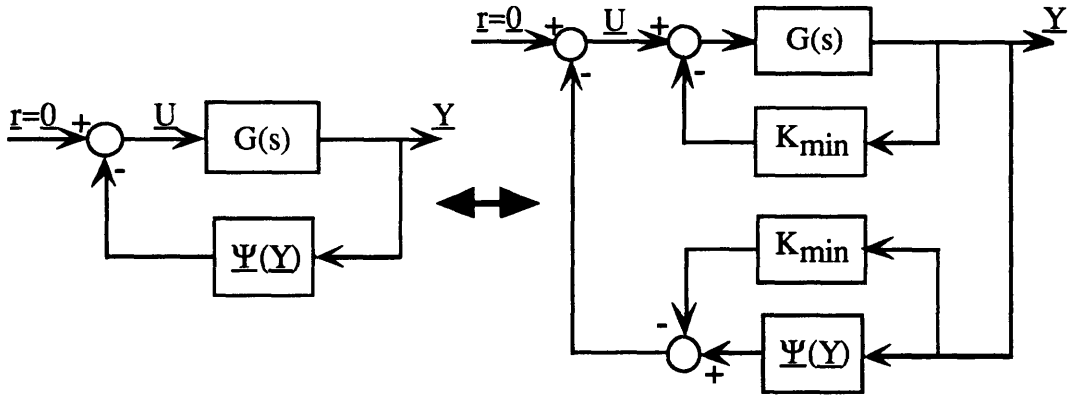

Figure 3.7: Loop transformation

Therefore, we consider now the asymptotic stability of the origin for the system (3.35) and all nonlinearities satisfying sector condition (3.36). The assumption is made that $A' = A - BK_{min}C$ is Hurwitz, i.e. stable (has all eigenvalues in the left half plane). The derivative of $V(\underline{X}) = \underline{X}^T \cdot P \cdot \underline{X}$ along the trajectories of the system is given by:

$$\dot{V}(\underline{X}) = \underline{X}^T \cdot \left(PA' + A'^T P\right) \cdot \underline{X} - 2\underline{X}^T PB\underline{\Psi}_t(\underline{Y})$$

Because of (3.36), $-2\underline{\Psi}_t^T(\underline{Y})\cdot[\underline{\Psi}_t(\underline{Y})-K\underline{Y}]\le 0, \forall \underline{Y}\in\Gamma\subset\mathbf{R}^p$ and its addition to the right hand-side of the last equality gives an upper bound of $\dot{V}(\underline{X})$.

$$\dot{V}(\underline{X})\le \underline{X}^T\cdot\left(PA'+A'^TP\right)\cdot\underline{X}-2\underline{X}^TPB\underline{\Psi}_t(\underline{Y})-2\underline{\Psi}_t^T(\underline{Y})\cdot\left(\underline{\Psi}_t(\underline{Y})-K\underline{Y}\right)$$

$$\dot{V}(\underline{X})\le \underline{X}^T\cdot\left(PA'+A'^TP\right)\cdot\underline{X}+2\underline{X}^T\cdot\left(C^TK-PB\right)\cdot\underline{\Psi}_t(\underline{Y})-2\underline{\Psi}_t^T(\underline{Y})\cdot\underline{\Psi}_t(\underline{Y})$$

Assuming that there exists $P=P^T>0$, L and $\varepsilon>0$ such that:

$$\begin{cases} PA'+A'^TP=-L^TL-\varepsilon P \\ PB=C^TK-\sqrt{2}L^T \end{cases} \tag{3.37}$$

Then, $$\dot{V}(\underline{X})\le -\varepsilon\underline{X}^T\cdot P\cdot\underline{X}-\left[L\underline{X}-\sqrt{2}\underline{\Psi}_t(\underline{X})\right]^T\cdot\left[L\underline{X}-\sqrt{2}\underline{\Psi}_t(\underline{X})\right]$$

and consequently, $$\dot{V}(\underline{X})\le -\varepsilon\underline{X}^T\cdot P\cdot\underline{X}<0$$

Moreover, $V(\underline{X})=\underline{X}^T\cdot P\cdot\underline{X}$ is then positive definite like P.

Thus, provided that we can find $P=P^T>0$, L and $\varepsilon>0$ solutions of Equations (3.37), we can show that $\dot{V}(\underline{X})<0$ for all trajectory $\underline{X}$ and, applying Lyapunov's theorem, the origin is globally asymptotically stable for all nonlinearities satisfying the sector condition (3.34).

Summary of the Multivariable Circle Criterion

Considering a class of nonlinearities $\underline{\Psi}(\underline{Y})$ that satisfy the sector condition

$$[\underline{\Psi}(\underline{Y})-K_{min}\underline{Y}]^T\cdot[\underline{\Psi}(\underline{Y})-K_{max}\underline{Y}]\le 0, \forall \underline{Y}\in\Gamma\subset\mathbf{R}^p$$

with K_{min} and K_{max} real, $K=K_{max}-K_{min}=K^T>0$ and the interior of Γ connected and containing the origin.

If $A-BK_{min}C$ is Hurwitz and if the system:

$$\begin{cases} P(A-BK_{min}C)+(A-BK_{min}C)^TP=-L^TL-\varepsilon P \\ PB=C^T(K_{max}-K_{min})-\sqrt{2}L^T \end{cases} \tag{3.37}$$

has a solution (P,L,ε) such that $P=P^T>0$ and $\varepsilon>0$,

then the system is absolutely stable and a suitable Lyapunov function is given by $V(\underline{X})=\underline{X}^T\cdot P\cdot\underline{X}$. If the sector condition is satisfied only on a set $\Gamma\subset\mathbf{R}^p$, the system is absolutely stable with a finite domain Γ.

By elimination of L, the system of equations (3.37) can be transformed into the following Ricatti equation:

$$A_{ric}{}^{T}P + PA_{ric} - PB_{ric}P + C_{ric} = 0 \qquad (3.38)$$

with

$$A_{ric} = A - \frac{1}{2}B(K_{min} + K_{max})C + \frac{1}{2}\varepsilon I_{2N+2}$$
$$B_{ric} = BR^{-1}B^{T}$$
$$C_{ric} = \frac{1}{2}C^{T}(K_{max} - K_{min})(K_{max} - K_{min})C$$
$$R = -2I_{6N+3}$$

In general, a Ricatti equation has many solutions P but only one of them is symmetric positive definite. A symmetric solution P to the Ricatti equation (3.38) can be constructed by using an eigenvalue decomposition of the Hamiltonian matrix H (see [19]).

$$H = \begin{bmatrix} A_{ric} & -B_{ric} \\ -C_{ric} & -A_{ric}^{T} \end{bmatrix} \qquad (3.39)$$

A key property of H is that if λ is an eigenvalue, so is $-\lambda$.

If $U = \begin{bmatrix} U_{11} & U_{12} \\ U_{21} & U_{22} \end{bmatrix}$ is the matrix of ordered eigenvectors of H, $P = U_{21}U_{11}^{-1}$ is the desired solution. P will be positive definite as soon as H has no eigenvalue on the $j\omega$ axis. This provides a simple test for the existence of the symmetric positive definite solution of the Ricatti equation (3.38).

We can now apply absolute stability theory and multivariable circle criterion to the nonlinear stability analysis of the model of rotating stall with unsteady losses. As an example, we will study compressor C2 of Section 2.4. The state-space representation of the model of rotating stall with unsteady losses is given in Section 3.1.

By definition, $\tilde{\underline{\Psi}}(\tilde{\underline{Y}}) = \begin{bmatrix} \tilde{\underline{H}}_i(\tilde{\underline{\phi}}) \\ \tilde{\underline{H}}_r(\tilde{\underline{\phi}}) \\ \tilde{\underline{H}}_s(\tilde{\underline{\phi}}) \end{bmatrix}$ where $\begin{cases} \tilde{H}_{ik} = \tilde{H}_i(\tilde{\phi}_k) \\ \tilde{H}_{rk} = \tilde{H}_r(\tilde{\phi}_k) \\ \tilde{H}_{sk} = \tilde{H}_s(\tilde{\phi}_k) \end{cases} \forall k \in [0;2N].$

$\tilde{H}_i$, $\tilde{H}_r$ and $\tilde{H}_s$ are functions of a single variable $\tilde{\phi}$. For compressor C2, ψ_i, $L_{ss}^{(r)}$ and $L_{ss}^{(s)}$ are of the form: $p(\phi) = c + d\phi + e\phi^2 + \frac{g}{\phi}$ which implies that to a third order approximation $\tilde{H}_i$, $\tilde{H}_r$and $\tilde{H}_s$ are of the form: $\tilde{p}(\tilde{\phi}) = h\tilde{\phi}^2 + l\tilde{\phi}^3$ with $h = e + \frac{g}{\phi^{*3}}$, $l = -\frac{g}{\phi^{*4}}$.

Therefore, they cannot satisfy any sector condition globally.

The nonlinearities $\tilde{H}_i$, $\tilde{H}_r$ and $\tilde{H}_s$ are shown on Figure 3.8 in the case of the compressor C2 of Section 2.4 for 2 extreme values of the explored range of throttle setting, K_t=9 and K_t=10.6. Both plots exhibit the same trends. The largest contribution in the nonlinear part of the compressor characteristic is due to the rotor. The third order term is negligible in $\tilde{H}_r$ and $\tilde{H}_s$. These functions can be considered even. $\tilde{H}_i$ is not even but it is very flat for positive $\tilde{\phi}$.

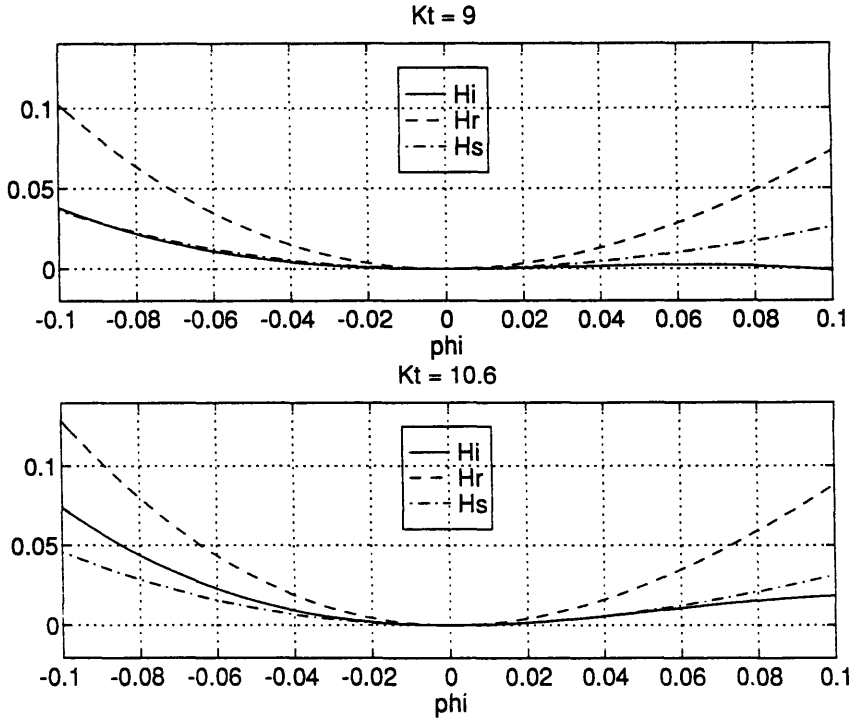

Figure 3.8: Nonlinearities $\tilde{H}_i$, $\tilde{H}_r$ and $\tilde{H}_s$ for K_t=9 and K_t=10.6.

If each one of the nonlinearities $\tilde{H}_i$, $\tilde{H}_r$ and $\tilde{H}_s$ satisfies locally the 1D sector condition:

$$\alpha_\bullet \tilde{\phi} \le \tilde{H}_\bullet\left(\tilde{\phi}\right) \le \beta_\bullet \tilde{\phi} \quad \forall \tilde{\phi} \in [a_\bullet; b_\bullet]$$

$\underline{\tilde{\Psi}}\left(\underline{\tilde{Y}}\right)$ satisfies the multidimensional sector condition in (3.34) with:

$$K_{min} = \begin{bmatrix} \alpha_i I_{2N+1} & & (0) \\ & \alpha_r I_{2N+1} & \\ (0) & & \alpha_s I_{2N+1} \end{bmatrix}$$

$$K_{max} = \begin{bmatrix} \beta_i I_{2N+1} & & (0) \\ & \beta_r I_{2N+1} & \\ (0) & & \beta_s I_{2N+1} \end{bmatrix}$$

$$\Gamma = [a_i; b_i]^{2N+1} \times [a_r; b_r]^{2N+1} \times [a_s; b_s]^{2N+1}$$

and the dimensions of the different matrices are:

A: (2N+2)(2N+2)	B: (2N+2)(6N+3)	C: (6N+3)(2N+2)
$\underline{X}$: (2N+2)(1)	$\underline{Y}$, $\underline{\Psi}$, $\underline{U}$: (6N+3)(1)	
P: (2N+2)(2N+2)	K_{min}, K_{max}: (6N+3)(6N+3)	
R: (6N+3)(6N+3)	A_{ric},B_{ric},C_{ric}: (2N+2)(2N+2)	

Considering a class of nonlinearities $\underline{\Psi}(\underline{Y})$ that satisfy the sector condition (3.34) with K_{min} and K_{max} as given before. In order to show that the system is absolutely stable with the finite domain Γ and that a Lyapunov function of the form $V(\underline{X}) = \underline{X}^T \cdot P \cdot \underline{X}$ is suitable, we must find a solution $P = P^T > 0$ to Equations (3.37) or equivalently to the Ricatti equation (3.38). The Ricatti equation is parameterized by:

$$\varepsilon,\ \alpha_i,\ \beta_i,\ \alpha_r,\ \beta_r,\ \alpha_s \text{ and } \beta_s.$$

The first parameter ε can be considered as a measure of how fast the trajectories converge to the origin since $\dot{V}(\underline{X}) \le -\varepsilon \underline{X}^T \cdot P \cdot \underline{X}$ for all trajectories. Setting ε to a certain value at the beginning of the nonlinear stability analysis will determine the kind of convergence we are looking for. If $\varepsilon \to 0$, we will get a larger domain of attraction for the system but the convergence will be penalized: it will be infinitely slow.

The second group of parameters is still free and comes from the definition of the sector conditions. Its number of parameters can be reduced to 3 if it is assumed that all 3 sectors are symmetric. Then, $\alpha_\bullet = -\beta_\bullet$ for $\bullet = i,r,s$. This assumption is valid for the compressor we are studying: compressor C2 since all 3 nonlinearities are flat or close to be even functions of $\tilde{\phi}$.

If we can prove that the system is absolutely stable with the finite domain Γ for a given sector condition, i.e. a given set $(\beta_i,\beta_r,\beta_s)$, the next step of the analysis is to find the largest sector condition, i.e. the sector condition with the set of largest β's and the largest domain of validity Γ, under which the system is still absolutely stable. Then, Γ defines the domain of attraction of the origin or equilibrium point.

Recall that a simple test of existence of the symmetric positive definite solution P of the Ricatti equation is: the Hamiltonian matrix H defined by Equation (3.39) has no eigenvalue on the $j\omega$ axis. Thus, the nonlinear stability analysis of compressor C2 proceeds as follows:

1) Choose ε, i.e. the speed of convergence of the trajectories.

2) Start with a large value of β_r.

3) Construct all 3 sector conditions from the only parameter β_r:

   * $\alpha_r = -\beta_r$

   * α_i and α_s are chosen so that $a_i = a_r = a_s$ as shown on Figure 3.9.

   * $\beta_i = -\alpha_i$ and $\beta_s = -\alpha_s$

4) Test H. If H has still some eigenvalues on the $j\omega$ axis, β_r is decreased and we go back to step 3. Otherwise, we have found the largest β_r such that the symmetric positive definite solution P of the Ricatti equation exists and the largest finite domain Γ over which the system is absolutely stable.

The result of the iteration $\Gamma = [a_i;b_i]^{2N+1} \times [a_r;b_r]^{2N+1} \times [a_s;b_s]^{2N+1}$ defines the region of negative $\dot{V}$ around the origin in the local coordinate system or equivalently around the equilibrium point (see Figure 3.6 for definition of $[a_\bullet;b_\bullet]$). The size of Γ (previously called Ω) defined as the distance of its boundary surface to the origin and is again called d. Here,

$$d = \min(|a_i|,|b_i|,|a_r|,|b_r|,|a_s|,|b_s|).$$

Rigorously, the domain of attraction of the equilibrium point is found by fitting the biggest ellipsoid $D_c = \{\underline{x} \mid V(\underline{x}) = c\}$ inside Γ and its size is c. However, as in Section 2.3, we prefer to use d as an estimate of the size of domain of attraction because c is dependent on V through P. d is not and makes sense physically: it is again a flow coefficient. Therefore, d's calculated at the same equilibrium point but using different methods can be compared whereas c's cannot. For example, in a next section we are going to introduce different basic controllers and for each controlled system apply the above nonlinear stability analysis iteration and calculate d. We will be able to compare the different d's but it does not make sense to compare the c's since in each case the P matrix we get is different.

Figure 3.9 (for which K_t=9) helps validating the choice made in step 3 of construction of all 3 sector conditions from the only parameter β_r so that $a_i = a_r = a_s$. It presents on 3 separate plots the nonlinearities $\tilde{H}_i$, $\tilde{H}_r$ and $\tilde{H}_s$ and the corresponding sector conditions resulting from the nonlinear stability analysis iteration. The dotted vertical lines picture the boundaries $\tilde{\phi} = -d$ and $\tilde{\phi} = +d$ of the hypercube $[-d;d]^{6N+3}$. Because of the shapes of $\tilde{H}_i$, $\tilde{H}_r$ and $\tilde{H}_s$, the hypercube is then very tightly fitted inside Γ. This constitutes a good configuration for the calculation of d: it will lead to greater d than for another configuration where a lot of space is wasted in some direction between the hypercube and Γ. For example, using the construction described in step 3 we get: d=0.0147. If all 3 sector conditions use the same α and β ($\alpha_i = \alpha_r = \alpha_s = -\beta_i = -\beta_r = -\beta_s$) then d=0.0093 and the interval [-d;+d] is much smaller than both $[a_i;b_i]$ and $[a_s;b_s]$. Therefore, an analogy can be made between the property that the result d of the iteration is larger if the set of parameters

$(\beta_i,\beta_r,\beta_s)$ is defined so that the hypercube $[-d;d]^{6N+3}$ is tightly fitted inside Γ and the property of Section 2.3 that the size of domain of attraction d is larger if the ellipsoid $D_c = \{\underline{x} \mid V(\underline{x}) = c\}$ is tightly fitted inside Ω. Since we are free to choose the way to define the set of parameters $(\beta_i,\beta_r,\beta_s)$, it makes sense to select the method that will lead to the largest d and the one described in step 3 is the best we have found.

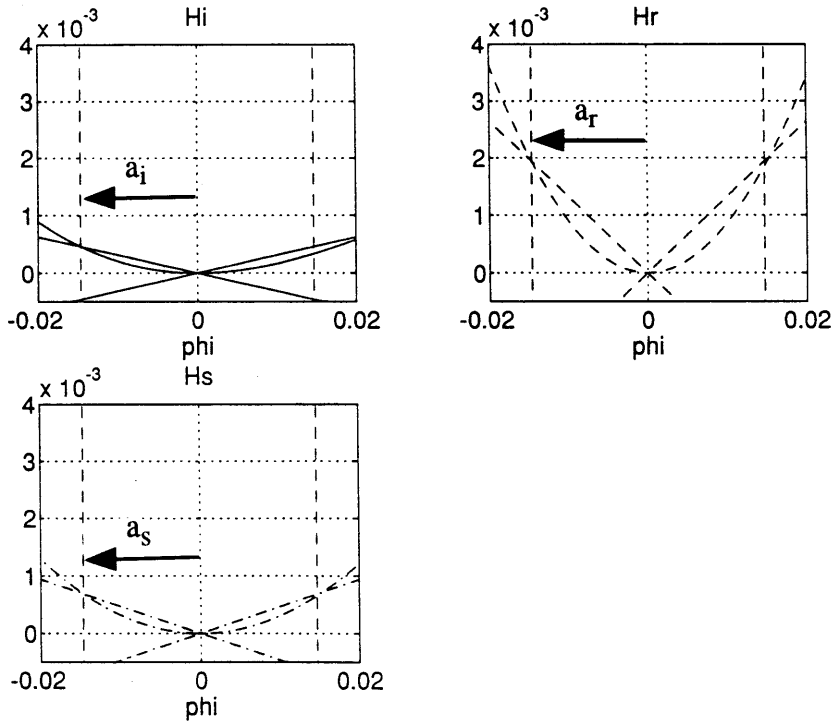

Figure 3.9: Nonlinearities $\tilde{H}_i$, $\tilde{H}_r$ and $\tilde{H}_s$ and the corresponding sector conditions resulting from the nonlinear stability analysis iteration for K_t=9.

In conclusion, a method has been developed using absolute stability theory to calculate d the size of domain of attraction of an operating (equilibrium) point on the compressor characteristic. For now, no assumption has been made about the linear stability of the considered operating point. We will see in the next section that for a linearly unstable operating point the Ricatti equation cannot be solved even when the 3 sectors are infinitely small ($\beta_r \to 0$). d is then 0. Except from the details of the construction of all 3 sector

conditions from the only parameter β_r in step 3, the ideas of the nonlinear stability analysis iteration apply to any compressor.

3.4 Validation of the Absolute Stability based Nonlinear Stability Analysis

The absolute stability based nonlinear stability analysis of Section 3.3 results from a theory and has no direct physical interpretation. The Lyapunov function it generates comes from some computation: resolution of a Ricatti equation and is not obviously energy-like. Comparing its result, the size of domain of attraction d, with the same quantity calculated by the Lyapunov based nonlinear stability analysis of Section 2.2 for compressor C2 of Section 2.4 would validate the absolute stability method because the Lyapunov one has proven to be physically meaningful. This validation is the purpose of the present Section.

In Chapter 2 the model of rotating stall did not include unsteady losses. Therefore, we have first to derive a state-space representation of rotating stall of the form:

$$\begin{cases} \dot{\tilde{\underline{X}}} = A\tilde{\underline{X}} + B\tilde{\underline{U}} \\ \tilde{\underline{Y}} = C\tilde{\underline{X}} \\ \tilde{\underline{U}} = -\tilde{\underline{\Psi}}\left(t, \tilde{\underline{Y}}\right) \end{cases} \qquad \text{where } \tilde{\underline{X}} \in \mathbf{R}^n,\ \tilde{\underline{U}} \in \mathbf{R}^p,\ \tilde{\underline{Y}} \in \mathbf{R}^p,$$

i.e. that is suitable for application of absolute stability theory, but which does not take into account unsteady losses. This is very straightforward. We just need to:

1) Recall the DFT form of the 2N+2 equations of rotating stall:

Equations (2.13) and (2.14) and the second equation in (2.2) directly written in the local coordinate system.

2) Decompose the compressor characteristic into linear and nonlinear parts:

$$\tilde{\psi}_c\left(\tilde{\phi}\right) = D_c\tilde{\phi} + \tilde{H}_c\left(\tilde{\phi}\right)$$

3) Linearize the throttle characteristic

$$\tilde{\phi}_T\left(\tilde{\bar{\psi}}\right) = \sqrt{\frac{1}{2K_t\bar{\psi}^*}}\cdot\tilde{\bar{\psi}}$$

4) Define again $d_n = \begin{cases} \frac{m}{|n|}+\mu, & \text{for } n \neq 0 \\ l_c, & \text{for } n = 0 \end{cases}$ as the (n+N+1)th element on the diagonal of the matrix D_E.

Through these steps, we get:

$$\underline{n\neq 0} \qquad \dot{\hat{\tilde{\phi}}}_n = \frac{(D_c - i\lambda n)}{d_n}\cdot\hat{\tilde{\phi}}_n + \frac{1}{d_n}\hat{\tilde{H}}_{cn} \tag{3.40}$$

$$\underline{n=0} \qquad \begin{cases} \dot{\hat{\tilde{\phi}}}_0 = \frac{D_c}{d_0}\hat{\tilde{\phi}}_0 - \frac{\sqrt{2N+1}}{d_0}\tilde{\bar{\psi}} + \frac{1}{d_0}\hat{\tilde{H}}_{c0} \\ \dot{\tilde{\bar{\psi}}} = \frac{1}{4B^2 l_c\sqrt{2N+1}}\hat{\tilde{\phi}}_0 - \frac{1}{4B^2 l_c\sqrt{2K_t\bar{\psi}^*}}\tilde{\bar{\psi}} \end{cases} \tag{3.41}$$

Equations (3.41) take the matrix form:

$$\begin{bmatrix} \dot{\hat{\tilde{\phi}}}_0 \\ \dot{\tilde{\bar{\psi}}} \end{bmatrix} = \underbrace{\begin{bmatrix} * & * \\ * & * \end{bmatrix}}_{\Lambda_a^0}\begin{bmatrix} \hat{\tilde{\phi}}_0 \\ \tilde{\bar{\psi}} \end{bmatrix} + \underbrace{\begin{bmatrix} * \\ * \end{bmatrix}}_{\Lambda_c^0}\hat{\tilde{H}}_{c0}$$

Defining the same state vector $\hat{\underline{\tilde{X}}} = \begin{bmatrix} \vdots & \\ \hat{\tilde{\phi}}_n & n=-N \\ \vdots & \\ \hat{\tilde{\phi}}_0 & n=-1 \\ \tilde{\bar{\psi}} & n=0 \\ \vdots & n=0 \\ \hat{\tilde{\phi}}_n & n=+1 \\ \vdots & n=+N \end{bmatrix}$ and the same matrix F_{ext} as in Section 3.1

so that $\dot{\hat{\underline{\tilde{X}}}} = F_{ext}\underline{\tilde{X}}$, Equations (3.40) and (3.41) can be written in a matrix form:

$$\dot{\hat{\underline{\tilde{X}}}} = \Lambda_a\hat{\underline{\tilde{X}}} + \Lambda_c\hat{\underline{\tilde{H}}}_c \tag{3.42}$$

with:
$$\Lambda_a = \begin{bmatrix} \ddots & & & & \\ & \frac{D_c - i\lambda n}{d_n} & & (0) & \\ & & \ddots & & \\ & & \left.\begin{bmatrix} ** \\ ** \end{bmatrix}\right\}\Lambda_a^0 & & \\ & & & \ddots & \\ & (0) & & \frac{D_c - i\lambda n}{d_n} & \\ & & & & \ddots \end{bmatrix} \begin{matrix} n=-N \\ \\ n=-1 \\ n=0 \\ n=0 \\ n=+1 \\ \\ n=+N \end{matrix}$$

and
$$\Lambda_c = \begin{bmatrix} \ddots & & & & \\ & \frac{1}{d_n} & & (0) & \\ & & \ddots & & \\ & & \left.\begin{bmatrix} * \\ * \end{bmatrix}\right\}\Lambda_c^0 & & \\ & & & \ddots & \\ & (0) & & \frac{1}{d_n} & \\ & & & & \ddots \end{bmatrix}$$

with dimension(Λ_a)= (2N+2)(2N+2) and dimension(Λ_c)= (2N+2)(2N+1).

Multiplying (3.42) on the left by F_{ext}^T we get:

$$\dot{\underline{\tilde{X}}} = F_{ext}^T \Lambda_a F_{ext} \underline{\tilde{X}} + F_{ext}^T \Lambda_c F_{ext} \underline{\tilde{H}}_c$$

Finally, if
$$\begin{cases} A = F_{ext}{}^T \Lambda_a F_{ext} \\ B = -F_{ext}{}^T \Lambda_c F \end{cases}$$

$$\underline{\tilde{Y}} = C\underline{\tilde{X}} = \underline{\tilde{\phi}} \qquad C = [I_{2N+1} \;\; \underline{0}]$$

$$\underline{\tilde{\Psi}}(\underline{\tilde{Y}}) = \underline{\tilde{H}}_c(\underline{\tilde{\phi}}), \qquad \underline{\tilde{U}} = -\underline{\tilde{\Psi}},$$

a state-space representation of the system of dimension 2N+2 is:

$$\begin{cases} \dot{\underline{\tilde{X}}} = A\underline{\tilde{X}} + B\underline{\tilde{U}} \\ \underline{\tilde{Y}} = C\underline{\tilde{X}} \\ \underline{\tilde{U}} = -\underline{\tilde{\Psi}}(\underline{\tilde{Y}}) \end{cases} \tag{3.43}$$

Then, the nonlinear stability analysis iteration based on absolute stability theory can be applied to the model of rotating stall without unsteady losses in a suitable form (3.43). It has to deal with only one nonlinearity $\tilde{H}_c(\tilde{\phi})$ which is symmetric for compressor C2. Therefore, the assumption $\alpha_c = -\beta_c$ is valid and there is no ambiguity in the construction of the sector condition. The iteration is simply done over β_c. Here, $d = b_c$. Using this method, the size of domain of attraction d is calculated for different operating points $(\overline{\phi}^*, \overline{\psi}^*)$ along the characteristic corresponding to a range of K_t from 8.5 to 9.5 and plotted as a function of $\overline{\phi}^*$, this is the dashed line on Figure 3.10. Meanwhile, the nonlinear stability analysis based on a Lyapunov analysis and presented in Section 2.2 is applied also to the model of rotating stall without unsteady losses. d is calculated for the same range of operating points and plotted on the same figure, this is the solid line in the figure. Figure 3.20 shows also the location of the peak of the compressor characteristic by a dashdotted vertical line.

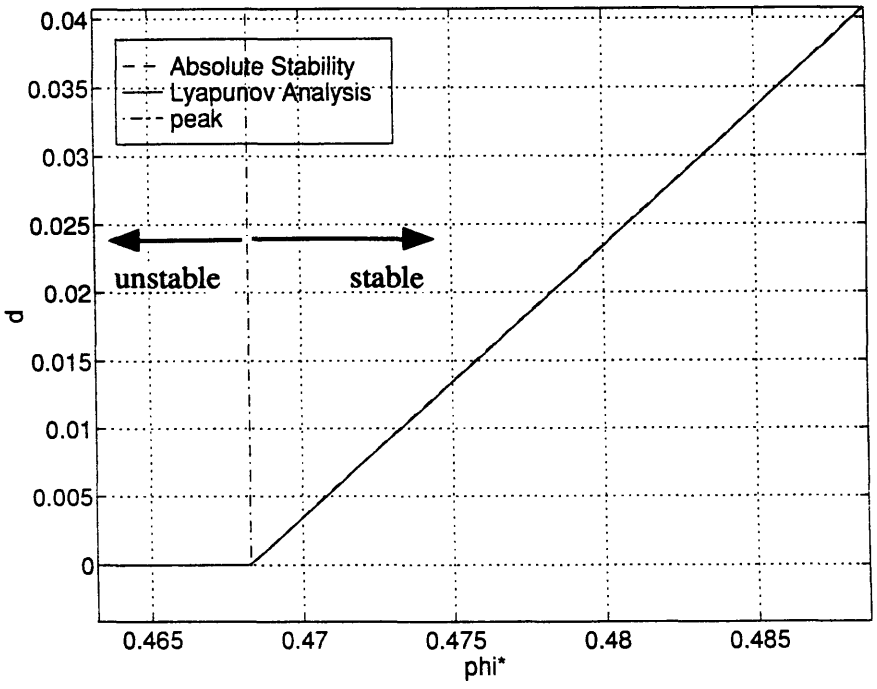

Figure 3.10: Comparison of Absolute Stability and Lyapunov based nonlinear stability analysis, evolution of d as the operating point moves along the compressor characteristic.

From this figure, there is obviously an excellent agreement between the 2 methods. Both curves go to 0 at the peak and are consistent with the linear stability theory: they show that in absence of perturbations the compressor goes unstable when the operating point reaches the peak of the characteristic. Even if the absolute stability method did not make any assumption on the linear stability of the operating point, it turns out that as soon as the operating point is linearly unstable the Ricatti equation cannot be solved out even for a very small β_c. The iteration stops when $\beta_c = 0$ and then $d = 0$.

In conclusion, the results shown on Figure 3.10 validate the absolute stability based nonlinear stability analysis by comparison with the Lyapunov based nonlinear stability analysis and consequently the absolute stability method appears to be as physically meaningful as the Lyapunov analysis.

3.5 Application of Absolute stability based Nonlinear Stability Analysis: Comparison of two Linear Controllers.

The purpose of this section is to introduce some basic linear controller in the nonlinear model of rotating stall with unsteady losses presented in Section 3.1 and to study how the presence of the controller modifies the function d, size of domain of attraction, as the operating point moves to the left along the compressor characteristic. The effects of 2 different linear controllers will be compared: a simple constant-gain feedback and a H_∞ controller. The compressor we will use is again compressor C2 of Section 2.4.

The nonlinear system of Section 3.1 is represented as a negative feedback connection of a linear dynamical system and a nonlinear element which contains all 3 nonlinearities due to the compressor characteristic. The linear control is wrapped around the linear system. Then, Figure 3.1 becomes Figure 3.11.

The linear controllers that are considered here stabilize the first 2 modes of rotating stall up to the throttle setting $K_t = 10.6$ for which the third mode becomes unstable.

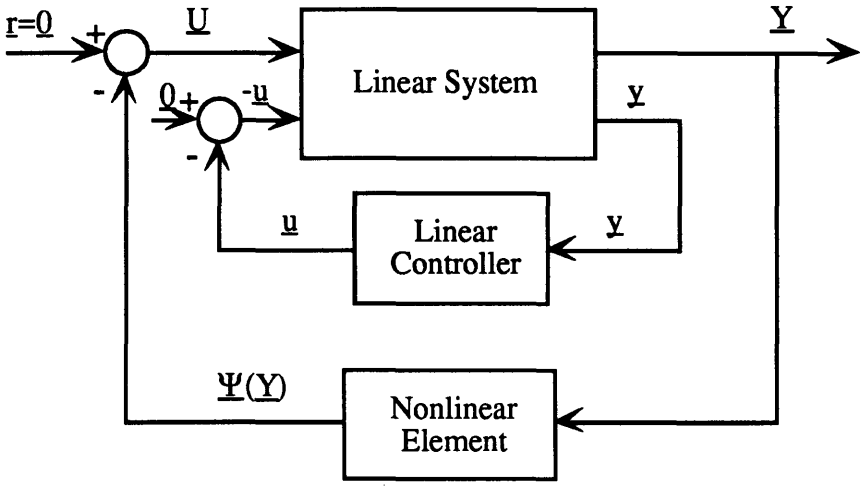

Figure 3.11: Linear control of the nonlinear model of rotating stall with unsteady losses

First linear controller: constant-gain feedback on the first 2 modes

A state-space representation of the uncontrolled linear system is given in Section 3.1 and takes the usual form:

$$\begin{cases} \dot{\tilde{X}} = A\tilde{X} + B\tilde{U} \\ \tilde{Y} = C\tilde{X} \end{cases}$$

The current controller modifies the eigenvalues of A for the first 2 modes. Using the notations of Section 3.1, the constant gains k_1 and k_2 applied respectively to the 1st and the 2nd modes are evaluated at $K_t = 10.6$ and defined by:

$$\begin{cases} k_1 = \text{real}\left(\lambda_1^{(1)}\right) \\ k_2 = \text{real}\left(\lambda_1^{(2)}\right) \end{cases}.$$

Then, for all K_t the closed-loop linear system has same eigenvalues as the open-loop one, except that:

$$\lambda_1^{(\pm 1)}{}_{C.L.} = \lambda_1^{(\pm 1)}{}_{O.L.} + k_1$$
$$\lambda_1^{(\pm 2)}{}_{C.L.} = \lambda_1^{(\pm 2)}{}_{O.L.} + k_2$$

The locations of both the open-loop and closed-loop eigenvalues of the linear system are shown on Figure 3.12 for K_t=10.6 (Figure 3.12 also shows the eigenvalues of the uncoupled dynamics of the model as in Section 3.1). By definition, the first 3 modes of the closed-loop linear system are neutrally stable for K_t=10.6 and stable for K_t<10.6.

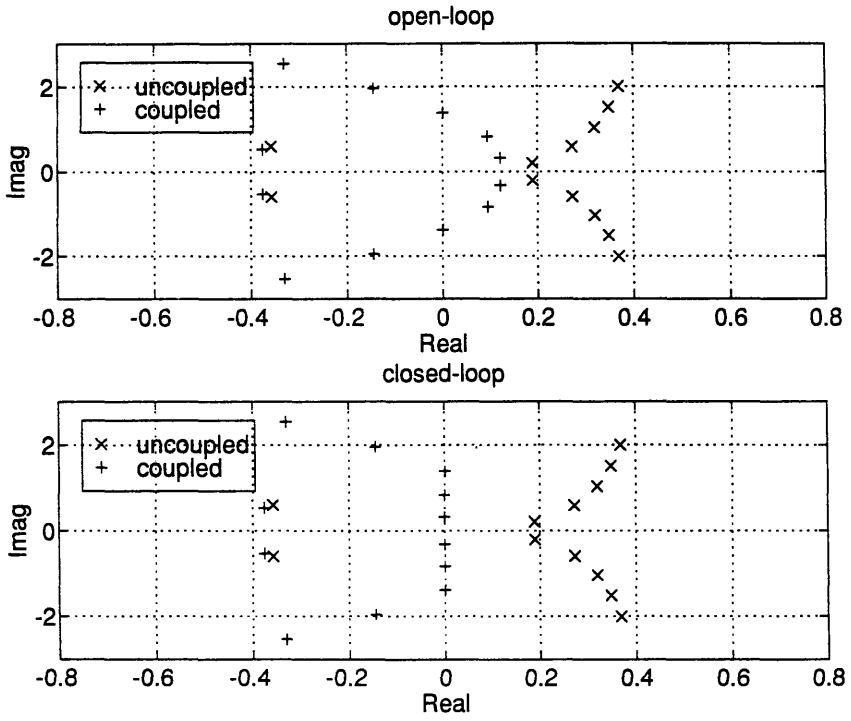

Figure 3.12: First linear controller: constant-gain feedback on first 2 modes, Eigenvalues of the open-loop and closed-loop linear systems for K_t=10.6.

Then, the absolute stability based nonlinear stability analysis of Section 3.3 is applied to the overall controlled system. The size of domain of attraction d is calculated for different operating points $(\bar{\phi}^*, \bar{\psi}^*)$ along the compressor characteristic corresponding to a range of K_t from 8.5 to 11.5 and plotted as a function of $\bar{\phi}^*$: solid line on Figure 3.13. The d function for the controlled system can be compared with the same d function for the

uncontrolled system which was calculated in Section 3.4 and is recalled by a dashed line on Figure 3.13. Figure 3.13 also shows by 4 successive dashdotted vertical lines the position of the peak of the compressor characteristic and where the first 3 uncontrolled modes become unstable.

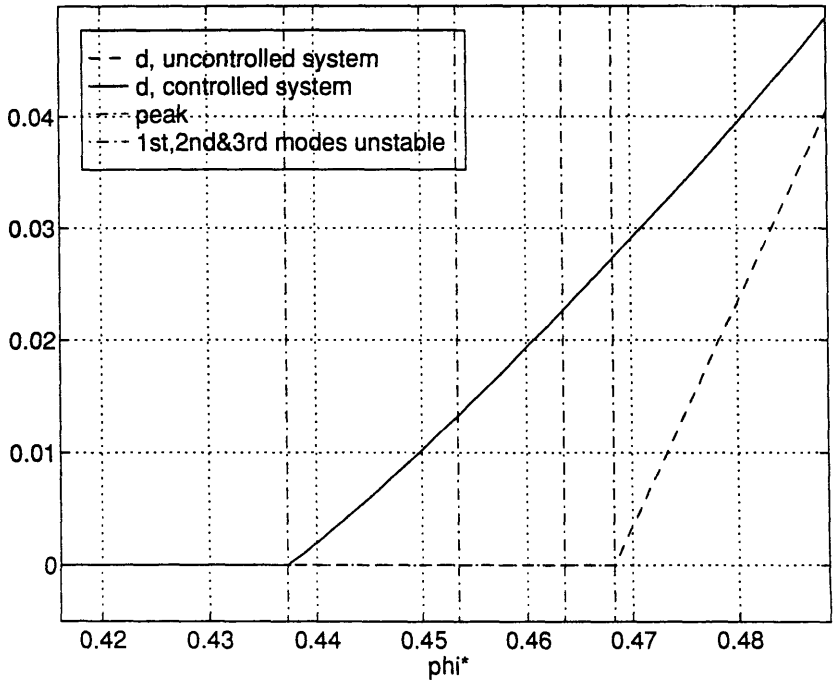

Figure 3.13: First linear controller: constant-gain feedback on first 2 modes, Size of domain of attraction d as the operating point moves along the compressor characteristic.

As expected, the d function for the controlled system is strictly positive for $K_t < 10.6$ or $\bar{\phi}^* > 0.4373$, i.e. as long as all modes are stable, and goes to 0 exactly at the neutral stability point $\bar{\phi}^* = 0.4373$ (which is simultaneous for modes 1, 2 and 3). This shows that in absence of perturbations the compressor will go unstable when the operating point reaches the flow coefficient $\bar{\phi}^* = 0.4373$ against $\bar{\phi}^* = 0.4683$ for the uncontrolled system. The range of linearly stable flow coefficients has been extended by a factor of 6.6%. Comparing both d functions, we can see that introducing this basic linear control has

dramatically increased the size of domain of attraction of the system as the operating point gets close to the peak and has even made it finite (strictly positive) instead of 0 in the range $0.4373 < \overline{\phi}^* \leq 0.46825$. Until its neutral stability point, the controlled system is much more robust as regards perturbations, i.e. much more stable nonlinearly speaking, than the uncontrolled system was. In that sense, the current linear control is very successful.

Second linear controller: H_∞ controller of the first 2 modes

A very rough dynamic compensator has been designed using the H_∞ algorithm in Matlab. Its purpose is to guarantee closed-loop stability and to reject worst case disturbances. Since the nonlinear model of rotating stall with unsteady losses does not include actuator dynamics nor delays and will involve only a simplified actuation, there is no need to design an elaborate H_∞ controller. The one we are considering is of second order mode by mode and is not optimized in frequency: no frequency weighting has been used. Again, the first 2 modes are controlled separately and the H_∞ controller is designed so that the first 3 modes are simultaneously neutrally stable at $K_t = 10.6$.

A state-space representation of the H_∞ controller is:

$$\begin{cases} \begin{bmatrix} \dot{\underline{z}}_1 \\ \dot{\underline{z}}_2 \end{bmatrix} = \begin{bmatrix} A_1 & 0 \\ 0 & A_2 \end{bmatrix} \begin{bmatrix} \underline{z}_1 \\ \underline{z}_2 \end{bmatrix} + \begin{bmatrix} B_1 & 0 \\ 0 & B_2 \end{bmatrix} \begin{bmatrix} \underline{y}_1 \\ \underline{y}_2 \end{bmatrix} \\ \begin{bmatrix} \underline{u}_1 \\ \underline{u}_2 \end{bmatrix} = \begin{bmatrix} C_1 & 0 \\ 0 & C_2 \end{bmatrix} \begin{bmatrix} \underline{z}_1 \\ \underline{z}_2 \end{bmatrix} + \begin{bmatrix} D_1 & 0 \\ 0 & D_2 \end{bmatrix} \begin{bmatrix} \underline{y}_1 \\ \underline{y}_2 \end{bmatrix} \end{cases} \tag{3.44}$$

where $\underline{z}_\bullet$, $\underline{y}_\bullet$ and $\underline{u}_\bullet$ are vectors of dimension 2.

An open-loop state-space representation of the linear dynamical element is:

$$\begin{aligned} \dot{\tilde{\underline{X}}} &= A\tilde{\underline{X}} + \begin{bmatrix} F_1 & F_2 \end{bmatrix} \begin{bmatrix} -\underline{u}_1 \\ -\underline{u}_2 \end{bmatrix} + B\tilde{\underline{U}} \\ \begin{bmatrix} \underline{y}_1 \\ \underline{y}_2 \end{bmatrix} &= \begin{bmatrix} G_1 \\ G_2 \end{bmatrix} \tilde{\underline{X}} \\ \tilde{\underline{Y}} &= C\tilde{\underline{X}} \end{aligned} \tag{3.45}$$

The inputs and outputs of the controller are:

$$\underline{y}_1 = \begin{bmatrix} \text{Real}\left(\hat{\tilde{\phi}}_{-1}\right) \\ \text{Imag}\left(\hat{\tilde{\phi}}_{-1}\right) \end{bmatrix} \qquad \underline{u}_1 = \begin{bmatrix} \text{Real}\left(\hat{\tilde{\gamma}}_{-1}\right) \\ \text{Imag}\left(\hat{\tilde{\gamma}}_{-1}\right) \end{bmatrix}$$

$$\underline{y}_2 = \begin{bmatrix} \text{Real}\left(\hat{\tilde{\phi}}_{-2}\right) \\ \text{Imag}\left(\hat{\tilde{\phi}}_{-2}\right) \end{bmatrix} \qquad \underline{u}_2 = \begin{bmatrix} \text{Real}\left(\hat{\tilde{\gamma}}_{-2}\right) \\ \text{Imag}\left(\hat{\tilde{\gamma}}_{-2}\right) \end{bmatrix}$$

where $\hat{\tilde{\phi}}_\bullet$ is nondimensional, $\underline{y}_\bullet$ is in m/s, $\underline{u}_\bullet$ in degrees and $\hat{\tilde{\gamma}}_\bullet$ in radians (γ is the stagger angle of the servo-controlled guide vanes).

Therefore, G_1 and G_2 are given by:

$$G_1 = \frac{U}{2}\begin{bmatrix} 1 & 1 \\ -i & +i \end{bmatrix}\begin{bmatrix} (F_{ext})_{N^{th}\text{row}} \\ (F_{ext})_{(N+3)^{th}\text{row}} \end{bmatrix}$$

$$G_2 = \frac{U}{2}\begin{bmatrix} 1 & 1 \\ -i & +i \end{bmatrix}\begin{bmatrix} (F_{ext})_{(N-1)^{th}\text{row}} \\ (F_{ext})_{(N+4)^{th}\text{row}} \end{bmatrix}$$

where U is the rotor speed and

$$\begin{bmatrix} \hat{\tilde{\gamma}}_{-\bullet} \\ \hat{\tilde{\gamma}}_\bullet \end{bmatrix} = \frac{\pi}{180}\begin{bmatrix} 1 & +i \\ 1 & -i \end{bmatrix}\underline{u}_\bullet$$

We use a simplified actuation: for n=±1 and n=±2, Equation (3.27) of the model of rotating stall with unsteady losses is replaced by:

$$\dot{\hat{\tilde{\phi}}}_n = \lambda_1 \hat{\tilde{\phi}}_n + \left[\frac{1}{d_n}\frac{\partial \psi_c}{\partial \gamma}\left(\bar{\phi}^*\right)\right]\hat{\tilde{\gamma}}_n + \frac{v_{11}w_{11}}{d_n}\hat{\tilde{H}}_{in} + \frac{v_{11}w_{14}}{\tau}\hat{\tilde{H}}_{rn} + \frac{v_{11}w_{15}}{\tau}\hat{\tilde{H}}_{sn}$$

For compressor C2, the function $\frac{\partial \psi_c}{\partial \gamma}(\phi)$ is found in [17]:

$$\frac{\partial \psi_c}{\partial \gamma}(\phi) = 0.8251 - 3.655\phi + 2.888\phi^2$$

if $f_\bullet = \frac{1}{d_\bullet}\frac{\partial \psi_c}{\partial \gamma}\left(\bar{\phi}^*\right)$, the actuation matrices F_1 and F_2 are given by:

$$F_1 = F_{ext}^T \begin{bmatrix} (0) \\ [f_1 \ 0] \\ (0) \\ [0 \ f_1] \\ (0) \end{bmatrix} \begin{matrix} \\ (N^{th}\text{row}) \\ \\ ((N+3)^{th}\text{row}) \\ \end{matrix} \cdot \frac{\pi}{180}\begin{bmatrix} 1 & +i \\ 1 & -i \end{bmatrix}$$

$$\text{and} \qquad F_2 = F_{ext}^T \begin{bmatrix} (0) \\ [f_2 \;\; 0] \\ (0) \\ [0 \;\; f_2] \\ (0) \end{bmatrix} \begin{matrix} \\ \left((N-1)^{th}\text{row}\right) \\ \\ \left((N+4)^{th}\text{row}\right) \\ \\ \end{matrix} \cdot \frac{\pi}{180} \begin{bmatrix} 1 & +i \\ 1 & -i \end{bmatrix}$$

Combining (3.44) and (3.45), we get the following closed-loop state-space representation for the linear dynamical element:

$$\begin{bmatrix} \dot{\tilde{X}} \\ \dot{z}_1 \\ \dot{z}_2 \end{bmatrix} = \underbrace{\begin{bmatrix} A - F_1D_1G_1 - F_2D_2G_2 & -F_1C_1 & -F_2C_2 \\ B_1G_1 & A_1 & 0 \\ D_2G_2 & 0 & A_2 \end{bmatrix}}_{A_{C.L.}} \begin{bmatrix} \tilde{X} \\ z_1 \\ z_2 \end{bmatrix} + \underbrace{\begin{bmatrix} B \\ 0 \\ 0 \end{bmatrix}}_{B_{C.L.}} \tilde{U}$$

$$\tilde{Y} = \underbrace{[C \;\; 0 \;\; 0]}_{C_{C.L.}} \begin{bmatrix} \tilde{X} \\ z_1 \\ z_2 \end{bmatrix}$$

The system is now of dimension 2N+6. Figure 3.14 shows the effect of the introduction of the H_∞ controller on the location of the eigenvalues of the linear component of the system for K_t=9.333 (at the peak). Eigenvalues of open-loop and closed-loop linear systems are marked by "o" and "x" respectively and those of the H_∞ controller by "+". Closing the loop stabilizes the first 2 modes and does not move the eigenvalues of the controller.

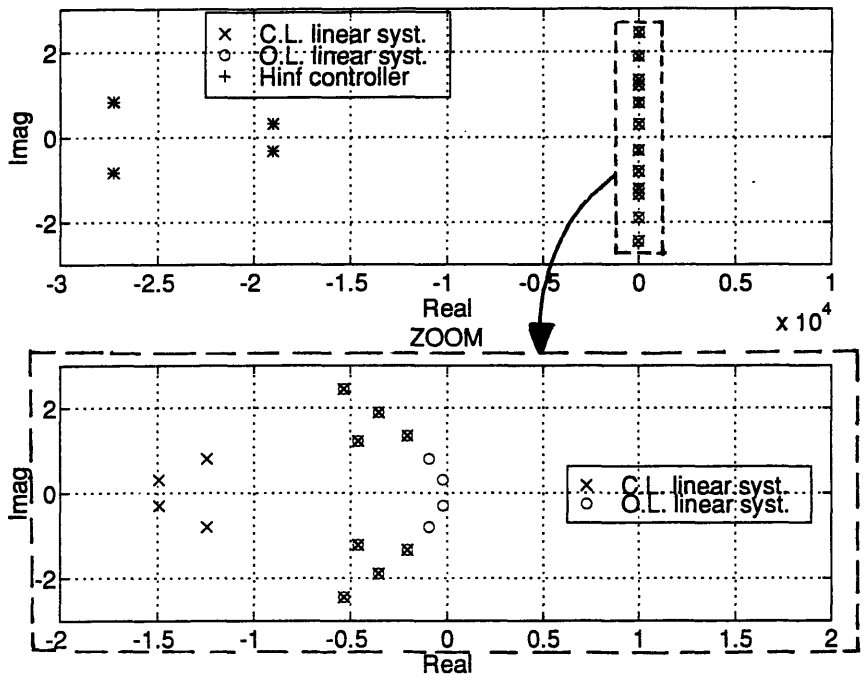

Figure 3.14: Second linear controller: H_∞ controller on the first 2 modes, Eigenvalues of the controller and both open-loop and closed-loop linear systems for $K_t = 9.333$.

Next, the absolute stability based nonlinear stability analysis of Section 3.3 is applied to the overall closed-loop system. System matrices $A_{C.L.}$, $B_{C.L.}$ and $C_{C.L.}$ are used instead of A, B and C and I_{2N+6} instead of I_{2N+2}. Again, the size of domain of attraction d is calculated for the operating points $(\bar{\phi}^*, \bar{\psi}^*)$ corresponding to a range of K_t from 8.5 to 11.5. d is plotted as a function of $\bar{\phi}^*$: solid line on Figure 3.15. It turns out that we get exactly the same results as with the constant-gain feedback controller. Figure 3.15 and 3.13 are identical. Thus, the same conclusions can be deduced regarding the improved stability of the system. The H_∞ controller has been designed to reject worst case disturbances and has therefore more stability robustness than the constant-gain feedback controller. Therefore, we expected an increase in the size of domain of attraction d. However, this is not the case. The function d does not distinguish between the linear controllers.

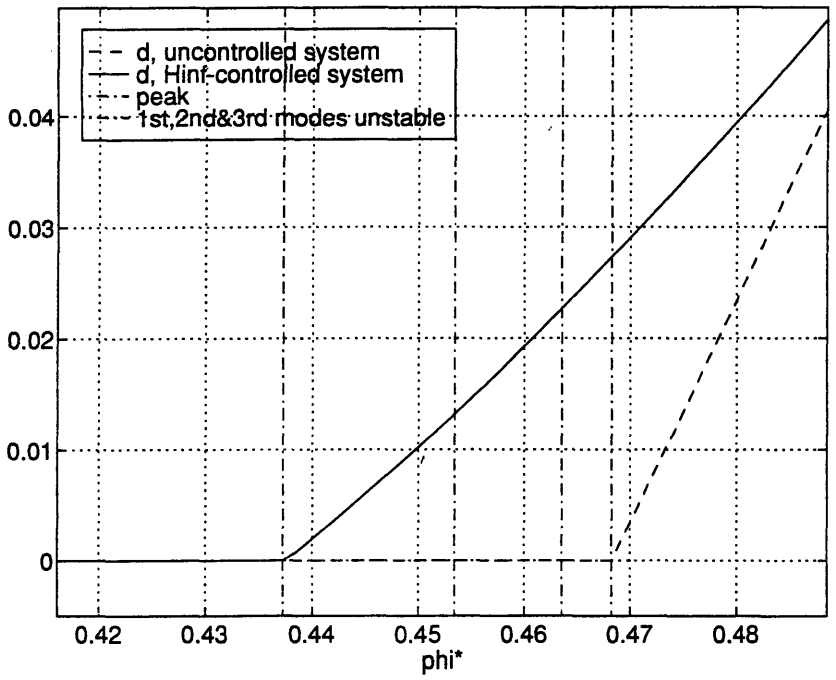

Figure 3.15: Second linear controller: H_∞ controller on the first 2 modes, Size of domain of attraction d as the operating point moves along the compressor characteristic.

The size of domain of attraction d is the same for both linearly controlled systems. In order to explain this phenomenon, we need to examine for a given operating point how the Hamiltonian matrix H behaves when the parameter β_r is decreased since the test on the eigenvalues of H decides when the iteration of Section 3.3 stops and thus how large d is. Figure 3.16 shows the location of the eigenvalues of H for $K_t = 9.333$ and $\beta_r = 0.2618$ when the system is stabilized using the constant-gain feedback controller. Figure 3.17 shows the same plot when the H_∞ controller is used.

H is of dimension twice the dimension of A (or $A_{C.L.}$). Each mode can be associated to 4 eigenvalues that are symmetric with respect to both real and imaginary axis. When β_r is very large, H has all eigenvalues on the $j\omega$ axis. Then as β_r decreases, its eigenvalues separate from the $j\omega$ axis mode by mode starting from the most stable to the least stable.

At K_t = 9.333, the order of separation by mode number is: 0, 5, 4, 1, 2 and 3 when constant-gain feedback is used and 1, 0, 2, 5, 4 and 3 when the H_∞ controller is used. In the second case, the 1st and 2nd modes separate earlier because their stabilization is better. But the key element is that in both cases the mode that is limiting (i.e. that separates last) is the 3rd mode. Improving the linear controller through its stability robustness and making the 1st and 2nd modes more stable does not change the 3rd one. It separates from the $j\omega$ axis for the same value of β_r and consequently d is not improved (d is determined by the domain of validity of the sector condition and thus by β_r).

In conclusion, the absolute stability based nonlinear stability analysis allows us to explain how a linear controller improves both the linear and the nonlinear stability properties of the system. We have also shown that 2 different linear controllers stabilizing the first 2 modes are the same from a nonlinear point of view: they generate the same domain of attraction. To improve the system, it is now necessary to design a more elaborate controller that takes into account higher modes.

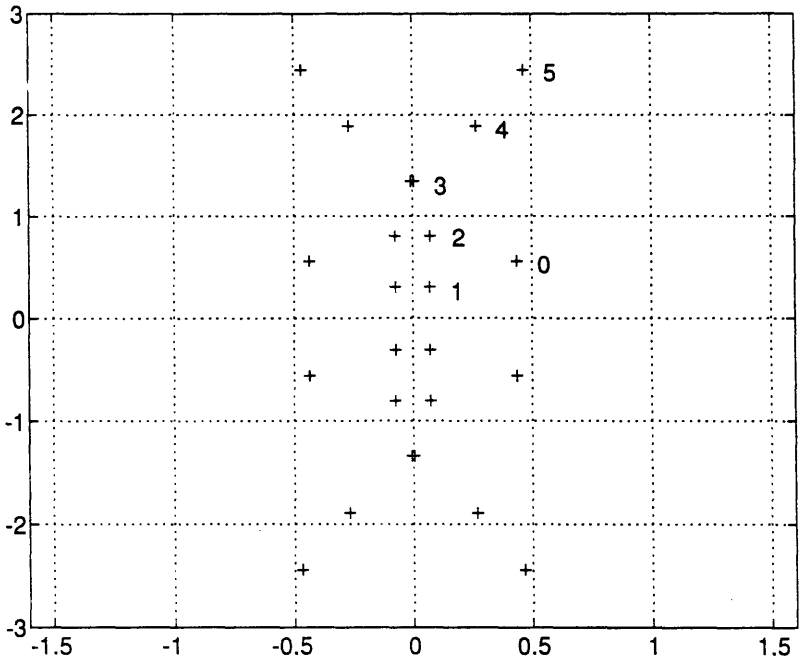

Figure 3.16: First linear controller: constant-gain feedback on the first 2 modes,

Eigenvalues of the Hamiltonian matrix H for $K_t = 9.333$ and $\beta_r = 0.2618$.

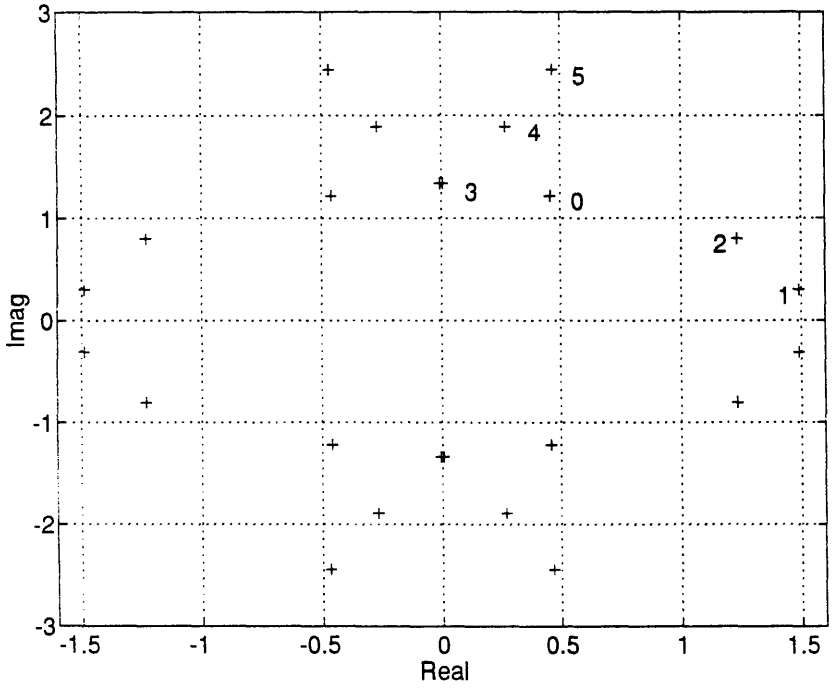

Figure 3.17: Second linear controller: H_∞ controller on the first 2 modes,

Eigenvalues of the Hamiltonian matrix H for $K_t = 9.333$ and $\beta_r = 0.2618$.

3.6 Attempt to reduce conservatism of the absolute stability based nonlinear stability analysis, Lyapunov function in Luré form

The reference used in this section is [20].

The absolute stability based nonlinear stability analysis of Section 3.3 has been restricted by its choice of Lyapunov function V. It deals exclusively with quadratic functions of the form: $V = \underline{X}^T \cdot P \cdot \underline{X}$ where P is symmetric positive definite. The result d of the nonlinear stability analysis iteration gives only an estimate of the size of the domain of attraction, the actual size being probably larger. Restricting the studied class of Lyapunov functions has introduced some conservatism. The purpose of the current section is to reduce it by allowing the Lyapunov function V to take a more general form than the quadratic one: the Luré form. New estimates of size of domain of attraction d will be calculated for compressor C2 at the peak (K_t=9.333) and compared with the previous one.

The new absolute stability based nonlinear stability analysis starts with the same assumptions as in Section 3.3. Then using Corollary 3.1 of [20], the multivariable circle criterion applied to compressor C2 is replaced by:

Considering a class of nonlinearities $\underline{\Psi}(\underline{Y})$ that satisfy the symmetric sector condition $\left[\underline{\Psi}(\underline{Y}) - K_{min}\underline{Y}\right]^T \cdot \left[\underline{\Psi}(\underline{Y}) - K_{max}\underline{Y}\right] \le 0, \forall \underline{Y} \in \Gamma \subset \mathbf{R}^p$

with $K_{max} = -K_{min} = K = \begin{bmatrix} \ddots & & (0) \\ & k_i & \\ (0) & & \ddots \end{bmatrix} = \begin{bmatrix} \beta_i I_{2N+1} & & (0) \\ & \beta_r I_{2N+1} & \\ (0) & & \beta_s I_{2N+1} \end{bmatrix}$

and $\Gamma = \left[a_i;b_i\right]^{2N+1} \times \left[a_r;b_r\right]^{2N+1} \times \left[a_s;b_s\right]^{2N+1}$,

if there exits: A) a multiplier $W(s) = I_{6N+3} + Ns$

with $N \in \left\{\mathbf{R}^{(6N+3)(6N+3)};\ n_{ij} = 0,\ i \ne j\ ;\ n_{ii} \ge 0\right\}$

B) $R = R^T > 0,\ R \in \mathbf{R}^{(2N+2)(2N+2)}$

such that: 1) $R_0 = \left[K^{-1} + NCB + (NCB)^T\right] > 0$

2) there exits a solution $P = P^T > 0$ to the equation:

$$(A + BKC)^T P + P(A + BKC) + R +$$
$$\left[C + NC(A + BKC) - B^T P\right]^T R_0^{-1}\left[C + NC(A + BKC) - B^T P\right] = 0 \qquad (3.46)$$

then the system is absolutely stable with finite domain Γ and a suitable Lyapunov function takes the Luré form:

$$V(\underline{X}) = \underline{X}^T \cdot P \cdot \underline{X} + 2\sum_{i=1}^{6N+3} n_{ii} \int_0^{C_i \underline{X}} (\Psi_i(\sigma) - k_i\sigma)\, d\sigma \qquad (3.47)$$

Note that Equation (3.46) is equivalent to the Ricatti equation:

$$A_{ric}{}^T P + PA_{ric} - PB_{ric}P + C_{ric} = 0 \qquad (3.38)$$

$$A_{ric} = A + BKC - BR_0^{-1}\left[C + NC(A + BKC)\right]$$

with $B_{ric} = B(-R_0)^{-1}B^T$

$$C_{ric} = R + \left[C + NC(A + BKC)\right]^T R_0^{-1}\left[C + NC(A + BKC)\right]$$

The nonlinear stability analysis iteration proceeds exactly as in section 3.3. It uses the same method of construction of the multivariable sector condition from the single parameter β_r and the same test over the location of the eigenvalues of Hamiltonian matrix:

$$H = \begin{bmatrix} A_{ric} & -B_{ric} \\ -C_{ric} & -A_{ric}^T \end{bmatrix}$$

The only difference is: instead of choosing ε, rate of convergence of the trajectories of the system towards the origin, we now have to select both matrices N and R prior to the iteration.

R is symmetric real positive definite and thus involves (N+1)(2N+3) degrees of freedom. It models the dissipation of the system and is thus analogous to ε. As with ε, if $R \to 0$ there is no dissipation, the convergence of the trajectories gets infinitely slow. It will be faster if R is chosen as "big" as possible (in a norm sense here).

N comes from the stability multiplier $W(s) = I_{6N+3} + Ns$ which is selected based on the known slope or gain properties of the nonlinearity $\underline{\Psi}(\underline{Y})$, i.e. based on K. This matrix is real diagonal and thus involves (6N+3) degrees of freedom.

For each choice of (N,R) a different d can be calculated using the iteration. If we want to optimize (N,R) (find (N,R) such that d is the biggest), we have to explore a space of dimension $2N^2+11N+6$ which gets very large indeed if N is as usual at least 5. This thesis will only show trends in the optimization. Simple particular forms are chosen for N and R:

$$R = rI_{2N+2},\ r > 0 \tag{3.39}$$

and $$N = nI_{6N+3},\ n > 0 \quad \text{or} \quad N = \begin{bmatrix} n_1 I_{2N+1} & & (0) \\ & n_2 I_{2N+1} & \\ (0) & & n_3 I_{2N+1} \end{bmatrix},\ n_1, n_2, n_3 > 0. \tag{3.40}$$

The last form of N is chosen by analogy with K since N is selected based on K.

First case: $n = r$.

Figure 3.18 shows the new estimate of size of domain of attraction, the flow coefficient d, as a function of n, in percent of $\bar{\phi}^*$. As expected, d gets bigger for small $n = r$, i.e. when a slower convergence of the trajectories is tolerated and is larger than the result of Section 3.3 (0.0273 or 5.83% of $\bar{\phi}^*$) only if $n = r \leq 10^{-1}$. Below $n = r = 10^{-2}$, the increase in d for a given decrease in $n = r$ and thus in convergence speed is not very dramatic. Therefore, we will keep the value of d at 10^{-2} as the optimum in the direction $n = r$.

$$n = r = 10^{-2} \quad d = 6.60\%.$$

Second case: $r = 10^{-2}$, n varies.

Figure 3.19 show the plot of d(%) as a function of n. It goes through a maximum at:

$$n = 0.16 \qquad d = 6.71\%.$$

Third case: $r = 10^{-2}$, N taken in the second form, n_1, n_2, n_3 vary.

Figure 3.20 shows a 3D plot of d(%) as a function of n_1, n_2 and n_3. d is maximum for

n_1 small, n_2 large and n_3=0.

$$\begin{cases} n_1 = 0.08 \\ n_2 = 0.34 \\ n_3 = 0 \end{cases} \quad d = 7.04\%.$$

In conclusion, extending the class of Lyapunov functions to Luré functions has increased the value of the size of domain of attraction d at the peak of compressor C2 characteristic from 5.83% to 7.04% of the equilibrium flow coefficient even if we use only basic forms for the matrices R and N, (3.39) and (3.40). Moreover, d is maximum for n_1, n_3 small and n_2 large. This makes a lot of sense since n_2 is associated to β_r and the nonlinearity due to the rotor is the predominant one. However, there is still room for optimization. Another form of multiplier W(s) should be considered since the present one is well adapted to third order nonlinearities and $\tilde{H}_i$, $\tilde{H}_r$ and $\tilde{H}_s$ are in a first approximation second order functions of $\tilde{\phi}$.

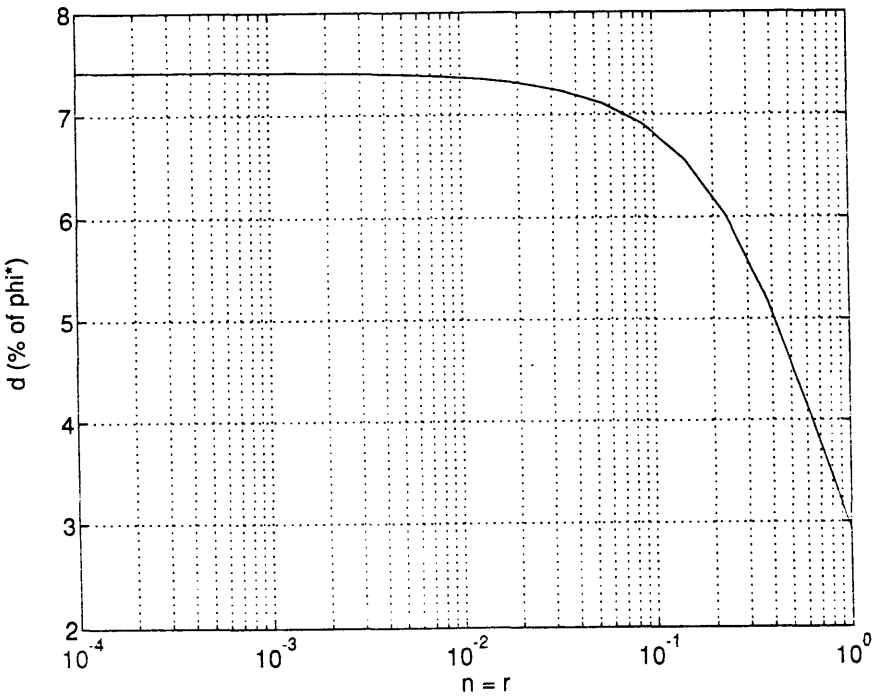

Figure 3.18: Size of domain of attraction d function of n = r.

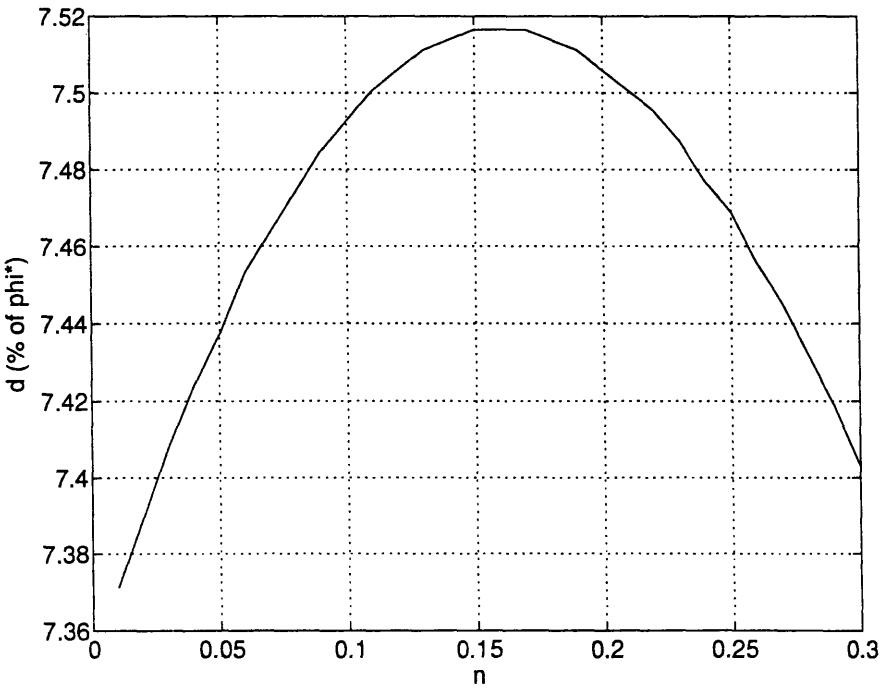

Figure 3.19: Size of domain of attraction d function of n, r = 0.01.

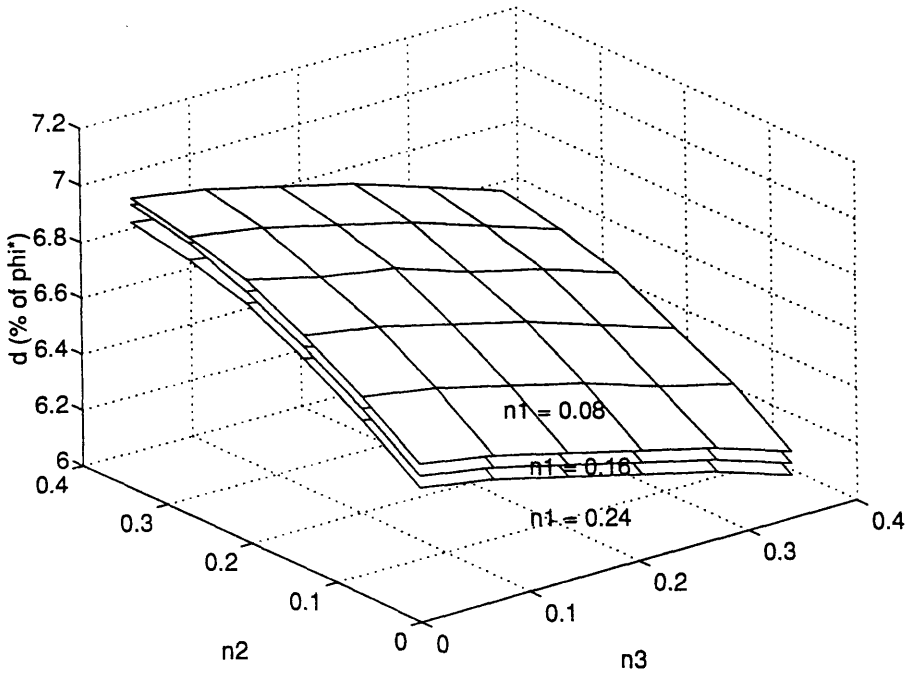

Figure 3.20: Size of domain of attraction d function of n_1, n_2, n_3, r = 0.01.

Conclusion and Future Work

Two methods of nonlinear stability analysis have been developed. The first one is based on a Lyapunov analysis and can be applied to the nonlinear model of rotating stall without unsteady losses. It provides a quantitative way to compare the stability of various compressors, and allows experimental stall inception behavior to be linked to the compressor characteristic nonlinear shape. This explains two experimentally observed phenomena, both of which are inexplicable using linearized arguments: 1) some compressors exhibit large traveling waves prior to stall, while others stall while traveling waves are still relatively small, 2) the experimentally determined damping ratios of pre-stall waves do not generally go to zero before stall inception occurs. A simple 1D Lyapunov analysis can also be used to explain the 'stabilization' of rotating stall by a basic nonlinear control scheme applied to the throttle. It shows that the system can operate safely at the peak of the compressor characteristic if the control moves the real throttle line to an apparent throttle line that is on the right of the compressor characteristic mid-line.

The second method of nonlinear stability analysis is based on Absolute Stability theory and is suitable for the analysis of a more elaborate model of rotating stall that can include both the effects of unsteady losses and a linear controller. Two linear controllers have been considered. Both stabilize the first 2 modes of the system up to the point where the third mode becomes unstable. The first controller is a constant-gain feedback over the first 2 modes, while the second one is a H_∞ controller. Domains of attraction have been calculated and compared with results from the first method. The second method allows to explain how a linear controller improves both the linear and nonlinear stability properties of

the system. The range of linearly stable operating points has been extended to the left of the peak of the compressor characteristic and over this range both linear controllers have dramatically increased the size of domain of attraction of the system. Until its neutral stability point, the controlled system is much more robust as regards perturbations, i.e. much more stable nonlinearly speaking, than the uncontrolled system was. The analysis also shows that 2 different linear controllers stabilizing the first 2 modes are the same from a nonlinear point of view: they generate the same domain of attraction. Therefore, the domain of attraction will only be increased if the controller takes into account higher modes.

The nonlinear stability analysis of rotating stall can still be improved. There are several areas of interest that call for further investigation in the future. First, an even more realistic model of rotating stall should be generated which includes the dynamics of the components in the feedback path: feedback time delay, zero order hold sampling of the filtered hot-wire signals by the A/D converter, and IGV actuator dynamics (see [17]). Then, the absolute stability based nonlinear stability analysis should be applied to this model and more complex controllers should be tried: linear controllers that take into account higher modes than the second one or even simple nonlinear controllers. Comparing the size of the domain of attraction for different control schemes will help in deciding what kind of controller to implement in the future. It seems that stabilization of the nonlinear phenomenon of rotating stall should be best enhanced by nonlinear control, precisely because of its nonlinear nature. The methods presented here will have to be adapted in order to deal with a nonlinear controller because, in the case of a nonlinear controller the control part of the state-space representation in a matrix form is no longer valid. The size of domain of attraction which results from the nonlinear stability analysis herein should also be checked and compared with a quantitative measure of the size of the perturbation

that destabilizes the system using a nonlinear simulation of rotating stall with unsteady losses.

References

1. Greitzer, E.M., "Review - Axial Compressor Stall Phenomena", Journal of Fluids and Engineering, Vol. 102, 1980, pp. 134-151.

2. Ludwig, G. R., and Nenni, J. P., "Tests of an Improved Rotating Stall Control System on a J-85 Turbojet Engine," ASME Paper 80-GT-17, presented at the Gas Turbine Conference and Products Show, New Orleans, March 10-13, 1980.

3. Paduano, J.D., Epstein, A.H., Valavani, L., Longley, J.P., Greitzer, E.M. and Guenette, G.R., "Active Control of Rotating Stall in a Low-Speed Axial Compressor", ASME Journal of Turbomachinery, Vol. 115, January 1993, pp. 48-56.

4. Day, I. J., "Active Suppression of Rotating Stall and Surge in Axial Compressors," ASME Journal of Turbomachinery., Vol. 115, No. 1, January 1993.

5. Badmus, O.O., Chowdhury, S., Eveker, K.M., Nett, C.N. and Rivera, C.J., "A Simplified Approach for Control of Rotating Stall, Part I and I", AIAA 93-2229 and 93-2234, 29th Joint Propulsion Conference and Exhibit, Monterey, June 1993.

6. Greitzer, E. M., Epstein, A. H., Guenette, G. R., Gysling, D. L., Haynes, J., Hendricks, G. J., Paduano, J. D., Simon, J. S., and Valavani, L., "Dynamic Control of Aerodynamic Instabilities in Gas Turbine Engines," AGARD Lecture Series 183, Steady and Transient Performance Prediction of Gas Turbine Engines, AGARD-LS-183, May 1992.

7. Hynes, T.P. and Greitzer E.M., "A Method for Assessing Effects of Circumferential Flow Distortion on Compressor Stability", ASME Journal of Turbomachinery, Vol. 109, July 1987, pp. 371-379.

8. Epstein, A.H., Ffowcs Williams, J.E. and Greitzer, E.M., "Active Suppression of Aerodynamic Instabilities in Turbomachines", Journal of Propulsion and Power, Vol.5. No. 2, March-April 1989, pp. 204-211.

9. Moore, F.K. and Greitzer, E.M., "A Theory of Post-Stall Transients in Axial Compression Systems, Part I - Development of Equations", ASME Journal of Engineering for Gas Turbines and Power, Vol.108, January 1986, pp. 68-76.

10. Chue, R.S., Greitzer, E.M., and Tan C.S., "An Analysis of General Post-stall Transients in Axial Compression Systems", May 1987.

11. Slotine, J.-J. E. and Weiping L., Applied Nonlinear Control, Prentice Hall, Englewood Cliffs, N.J., 1991.

12. D'Azzo, J.J. and Houpis, C.H., Linear Control System Analysis and Design: conventional and modern, McGraw-Hill, New York, 1975.

13. Simon, J.S. and Valavani, L., "A Lyapunov Based Nonlinear Control Scheme for Stabilizing a Basic Compression System Using a Close-Coupled Valve", American Control Conference, Boston, June 1991.

14. Greitzer, E.M., "The Stability of Pumping Systems"- the 1980 Freeman Scholar Lecture, ASME Journal of Fluids Engineering, Vol. 103, June 1981, pp. 193-242.

15. Gysling, D.H., "Dynamic Control of Rotating Stall in Axial Flow Compressors Using Aeromechanical Feedback", Ph.D. Thesis, MIT Department of Aeronautics and Astronautics, September 1993.

16. Mansoux, C., Gysling, D.L. and Paduano, J.D, "Distributed Nonlinear Modeling and Stability Analysis of Axial Compressor Stall and Surge", to appear, Proceedings of the American Control Conference, Baltimore, June 1994.

17. Haynes, J.M., "Active Control of Rotating Stall in a Three-Stage Axial Compressor", M.S. Thesis, MIT Department of Mechanical Engineering, February 1993.

18. Khalil, H.K., Nonlinear Systems, Macmillan, New York, 1992.

19. Maciejowski, J.M., Multivariable Feedback Design, Addison-Wesley, 1989.

20. How, J.P., "Robust Control Design with Real Parameter Uncertainty Using Absolute Stability Theory", Ph.D. Thesis, MIT Department of Aeronautics and Astronautics, February 1993.

5740-18